RICE UNIVERSITY

Manipulation and Biological Applications of Gold Nanorods

by

Betty Catalina Rostro-Kohanloo

A THESIS SUBMITTED
IN PARTIAL FULLFILLMENT OF THE
REQUIREMENTS FOR THE DEGREE

Doctor of Philosophy

APPROVED, THESIS COMMITTEE:

Jason H. Hafner, Chair, Associate Professor of Physics and Astronomy and Chemistry

Sibani Lisa Biswal, Assistant Professor in Chemical and Biomolecular Engineering

Jennifer West, Isabel C. Cameron Professor of Bioengineering and Chair, Bioengineering

HOUSTON, TEXAS
DECEMBER 2010

ABSTRACT

Manipulation and Biological Applications of Gold Nanorods

by

Betty Catalina Rostro-Kohanloo

This thesis compared anionic polyelectrolyte wrapping stabilization with poly(sodium 4-stryene-sulfonate), (PSS), polyelectrolyte and methoxy (polyethylene glycol)-thiol ($mPEG_{(5000)}$-SH) strategies. From this data the critical gold nanorod (GNR) and cetyl-trimethylammonium bromide (CTAB) concentration ratio needed for GNR stabilization was determined using optical and chemical extraction methods. This was followed by functionalization with a heterobifunctional Polyethylene glycol (PEG) linker, such as a-thio-w-carboxy poly(ethylene glycol) termed t-PEG-c and carbodiimide chemistries for antibody linkage with Immunoglobulin G (IgG), and epidermal growth factor receptor (EGFR) based Human Epidermal growth factor Receptor 2 (Her2), and Cetuximab (C225) antibodies, for in vitro cancer cell targeting. Confocal, two-photon luminescence (TPL), and dark scattering microscopy, and fluorescence, zeta potential, and Nanoparticle Enzyme-linked immunosorbent assay (ELISA) were used to monitor changes to the GNR surface. An untreatable form of bladder cancer was then studied using the t-GNR-PEG-c-Ab bioconjugates with C225 antibody, which housed a glyceraldehyde-3-phosphate (GAPDH), Fluorescein isothiocyanate (FITC) labeled siRNA, termed GAPDH-siRNA-FITC, which was included within a Luciferase based plasmid. A salt based electrostatic heating method was used to trap the GAPDH-siRNA-

FITC from the PEG layer by activating the PEG polymer pour point, while a laser based heating system was used for in vitro release inside cancer cells. The down regulation of the GAPDH gene was targeted by the siRNA, as GAPDH has been shown to be up-regulated in many cancers and down-regulated by chemotherapeutic drugs. Cell culture, and subsequent imaging by transmission electron microscopy (TEM), TPL and confocal microscopy were used to view the internalized conjugates, and reverse transcriptase polymerase chain reaction (RT-PCR) were used to determine if the release of the GAPDH-siRNA caused a reduction in the expression of GAPDH-mRNA. Plasmonic gene silencing of the gene by the GAPDH-siRNA was then compared to a lipid based Dharmafect control in terms of transfection ability. RT-PCR results evidenced gene silencing of the plasmonic-GAPDH-siRNA vector when compared to the Dharmafect control. Silencing likely resulted from the zwitterionic charges of the plasmonic vector and the encapsulated GAPDH-siRNA, which yielded near neutral charge tendencies. This differs significantly from the Dharmafect lipid vector, which is cationic in nature. Endosomal release of the plasmonic vector is further enhanced by the laser excitation of the GNR at the longitudinal surface plasmon resonance (LSPR), which allows for the endosomal release of the GAPDH-siRNA through pore formation leading to cytoplasmic transport and subsequent gene silencing. Near neutral charges were welcomed in this plasmonic gene therapy study as they tend to favor endosomal release, pore formation, and transport.

ACKNOWLEDGEMENTS

Within these pages I give to you my "formalized curiosity," a work that took a monumental time to complete. It is because of this, that I must be grateful to the few. My parents, cousins, and siblings are purposely mentioned for allowing me, the L'enfant terrible, to experiment with my educational endeavors. For in spite of my many adventures, it seems, I have finally finished with my education; they must be very, very grateful for that, I am as well.

Of the knowable and eminent I provide a notable mention; Ellen & Dr. Harvey Loomstein, Dr. Olga Pupysheva & Dr. Amir A. Farajian, Dr. Catalina Garcia, Dr. Jennifer Caldwell-Johnson, Dr. Skedros, Dr. Lothar Esser, Dr. Peter Sun, NCI-NIH, NIAID-NIH, GPP-NIH, The Department of Biomedical Engineering and The Whitaker Institute at John Hopkins University, STLE, Nancy Nalence, Dr. Shina Philips, Metal Oxide Technologies, UofH, NASA, Dr. Kelly Bradley, CBEN, RQI, Dr. Dmitri Lapotko, Dr. Liana Adams, Dr. Rebecca Drezek, Dr. Jennifer West, Dr. S. Lisa Biswal, and Dr. Jason Hafner, for maintaining confidence, in spite of reputational risks. Honorable mention is given to graduate students Katie, Sean, Lindsey, Courtney, Hong Wei, Lisette, Ivana, Oara, Danny, Nikolai, Merlyn, Sandra, Abhi, post-doc Stefan, for years of indicating and contraindicating. A notorious, and unwarranted mention, is given to the Wagner Lab for their help with many loquacious and malapropistic, yet somatoformic endeavors with both non-Bachelor and Bachelor stimulating studies, with stimulating applying only, and only, to the latter. Note that somatoformic here refers solely to the

female hysteria type, a condition that has been historically known to plague high-IQ women.

Secured mentions are given to friends Krista, Jane, Lynn, Mary, Touran, Rezza, Sharon, Stephanie, and Ben, for achieving high diplomatic relations between all kinds of ambassadors. My husband Prince Farshid, his family (Luke, Ana, Nahid, Ali & Maria) & friends (Reza, Jesus, Fiona), and my little micro human Talis, who gives me more of a human touch, well these mentions are expected by both parties, them and me.

A liberating definition, is given to the Applied Physics program, which I define as a top notch (top 10 program in optics to be exact); housed within an institution that has provided a cozy lab, respectable library (notable for its summum bonum resources); and an extremely competent and knowledgeable advisor - who is open-minded, and not afraid to do novel research with the "creatively inclined." To my fellow comrades - Yvonne, Barbara, Angela, and Bridgitt, whom I term the consul-general, well they require a sincere expression of gratitude for hearing, and rehearing, the many complaints, stemming from the proletariat whom comprise, and compose, the Institute of Physical Problems.

Alas, after many years of trepidation through the halls of knowledge, this PhD yielded conclusive evidence of the close-knit relationships that exist between science, resourcefulness, creativity, and some genius inspired insanities. After all exhaustion-inspired insanities, are amongst the formal requirements for inducing creative and original thought. However, those who came before me, have said that, "*no man is sane who does not know how to be insane on proper occasion, after all, there's a fine line*

between genius and insanity." Alas, I have erased this line, time and time again, often purposely, rarely accidentally. But the well informed, have given me countless lectures relating to me that, *"insanity is often the logic of an accurate mind over tasked; and there is no great genius without some touch of madness, for alas, the distance between insanity and genius is measured only by success."* Yet, while greatly informed, I may believe those who came before me, only upon seeing names signed with bold, dark ink; we can then, thank the committee.

Until then, I am still in disbelief, yet we hope for some success. Again we hope. Otherwise, what be the use of the bright splinters of the mind, those damn moments of eureka, which bless the saint and damn the demon? Ergo, "*O livro de como se fazem as cores*" applies here as petitio principii, something which has plagued me, and my field(s) of study for years. Consequently, this is a thesis dictated unneurotically, we exclude the *in biblio*, flagship security, and propaganda sections here, lest we forget the damn "*blue screen of death (BSOD)*". Nevertheless, following a neurotic, yet *avante-garde* delivery given by the ***Eternal Eureka Vagabond***, we thus celebrate an infamous, yet notable departure, from The Institute of Physical Problems. 'Elaka de'Meir, Aneni!'x3

.....To be accepted sometime in 2010. This being--- early if hopeful,

mid year if lucky, or later if suffering from a bad case of dolce far niente.

LIST OF FIGURES

Figure 4-9. TPL of nonspecific IgG-GNR (red pixels). Alexa-488 labeled WGA was added to live bladder mesenchymal UC3 cells cell 10 min before fixation Alexa-488 WGA with C225-GNR seen in red (far right), and Alexa488-WGA in green no GNR (lower left).

Figure 4-10. Confocal microscopy of KU7 Cells shown (top left) NR-C225-EGF, (middle top) NR-C225, (top right) Phenyl red-EGFR, (bottom left) EGF control, (bottom right) C225-EGF control. Green images shown GNR binding in KU7 cells with and without EGF, DNA is shown in blue.

Figure 4-11. Cellular integration of bi-functionalized gold nanoparticles as observed by confocal. The images of live cells were taken 12 hrs post-transfection using a 40x objective-Zeiss Observer-Z1.

Figure 4-12. Measurement of GAPDH-mRNA using real-time RT-PCR. KU7 cells were incubated for 48 hours with non-targeting Glyceraldehyde (NTG) and GAPDH targeted siRNA-FITC that was housed with the t-GNR-PEG-Ab with C225. The RNA was extracted and GAPDH-mRNA was measured. The mRNA normalization was done by measurement of 18S ribosomal RNA (internal control).

LIST OF TABLES

LIST OF EQUATIONS

NOMENCLATURE

(NIR)	Near-Infrared
(LSPR)	Localized Surface Plasmon Resonance
(GNR)	Gold nanorod(s)
(TPL)	Two-photon Luminescence
(AFM)	Atomic Force Microscopy
(SEM)	Scanning Electron Microscopy
(cPEG-GNR-Ab)	α-thio-ω-carboxy poly(ethylene glycol)–GNR-antibody
(CTAB)	Cetyltrimethylammonium Bromide
(PAA)	Polyaspartic Acid
(tPEG)	PEG-thiol
(tcPEG)	Thiol-carboxyl-PEG
(cPEG)	carboxyl-PEG
(cmc)	Critical Micelle Concentration
(DNA)	Deoxyribonucleic Acid
(RNA)	Ribonucleic Acid

(mtPEG)	Thiol-terminated methoxypoly(ethylene glycol)
(MES)	2-(N-morpholino)ethanesulfonic acid
(PSS)	Poly(sodium 4-styrene-sulfonate)
(QCM)	Quartz Crystal Microbalance
(MS)	Mass Spectrometry
(FWHM)	Full Width Height Max
(NHS)	N-Hydroxysuccinimde
(EDC)	1-Ethyl-[3-dimethylaminopropyl]carbodiimides
(PBS)	Phosphate buffered saline
(AF-Ab)	Alexa Fluor 488 labeled rabbit IgG
(BSA)	Bovine Serum Albumin
(IgG)	Immunoglobulin G
(HRP)	Horse Radish Peroxidase
(FBS)	Fetal Bovine Serum
(MEBM)	Mammary Epithelial Basal Medium
(WGA)	Alexa-488-wheat germ agglutinin
(HER2)	Human Epidermal Growth Factor Receptor 2

(MPS)	Mononuclear Phagocytic System
(EGF)	Epidermal Growth Factor
(siRNA)	silencing-interfering-RNA
(miRNA)	micro-RNA
(UC)	Urothelial Carcinoma
(M-VAC)	Methotrexate-Vinblastine-Adriamycin-Cisplatin
(HB-EGF)	Heparin Binding-EGF
(bFGF)	Basic Fibroblast Growth Factor
(nt)	Nucleotide
(dsRNA)	double-stranded-RNA
(RNAi)	RNA interference
(C225)	Cetuximab-225
(TBE)	1xTris-Borate-EDTA buffer
(BLI)	Bioluminescence Imaging
(siGAPDH)	Small Inhibiting RNA for Glyceraldehyde-3-Phosphate
(RT-PCR)	Reverse Transcriptase Polymerase Chain Reaction
(NTG)	non-targeting Glyceraldehyde

(SPDP)	Succinimidylpyridyldithiopropionamidohexanoate
(PIs)	Isoelectric Points
(TEM)	Transmission Electron Microscopy
(DF-1)	Dharmacon, Dharamafect-1
(RTK)	Receptor Tyrosine Kinases
(ncRNAs)	non-coding RNAs
(DF-1)	Dharmacon, Dharamafect-1
(PY-20)	Phosphotyrosine-20 antibody
(HCl)	Hydrochloric acid
(APTES)	Aminopropyltriethoxy silane

TABLE OF CONTENTS

CHAPTER 1

Plasmon Resonances

Reducing the size and dimensionality of a material can affect its interactions with electromagnetic radiation, as well as its surface chemistry.[1-3] In noble metal particles that are much smaller than the wavelength of incident light, the surface properties of the material govern interactions at visible and near-infrared (NIR) wavelengths, and lead to the ability to manipulate light at the nanometer scale. The gold nanoparticles that are the subject of this work manipulate light through resonant collective oscillations of the conduction electrons, termed localized surface plasmon resonances, which result in strong optical absorption and scattering.[2-6] This exotic behavior can be seen in the reddish-orange hues of stained glass windows in many medieval churches and in the Lycurgus Cup from the 4th century AD. The presence of colloidal gold in the glass absorbs the green wavelength of light, producing a deep ruby red in transmitted light, as shown in **Figure 1-1**.[10]

Figure 1-1. **a**) Stained glass and, **b)** Lycurgus cup colored with colloidal gold nanoparticles that yields unusual optical properties.

1.1 Nanoparticle Analysis

1.1.1 Plasmons

When light strikes the metal nanoparticles, it creates an electromagnetically induced oscillation of the conduction electrons in the particles. The restoring force,

which is the Coulombic attraction of the electrons towards the nuclei in the lattice, creates a resonant condition within a relatively narrow spectral band termed a localized surface plasmon resonance.[8] Excitations of the surface plasmons generate large local fields within the vicinity of the nanoparticle surface, which strongly exceed the intensity of the incident light field. This produces enhanced optical phenomena at the nanoparticle surface such as fluorescence, Raman scattering, second-harmonic generation, and other non-linear optical responses. The plasmon resonance also results in enhanced absorption and scattering of incident light by the nanoparticles. The type of metal, its size, and geometry will ultimately dictate the strength and peak wavelength of these effects. Noble-metal gold and silver nanoparticles have small losses at the optical frequencies, and tend to exhibit strong resonant behavior, with the resonance of silver being stronger than that of gold.[4-5] Plasmon resonances cause a peak in the spectral extinction of nanoparticle solutions, as seen in **Figure 1-2**.

The observed reddish-purple hues of spherical gold nanoparticle solutions result from a strong absorption band centered around 520 nm (2.3 *eV*), which is when the frequency of the electromagnetic field of the incoming light is resonant with the collective oscillation of the conduction electrons.[1,4-5] We will discuss gold nanoparticles of 10 nm through 60 nm in diameter, where the dissipation regime of the plasmon decay dominates the dephasing of the collective electron motion, and reradiation, which is present in larger particles, is highly diminished.[1-5] We will discuss these absorbing particles and their subsequent plasmons, shape dependence, functionalization with polymers, and their biological applications such as cell targeting, internalization, cell receptor specific binding, and gene therapies.

1.1.2 GNR Shape

If the nanoparticle shape is significantly altered it will have a tremendous affect on the plasmon absorption band.[13-15] The boundary conditions of the gold nanoparticles affect the coherent electron oscillations and the interband d to sp electronic transitions, which in turn affect the optical absorption properties. Nanoparticle size also affects the resonance frequencies and width of the plasmon absorption band. Altering the shape and size of such nanoparticles gives control over spectral variations in how the captured electromagnetic energy is distributed.[12] Gold nanorod(s), (GNR), support a large absorption cross-section at NIR frequencies per unit volume when compared to other nanostructures and have narrower linewidths due to reduced radiative damping effects, with higher optothermal conversion efficiencies. For GNR the plasmon absorption band is split into two bands, transverse and longitudinal, these stemming from the oscillation of free electrons along and perpendicular, to the long axis of the rods, **Figure 1-2, Figure 1-3**.[4-6,12] The transverse band of the GNR occurs at a wavelength of 520 nm, note that this is also seen in spherical nanoparticles. The longitudinal plasmon band, can red shift into the NIR, and is approximately linear with aspect ratio, and with the dielectric function of the medium.[2] The aspect ratio of the GNR can be tailored by varying the ratios of surfactants to cosurfactant molecules during their synthesis.[13-15]

The width and height of the plasmon band is directly related to the associated decay mechanisms of the electrons which occur due to the dephasing of the collective electron motion arising from radiative damping, and electron scattering, off phonons and

defects.[1-3] Due to the longitudinal localized surface plasmon resonance (LSPR), nonlinear optical effects can also arise. Two-photon absorption can also present itself in the GNR, due to an electronic transition from the *d*- to *sp*-bands, leading to an electron-hole pair. Recombination of the separated charges would then result in two-photon luminescence (TPL) emission. The conversion of optical energy into heat arises from the nonradiative electron relaxation dynamics, which creates the resulting electron-phonon collisions. This provides gold nanoparticles with photothermal properties such as localized heating that can be of use in medical therapeutics and biomedical imaging.

1.1.3 Mie Theory

Mie was the first to explain the surface plasmon resonance behavior of spherical metal nanoparticles by solving Maxwell's equation for the interaction of an electromagnetic plane wave with an interacting small sphere.[1-12] It then became possible to calculate a particle's extinction spectrum by simply using the material's dielectric function.[4-5] The total extinction coefficient of the metal nanoparticles was taken to be the summation over electric and magnetic multipole oscillations, which would contribute to the absorption and scattering of the interacting electromagnetic field. Nanoparticles that are well below the wavelength of light, these being particles that are smaller than 100 nm, show a strong contribution from the dipole oscillation, and so only this term is relevant when tabulating the absorption spectra.[4-5]

In the quasi-static regime the plasmon resonant extinction can be tabulated by using **Equation 1-1**, where κ is the extinction coefficient, for N particles of volume V. ε_m is the dielectric constant of the medium, λ is the radiation wavelength, ε_1 is the real part

of a material's dielectric function, ε_2 is the imaginary part of a material's dielectric function.[5]

$$\kappa = \frac{18\pi N V \varepsilon_m^{3/2}}{\lambda} \frac{\varepsilon_2}{(\varepsilon_1 + 2\varepsilon_m)^2 + \varepsilon_2^2} \qquad \textbf{(Equation 1-1)}$$

The materials dielectric function can in turn be expressed as a summation of ε_1 and ε_2, where ω is the angular frequency of light, this is given in **Equation 1-2**.[1-12]

$$\varepsilon(\omega) = \varepsilon_1(\omega) + i\varepsilon_2(\omega)$$

(Equation 1-2)

In order to tabulate the absorbance of a colloidal solution containing N particles in an optical cell of path length L, you would take the extinction coefficient, κ and use **Equation 1-3**.[5]

$$A = (\kappa / \ell n 10) L \qquad \textbf{(Equation 1-3)}$$

Noble metal nanoparticle have small, negative ε_1 in the visible, and a small ε_2, which are responsible for their sharp plasmon resonances.[2,5] The resonance condition for the plasmon absorption band is fulfilled when $\varepsilon_1(\omega)=-2\varepsilon_m$. While the minimum plasmon bandwidth depends on ε_2, it is also size dependent.[2,5]

1.1.4 Gans Theory

These shifts in the plasmon wavelength, which are altered with respect to shape and environment, can be calculated by Gans' theory, which is a more modified form of Mie theory.[4-6] The extinction coefficient, κ, shown in **Equation 1-4** is given in terms of the number of particles N, volume V, P_j depolarization factors, whereby the material dielectric constant ε_m is frequency independent, and ε_1 and ε_2 are the real and imaginary part of a material's dielectric function.[4-6]

$$\kappa = \frac{2\pi N V \varepsilon_m^{3/2}}{3\lambda} \sum_j \frac{(1/P_j^2)\varepsilon_2}{\left(\varepsilon_1 + \frac{1-P_j}{P_j}\varepsilon_m\right)^2 + \varepsilon_2^2}$$ **(Equation 1-4)**

The depolarization factors for axes *A*, *B*, *C*, are shown as P_A and P_B=P_C, with the aspect ratio, R, and λ, which is the radiation wavelength, are then used to tabulate the extinction coefficient, this is shown in **Equation 1-5**.[4-6]

$$P_A = \frac{1-e^2}{e^2}\left[\frac{1}{2e}\ln\left(\frac{1+e}{1-e}\right) - 1\right]$$
$$P_B = P_C = \frac{1-P_A}{2}$$ **(Equation 1-5)**
$$e = \sqrt{1-\left(\frac{B}{A}\right)^2} = \sqrt{1-\frac{1}{R^2}}$$

where P_j are depolarization factors for axes *A*, *B*, *C*, where $A > B = C$ for a prolate spheroid.

1.1.5 Analysis

For GNR, their aspect ratio is tabulated in terms of the ratio of the length and width of the rod, where the average nanorod length is 44 nm and width is 11 nm, these being parameters that were determined by Atomic Force Microscopy (AFM), and Scanning Electron Microscopy (SEM), this is shown in **Figure 1-2**. This can be compared to the calculated absorption spectrum shown in **Figure 1-3.** Aggregated GNR and other nanoparticles will show a red-shifted plasmon absorption band and longer wavelengths, due to the nanoparticles being electronically coupled.[2] This occurs since the oscillating electron in one particle will feel the electric field due to the oscillating free electron in a second particle, which is a short distance away, leading to a collective

plasma oscillation of aggregated particles. The frequency and intensity of the resulting band will be determined by the degree of aggregation, orientation of nanoparticles, and interparticle coupling.[2]

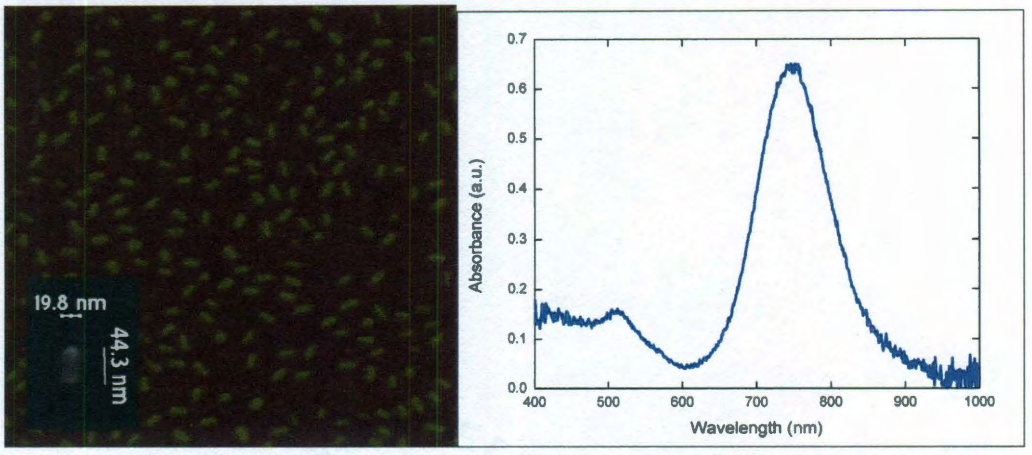

Figure 1-2. AFM of 20 nm by 45 nm GNR (background) and HiVac SEM (overlay) and LSPR bands that are optically evident (right).

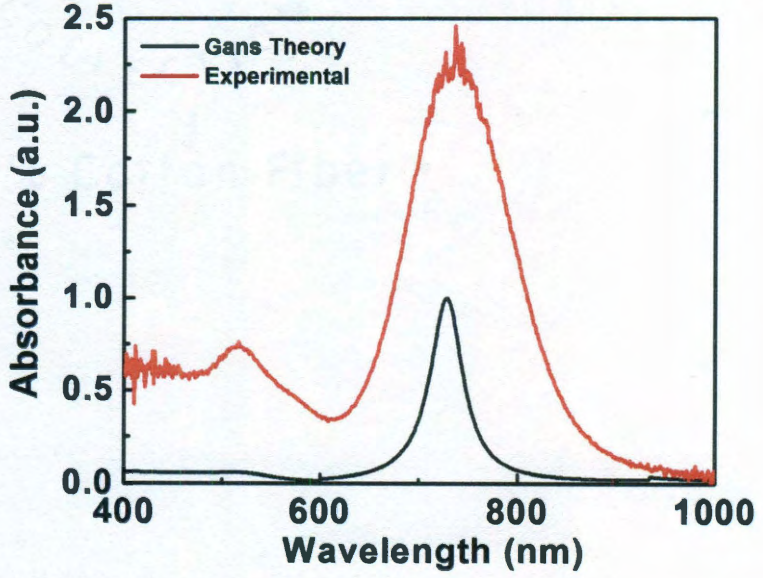

Figure 1-3. A comparison of the extinction spectrum calculated for prolate spheroids (Gans theory) and gold nanorods (experiment).

1.2 Conclusion

Noble metal particles are much smaller than the wavelength of incident light, and their material surface properties govern interactions at visible and NIR wavelengths, which lead to the ability to manipulate light at the nanometer scale. The gold nanoparticles can then manipulate light through resonant collective oscillations of the conduction electrons, which are LSPR that result in strong optical absorption and scattering, at visible and NIR wavelengths. These shifts in the plasmon wavelength, which are altered with respect to shape and environment, can be calculated by Gans' theory, which is a more modified form of Mie theory, and are dependant on the material's dielectric function and the particle's environment. This can be of considerable interest in biomedical applications, since the plasmon resonances can affect localized heating and light scattering, which can benefit biological systems that require relatively inert gold nanoparticle based therapies. To date tunable gold nanoparticles have already been implemented in applications ranging from photothermal therapies, drug delivery, and diagnostic imaging which make use of the nanoparticle shape biased LSPR.[73-79]

CHAPTER 2

Gold Nanorod Stabilization

CTAB, which is needed for the synthesis and stability of the GNR, produces various unwanted effects for biological GNR applications due to its cytotoxicity and nonspecific binding.[16-18] The CTAB plays an important role in determining the aggregation behavior of GNR, for example, high CTAB concentrations serve as a stabilizer that prevents nanorod agglomeration. CTAB is beneficial in that it imparts the rods with a positive charge, leading to repulsive forces that electrostatically stabilize the GNR against the attractive van der Waals forces of the bare metal, which is thought to occur through the formation of CTAB bilayers on the surfaces.[19-21,23,72] This helps in offsetting the GNR aggregation behavior by preventing the bare gold surfaces of the rods from binding to each other.[19-21] Lowering the CTAB concentration leads to a loss of bilayers often leading to immediate GNR aggregation.[24-36,72] The strong binding of CTAB-gold surfaces, and the resulting slow exchange at the GNR surface, has led to extensive surface modification and functionalization techniques that can displace or overcoat the CTAB and stabilize the GNR. Yet, the strong CTAB-gold absorption continue to make such techniques a significant challenge.[24,26]

2.1 GNR Surface Modification

In order to overcome such problems several strategies have been developed to modify the surface chemistry of the GNR in order to either bind and/or displace the

CTAB surfactant layer. Some groups have used electrostatic polymer methods to bind the CTAB layers through wrapping with anionic polyelectrolytes like polyaspartic acid (PAA), while others have focused on displacing the CTAB layer using thiol-terminal polyethylene glycol (tPEG) functionalization strategies.[30-31,34-44] Other strategies have focused on experimenting with displacement with alkanethiols, and lipids, however, all of these strategies must be studied further, as reproducibility issues still arise.[32-33] In this study, a suitable method to overcome such issues was developed through the use of previously described poly(sodium 4-stryene-sulfonate) (PSS) polyelectrolyte wrapping methods and compared this to (polyethylene glycol)-thiol ($mPEG_{(5000)}$-SH) strategies. Here we identify the sensitivity of GNR to CTAB concentration and determined the critical GNR/CTAB concentration ratio which was needed for CTAB stabilization. A comparison of electrostatic polymer wrapping to covalent $mPEG_{(5000)}$-SH stabilization through water dilution, chloroform extraction, and optical characterization techniques provided the critical CTAB concentration that was needed for GNR stability.

2.2 Methods

2.2.1 GNR synthesis

GNR were prepared using the seed-mediated synthesis, and scaled up to increase the quantity.[80-82] Gold seed particles were prepared by adding 250 μL of 10 mM $HAuCl_4 \cdot 3H_2O$ (Sigma, #520918) to 7.5 mL of 100 mM CTAB (Sigma, #H9151) with brief, gentle mixing by inversion. To this was immediately added 600 μL of freshly prepared, ice-cold 10 mM $NaBH_4$ (Acros, #H9151) solution (2-8°C), followed by mixing by inversion for 2 minutes, leading to a pale brown seed solution that was stable and usable for several days. The nanorod growth solution was prepared in a plastic tube, by

adding the following reagents in the order given, 425 mL of 100 mM CTAB, 18 mL of 10 mM $HAuCl_4 \cdot 3H_2O$, 2.7 mL of 10 mM $AgNO_3$ (Acros, #19768), and then gently mixed by inversion. To this mixture was added 2.9 mL of 100 mM ascorbic acid (Fisher, #A61) and mixed by inversion, which changed the solution from a brown-yellow to a clear colorless solution. GNR growth was initiated by adding 1.8 mL of the seed solution to the growth solution, which was followed by gentle mixing. The solution was then incubated for 3 hours at room temperature, which produced a color change to dark purple, mostly within the first hour. This dark purple color change is representative of GNR growth.

2.2.2 PSS stabilization

GNR solutions were heated to 30°C to melt CTAB crystals which form at room temperature, leading to a known initial CTAB concentration of 100 mM. 5 mL aliquots were pelleted by centrifugation at 10,000 RPM (6,800 rcf) for 60 minutes. 4.5 mL of the clear supernatants were decanted, and the pellets were resuspended with deionized (DI) water. The GNR solutions were pelleted again at 10,000 RPM (6,800 rcf) for 60 minutes, and the clear supernatants were decanted. For anionic polymer stabilization, the GNR pellets were resuspended with 4.5 mL of a solution containing 30 mg/mL poly(sodium 4-stryene-sulfonate) (PSS, Aldrich, #243051) and 1 mM NaCl. The GNR solution was incubated overnight at room temperature.

2.2.3 Thiol-terminated PEGylation (mPEG-SH)

GNR solutions were heated to 30°C to melt CTAB crystals which form at room temperature, providing a known initial CTAB concentration of 100 mM. 5 mL aliquots were pelleted by centrifugation at 10,000 RPM (6,800 rcf) for 60 minutes. 4.5 mL of the

clear supernatants were decanted, and the pellets were resuspended with water. The GNR solutions were pelleted again at 10,000 RPM (6,800 rcf) for 60 minutes, and the clear supernatants were decanted. For PEGylation, the GNR pellets were resuspended with 4.5 mL of a solution containing 200 μM K_2CO_3 and 10 μM methoxy (polyethylene glycol)-thiol ($mPEG_{(5000)}$-SH) (Nektar Therapeutics, #2M4E0H01) in DI water. The GNR solution was incubated overnight at room temperature.

2.2.4 Chloroform Extraction

To study the dependence of the effect of GNR stabilization with CTAB concentration, a chloroform extraction of CTAB was performed. CTAB was extracted from the 10 mL nanorod solution using a separatory funnel and 100 mL of chloroform. The mixture was vigorously shaken and allowed to separate overnight, while the aqueous nanorod solution was extracted and 500 μL aliquots were placed in the test tubes. To theses test tubes, increased chloroform aliquots were added from 0, 50, 100, 150, 200, 250, and 300 μL. After vigorous mixing, the samples were allowed to separate overnight, the following day the solutions were removed and analyzed.

2.2.5 GNR Optical Data

Subsequent rounds of centrifugation at 10,000 RPM (6,800 rcf) for 60 minutes, greater than 95% decantation, and resuspension with DI water were carried out on the CTAB stabilized nanorods (CTAB-GNR), PSS stabilized nanorods (PSS-GNR), and PEGylated nanorods (mPEG-GNR). At each round, the supernatant was replaced by DI water in such a way as to reduce the CTAB concentration by a factor of 10. The extinction spectra were recorded at each stage, and the LSPR peak wavelength, peak width, and peak height were recorded and plotted.

2.2.6 GNR mass spectrometry

The MALDI-TOF mass spectrum was taken on a Brunker MS Reflex IV MALDI-TOF. DCTB (*trans*-2-[3-(4-*tert*-Butylphenyl)-2-methyl-2-propenylidene] malononitrile) was used as the matrix, solvents were removed by lyophilization using a SpeedVac.

2.3 Results and Discussions

2.3.1 PEGylation –vs.- Polyelectrolyte Stabilization

To characterize the critical CTAB concentration, the LSPR spectrum of the GNR solutions was monitored by sedimentation. In order to determine the critical CTAB concentration that was needed for GNR stability, GNR solutions were heated to melt the CTAB crystals, which provided a well-defined initial concentration of 100 mM. Subsequent rounds of sedimentation by centrifugation, 90% decantation, and resuspension with DI water were carried out on CTAB stabilized nanorods (CTAB-GNR), PSS stabilized nanorods (PSS-GNR), and $mPEG_{(5000)}$-SH stabilized GNR (mPEG-GNR). At each round, the supernatant was replaced by DI water in such a way as to reduce the CTAB concentration by a factor of 10, leading to a negligible quantity of CTAB that is bound to the GNR surface compared to the initial CTAB concentration.[60] The extinction spectra were recorded at each stage, and the LSPR peak wavelength, peak width, and peak height were recorded and are plotted in Figure 2-1.

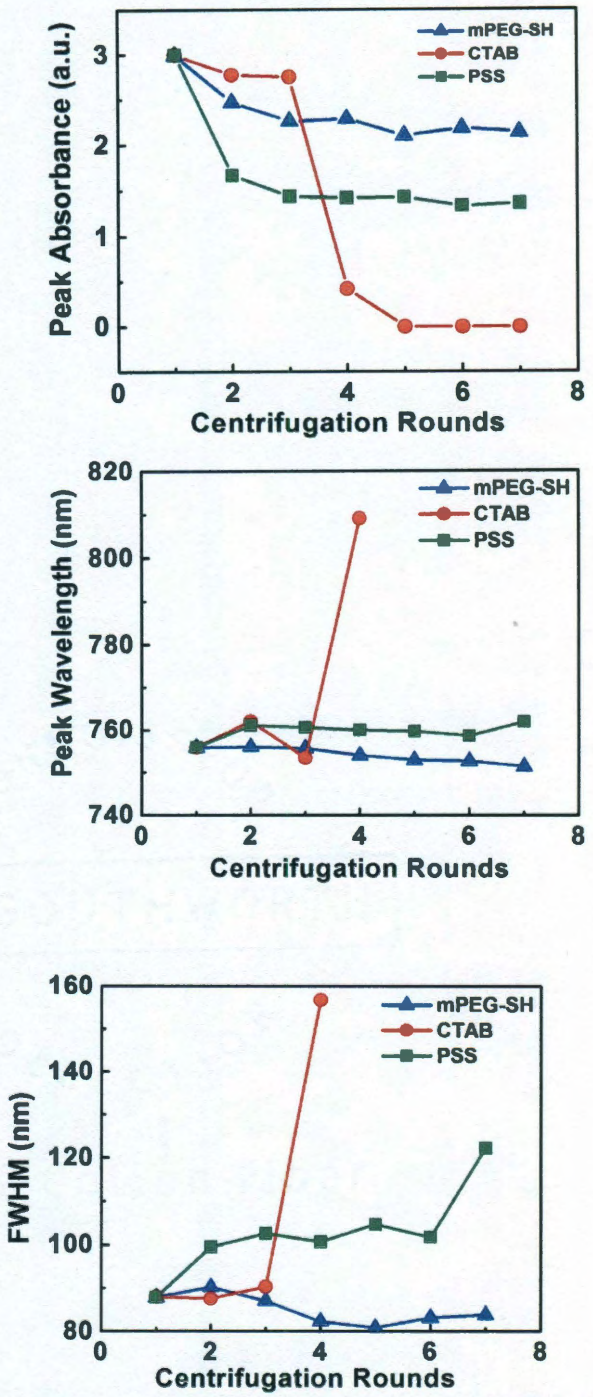

Figure 2-1. The evolution of the plasmon resonant peak of nanorod solutions after reduction of the CTAB concentration by sedimentation. The absorbance peak height (top), peak wavelength (middle), and peak width (bottom) for CTAB-GNR (λ), anionic PSS-GNR (ν), and $mPEG_{(5000)}$-GNR (σ).

LSPR peak height reduction, broadening, and red shifting were observed around the third round of sedimentation, which suggested GNR aggregation. This aggregation was noted during the third round of centrifugation, which is when the CTAB concentration is around 1 to 0.1 mM. Both polyelectrolyte PSS and $mPEG_{(5000)}$-SH stabilized the GNR against lower CTAB concentrations. The $mPEG_{(5000)}$-SH, however, evidenced reduced aggregation when compared to PSS polyelectrolyte. PSS is a strong polyanion polyelectrolyte that is thought to wrap the cationic CTAB bilayer and stabilize the nanorods by electrostatic interparticle repulsions.[27-47] PSS polyelectrolyte electrosteric stabilization requires the adsorption of charged polyelectrolyte that wraps the CTAB, yielding both electrical double layer repulsive forces and a steric barrier.[45-46] Since PSS is more strongly bound than CTAB, it does not require a bulk concentration of PSS in solution, which is required for CTAB. The PSS yield for stabilization was only about 50% based on the height of the LSPR absorbance peak (from 3 to 1.5). It resulted in a small red shift, but significant increase in peak width indicates some level of GNR aggregation.

The $mPEG_{(5000)}$-SH also stabilized the GNR, through the covalent attachment of polymeric chains around the particles forming a sterically protective layer.[47] Rather than wrapping, the $mPEG_{(5000)}$-SH displaces the CTAB layer to directly form a covalently bound gold-thiol polymer film on the GNR surface.[46-48] Once PEGylated, the GNR surfaces do not come into contact due to simple steric interference. The less dense packing stemming from the binding of the thiol-PEG polymer chains provides a steric barrier which offsets interparticle GNR interactions. This is distinct from the role of PEGylation in stabilizing nanoparticles and drugs in vivo, where it shields the PEGylated

object from the immune system. PEGylation is superior to polyelectrolyte wrapping based on **Figure 2-1**. The yield remains above 67%, and the red shift and peak broadening are negligible indicating no significant GNR aggregation. In addition, the covalent GNR stabilization by $mPEG_{(5000)}$-SH will be stable over a wider range of pH conditions than electrostatically CTAB stabilized GNR or PSS-GNR. Further evidence of the improved monodispersity of PEG stabilized nanoparticles can be seen by comparing films produced with $mPEG_{(5000)}$-SH nanoparticles versus those produced with polyelectrolyte-stabilized particles.[30-31]

2.3.2 GNR stability against sedimentation

Below a 100 μM CTAB concentration, the GNR begin to experience significant aggregation. This value is, however, much larger than that required to coat the nanorod surfaces. The GNR surface area is:

$$area = \pi d l + 2\pi (d/2)^2 \qquad \textbf{(Equation 2-1)}$$

neglecting the spherical shape of the end caps.[83] For a typical nanorod of 15 nm diameter and 50 nm length, the area is 2708 nm^2. Given a typical CTAB headgroup area of 0.3 nm^2, and the fact that the CTAB is thought to form a bilayer, one would expect approximately 9000 CTAB molecules per nanorod. Given that the GNR concentration is approximately 0.2 nM, the effective concentration of the CTAB that actually covers the nanorods is only 1.8 μM. Since that is much smaller than the required solution concentration, it is clear that there is significant exchange between the CTAB molecules on the nanorod and those in solution. Also, the critical concentration for nanorod

stability, 100 μM, is near typical values of the critical micelle concentration for charged surfactants.

2.3.3 GNR stability against dilution

In addition to sedimentation, the GNR stability against water dilution was tested. The CTAB concentration was reduced by slow dilution with DI water directly in a cuvette. The spectra were monitored during dilution, and the peak wavelength, height, and width results are shown in **Figure 2-2**. One can see that there is no sign of aggregation even to a CTAB concentration of 50 μM, which apparently contradicts the results of **Figure 2-1**. This contradiction can be explained if one considers that it is not the absolute CTAB concentration that is important, but the ratio between the CTAB and GNR concentrations. When diluting the GNR and CTAB solutions with water, the peak height underwent a linear decrease due to dilution of the nanorods. We observed no significant peak wavelength shift and no peak broadening, so the nanorods did not aggregate. The lack of aggregation to 50 μM suggests that it is the ratio of CTAB to GNR concentration that critically determines stability, rather than the CTAB concentration alone. However there are various thermally induced effects that can often interfere with the optical response of GNRs. These include heating of the CTAB and water molecules that surround the GNRs, which often results in their thermal activation and subsequent migration away from the GNR surface. Such thermal effects can interfere with the GNR optical signals often producing changes to the refractive index, and shifts to the LSPR bands.

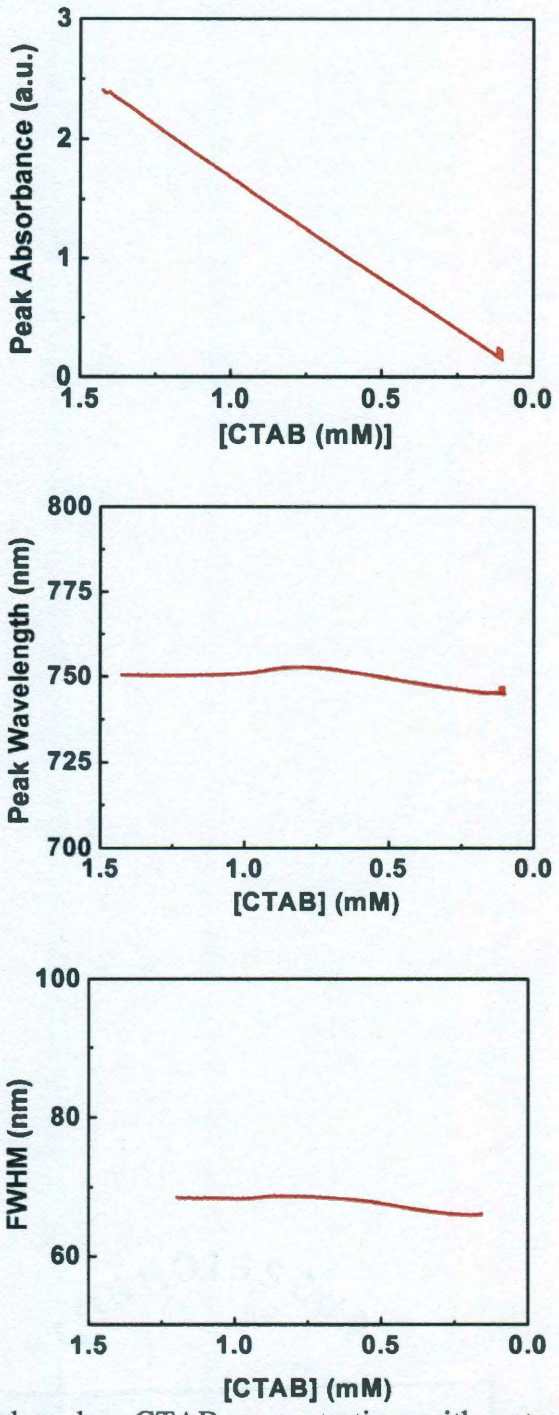

Figure 2-2. Aggregation based on CTAB concentration, with water dilution the CTAB concentration drops, but no aggregation is evidenced, this suggests that CTAB/particle loading ratios determine aggregation behavior.

2.3.4 GNR stability against extraction

Sedimentation is not effective as a means to adjust the CTAB/GNR concentration ratio. Upon sedimentation, the nanorods form a pellet that spikes the GNR concentration before the pellet is diluted. To more controllably alter the CTAB/GNR concentration ratio, we extracted the CTAB with chloroform. Since the nanorods remain in the aqueous phase, the CTAB/GNR ratio is gently lowered as the CTAB concentration lowers. The results of the chloroform extraction are shown in **Figure 2-3.** Note that the GNR aggregate suddenly as the CTAB concentration in reduced by the addition of increasing

chloroform volume.

Figure 2-3. A photograph of 500 μL nanorod solutions that were extracted with the stated volume of chloroform.

To quantitatively determine the critical CTAB/GNR concentration ratio for GNR stability, the distribution ratio of CTAB between water and chloroform was measured to be approximately 4. The experiment was repeated and the chloroform volume was carefully adjusted to find the exact concentration at which the GNR aggregate. **Figure 2-4** displays LSPR spectra of a GNR solution at two CTAB concentrations adjusted by chloroform extraction.

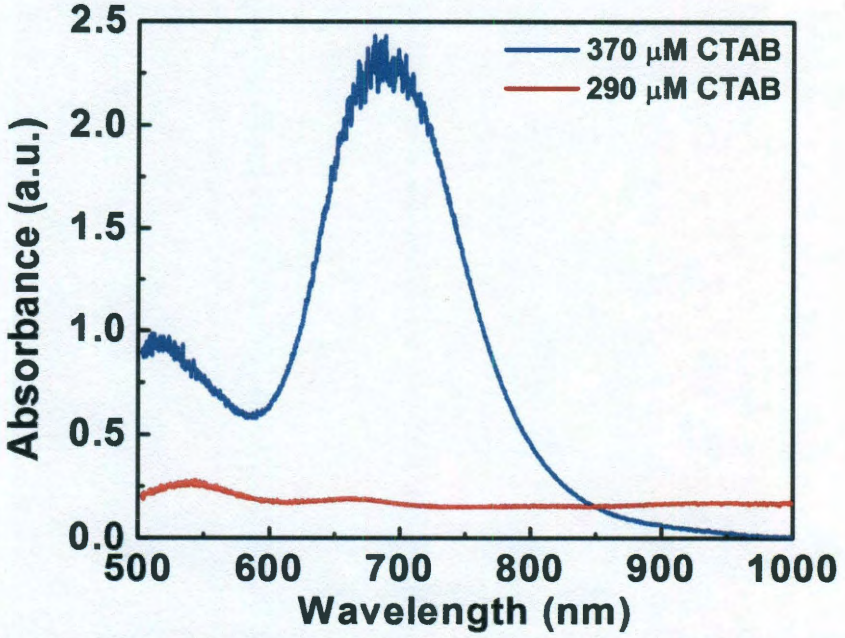

Figure 2-4. The LSPR extinction spectra of nanorod solutions at two CTAB concentrations achieved by chloroform extraction. The nanorod concentration was 0.5 nM.

With this precise critical CTAB concentration, the critical CTAB/GNR concentration ratio can be calculated. Since the GNR concentration was at 0.5 nM, when the CTAB concentration was 370 μM the ratio of CTAB/GNR was 740,000, and when the CTAB concentration was 290 μM, the ratio of CTAB/GNR was 580,000. So, according to the spectra in **Figure 2-4**, aggregation occurs rapidly at a critical CTAB/GNR ratio of 740,000. This large ratio further confirms that the CTAB concentration required for stabilization is much greater than that required to simply cover the GNR, and that the [CTAB]/[GNR] ratio is critical for GNR stability due to the dynamic interactions between CTAB in solution and the bilayer.

As shown above, the exact CTAB concentration that is needed for GNR stability will depend on many parameters that are not usually well controlled, these include the

GNR concentration and initial CTAB concentrations that vary with particle surface area. These results highlight the widely varying reports regarding the amount of CTAB required to stabilize gold nanorods. Therefore, the CTAB must be in a dynamic equilibrium between the GNR surface, and bulk CTAB micelle solution. Furthermore, the CTAB concentration is not usually reduced in a controlled manner since a certain amount of CTAB is needed for each GNR, thus requiring a certain CTAB/GNR ratio of adsorbed CTAB at the GNR particle, to offset the van der Waals. This is consistent with colloidal stability, which requires stabilization agents that provide a repulsive barrier to offset the van der Waals forces at the particle surface, which lead to the nanoparticle aggregation tendencies.

2.3.5 Mass Spec and trace CTAB

We also studied residual CTAB in the PEGylated GNR samples by mass spectrometry (MS), which showed that even after PEGylation and extensive washing/decants, some residual CTAB remains bound to the GNR surface. This is shown in the mass spectras below, **Figure 2-5** and **Figure 2-6**, where even after 10 decants a residual $[CTAB\text{-}Br]^+$ ion peak is evident at m/z, 284.53), in the lyophilized solutions followed by an Au^- peak at m/z, 197.976. Note that the GNR solutions had to be lyophilized as the CTAB was not seen in the liquid solutions. This suggested that the CTAB-gold interaction is quite strong, that even long PEG incubations and extensive rinsing- over 10 cycles of decants, will not entirely remove the adsorbed CTAB. CTAB-metal surface adsorption can often be weak and completely reversible in metals other than gold. Quartz Crystal Microbalance (QCM) studies have shown that the CTAB-gold

adsorption is partially irreversible, except upon acid exposure, as this alters the surfactant-gold electrostatics.[50]

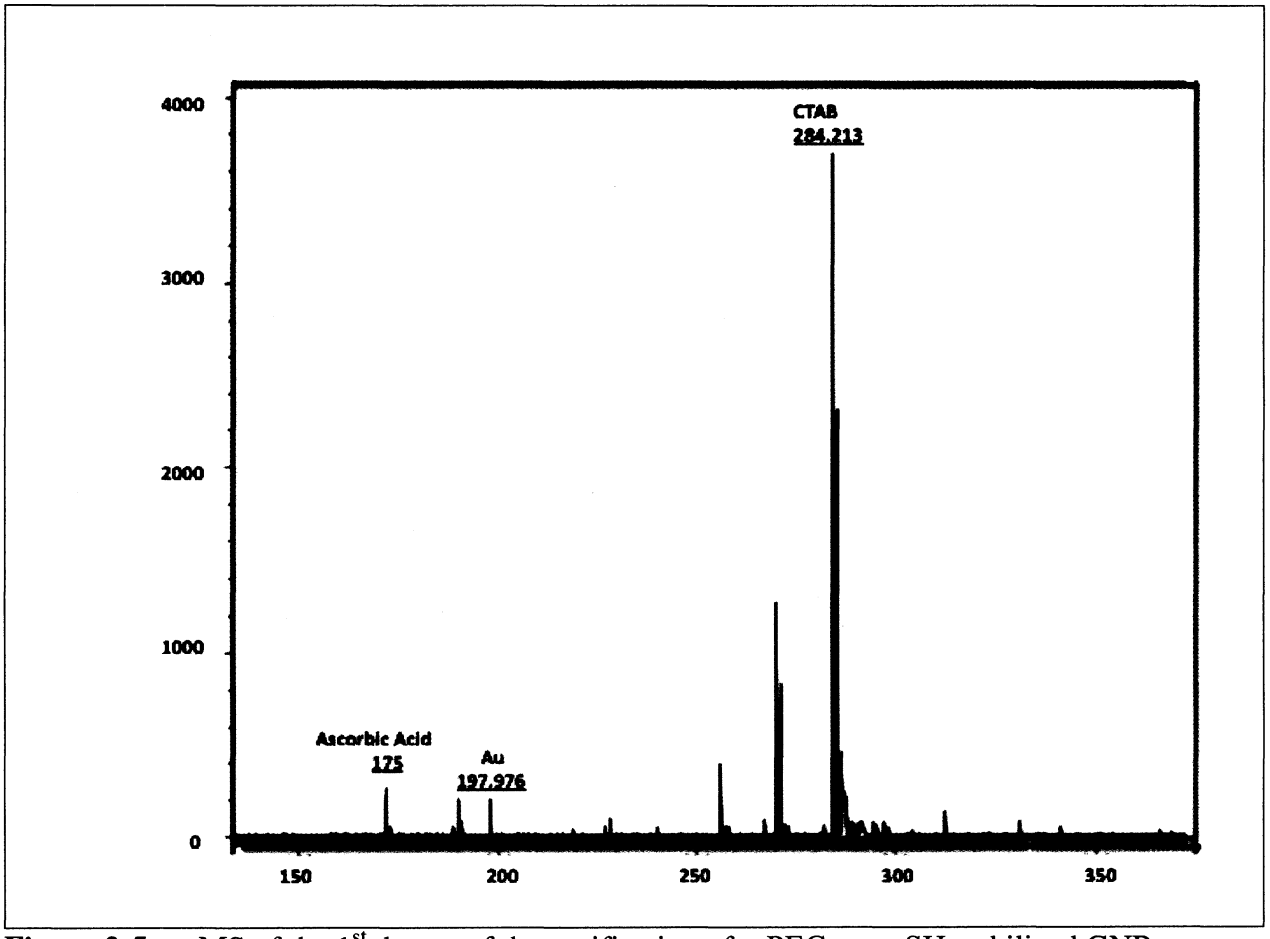

Figure 2-5. MS of the 1st decant of the purification of mPEG $_{(5000)}$-SH stabilized GNR with [CTAB-Br]+ ion (m/z, 284.213), Au- (m/z, ~197.976), and Ascorbic acid (m/z, ~175), note that PEG is not shown due to the higher molecular weight of the PEG polymer chains.

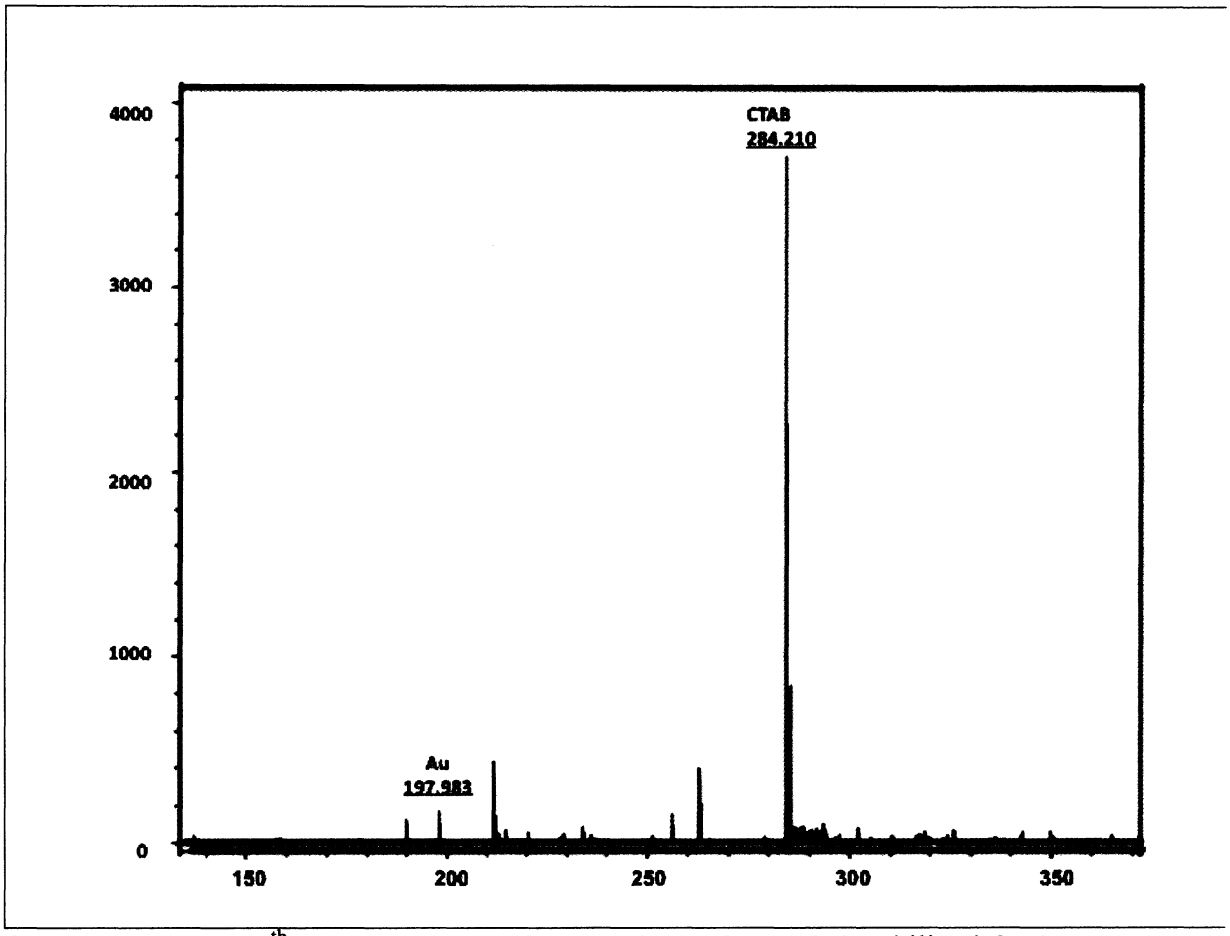

Figure 2-6. MS of the 10th decant of the purifcation of $mPEG_{(5000)}$-SH stabilized GNR with $[CTAB\text{-}Br]^+$ ion (m/z, 284.10) and Au- (m/z, ~197.983), with no Ascorbic acid noted.

This suggests that the residual CTAB was trapped within the PEG surface of the GNR, and would still be present despite the number of decants and PEG displacement.[24] This is why future studies of the CTAB displacement during the $mPEG_{(5000)}$-SH functionalization and surface chemistry modification of the GNR are needed.[24] However, it should be noted that the remaining trace CTAB is likely trapped within the t-PEG layer of the GNR, and is at a sufficiently low concentration (below 10 μM), which is not cytotoxic to cells. In our targeting experiments described in chapters 3 and 4 we have not observed any cytotoxic effects associated with PEGylated nanorods that were prepared by this method.

2.3.6 GNR Stabilization Discussion

The CTAB surfactant, which is needed for GNR synthesis is also needed to maintain the colloidal stability of the GNR. The CTAB concentration at which this stability is lost has not been well characterized, and stems from a number of factors. Since sedimentation, decantation, and resuspension of GNR into pellets is often used to reduce the CTAB concentration, lack of analytical techniques in these procedures can lead to unknown initial CTAB concentrations. Further, GNR synthesis is carried out in 100 mM CTAB, which is above the saturation concentration at room temperature. This causes the crystallization of the CTAB upon storage, leading to unknown concentrations of the surfactant being drawn up from the bulk solution phase. Finally, micellization and association of CTAB with gold and silver ions in solution can complicate the analysis, i.e. spectroscopic characterization, of the CTAB concentrations. However, below 1 mM, CTAB can stabilize the GNR solutions, and this is often perplexing, as decreased surfactant concentrations are notable at causing aggregation. Furthermore, the GNR

stability has shown to fail at a critical value, since it is the ratio of the CTAB/GNR concentration that determines stability, rather than the CTAB alone. This means that for a known concentration of a GNR sample, a certain CTAB concentration will be needed, since it is the CTAB/GNR ratio which ultimately determines the samples stability. The surface area parameters of the GNR are also relevant, as this is what ultimately determines the degree of CTAB bilayer formation that is needed to coat the GNR surface. This implies that the critical CTAB concentration for a given sample really is determined by the GNR size parameters. Such factors can lead to a variability in defining the critical CTAB concentration per GNR sample, which often complicates the reproducibility of the stabilization and bioconjugation methods.

A thiol-PEG strategy was then compared to PSS stabilization methods. The GNR were stabilized using $mPEG_{(5000)}$-SH functionalization, as this can be used to effectively displace the CTAB bilayers. This allows the CTAB to be reduced to an arbitrarily low concentration suggesting that the PEG is responsible for maintaining GNR stability.[30] PSS stabilization was likewise able to stabilize the GNR as the anionic polymer is attracted to the CTAB bilayers, this occurs due to wrapping of the CTAB and the formation of multiple polyelectrolyte layers around the CTAB layers.[31] Stabilization comparison of CTAB-gold nanorods shows significant aggregation following only two rounds of centrifugation. $mPEG_{(5000)}$-GNR stabilization shows significantly higher yields, and narrower LSPR linewidths when compared to electrosteric polyelectrolyte stabilization methods and CTAB stabilization. Microscopic characterizations of GNR substrates also suggest that PEGylated GNR solutions yield more monodisperse GNR

substrates when compared to aggregated polyelectrolyte wrapped GNR glass substrates.[30-31]

2.4 Conclusion

$mPEG_{(5000)}$-SH functionalization can displace the CTAB while polyelectrolytes can wrap the CTAB present on the surface of the GNR. Chloroform extractions of CTAB showed that a critical CTAB/GNR ratio is needed in order to maintain colloidal stability of the GNR, this was found to be 740,000:1. Yet in spite of $mPEG_{(5000)}$-SH covalent functionalization methods, some residual CTAB remains bound to the particles, as shown by the MS data. Nevertheless at these CTAB concentrations, which are below 10 μM, cell cytotoxic effects are typically absent. Both the $mPEG_{(5000)}$-SH and PSS stabilization methods were effective methods by which to stabilize the GNR. However, the $mPEG_{(5000)}$-SH covalent functionalization method leads to higher yields and more monodisperse GNR samples.

CHAPTER 3

Gold Nanorod Bioconjugation

The physical and chemical nature, surface charge, and nanoparticle size of the GNR often makes it difficult to predict their uptake and delivery into cells, tissues, and organisms, and is therefore an area that is currently under serious scientific investigation.[16-17,25,27,30,55-63] A way by which to overcome such problems is to couple proteins such as antibodies with a heterobifunctional PEG linker, such as α-thio-ω-carboxy poly(ethylene glycol) which we term t-PEG-c. The t-PEG-c linker allows for covalent conjugation strategies to antibodies using zero length carbodiimide chemistries. The 1-ethyl-[3-dimethylaminopropyl]carbodiimide (EDC) chemistry allows for a hydrophobic C=O from acylisourea to be stabilized with N-hydroxysuccinimde (NHS). This stable NHS can then form an amide bond with the antibody, which can then facilitate a drug's hydrophobic loading onto the amphiphilic PEG. In this study t-PEG-c conjugation strategies were employed to stabilize GNR followed by subsequent activation with a stabilized EDC carbodiimide linking agent, and conjugation with antibodies ranging from Immunoglobulin G (IgG), Human Epidermal growth factor Receptor 2 (Her2), and Cetuximab (C225), for in vitro cancer cell targeting. Conjugates with biomolecular targeting ligands of monoclonal antibodies were then used for in vivo tumor targeting strategies, and as therapeutic anti-cancer agents. Confocal, two-photon luminescence (TPL), and dark scattering microscopy methods coupled with fluorescence,

zeta potential, and Nanoparticle Enzyme-linked immunosorbent assay (ELISA) were used to monitor changes to the conjugated GNR surface.

3.1 Methods

3.1.1 t-GNR-PEG-c Conjugation

Corning® 15mL clear polyethylene terephthalate (PET) centrifuge tubes with maximum RCF of 3,600 x g were initially rinsed out with 50 mM Borate Buffer pH 8.6 (Pierce #28384) in DI water. A 15-minute incubation in 50 mM Borate Buffer pH 8.6 was followed by homogenization of the buffer using a Vortex genie for 5 minutes. Buffer rinse or use of antistatic devices is highly recommended as this can offset any residual static charge that naturally builds up on the PET vial surface. Extra care should also be taken to avoid rubbing the vial to the packaging when removing the vial from its plastic bag, as this is known to increase static charge that occurs due to low air humidity. Reduction of static charge will help decrease the aberrant GNR particle binding to plastic walls which can be a major factor in the aggregation of GNR at low CTAB concentrations.

CTAB-GNR stock solutions were heated to 30°C to melt CTAB crystals which form at room temperature, and therefore provided a known initial CTAB concentration of 100 mM. 5 mL aliquots of CTAB-GNR were pelleted by centrifugation at 10,000 RPM (6,800 rcf) for 60 minutes. 4.5 mL of the clear supernatants were decanted to greater than 95%, and the GNR pellets were resuspended with DI water. The GNR solutions were pelleted again at 10,000 RPM (6,800 rcf) for 60 minutes, and the clear supernatants

were decanted to greater than 95% and resuspended in 50 mM Borate buffer pH 8.6, leading to a 1 mM CTAB concentration. For t-PEG-c functionalization, the GNR pellets were resuspended with 4.5 mL of 50 mM Borate buffer pH 8.6, to which was added 200 mM of the t-PEG-c linker (Iris Biotech, #HOOCPEG-SH) in DI water, and incubated overnight at room temperature, with the vials being wrapped in aluminum foil. The yield of the t-GNR-PEG-c conjugates could be increased with a 5 day overnight incubation, foil wrapping of the outer walls of the PET tubes, and inclusion of 50 mM Borate buffer at pH 8.6, as this environment helps to offset thiol-thiol formation. Sedimentation at 10,000 RPM (6,800 rcf) for 60 minutes, and greater than 95% decantation of the supernatant and resuspension into 100 mM MES buffer pH 6.1 (Sigma #M-0164) in DI water, helped to further increase conjugate yield. The 9 round centrifugation, and greater than 95% decantation, and resuspension into MES buffer pH 6.1, needed to include a gentle decantation-resuspension for decants 1-3. This initial gentle decantation was needed as residual hydrophobic groups from the CTAB hydrocarbon chains become exposed due to changes to its micellization. The CTAB hydrophobicity can in turn modulate the hydrophobic nature of the PET vial walls, causing some of the GNR to bind onto the wall of the container leading to a reddish film. However, the inclusion of the hydrophilic COOH end groups from the t-PEG-c linker and inclusion of 100 mM MES buffer at pH 6.1 help offset the GNR particle binding onto the walls of the container by promoting PET hydrophilicity. t-GNR-PEG-c conjugates were concentrated in 100 mM MES buffer at pH 6.1 to OD~10 at the LSPR peak wavelength .

3.1.2 Antibody Bioconjugation

In order to perform the antibody conjugation a 5 mL aliquot of t-GNR-PEG-c with an OD~10 at the LSPR peak wavelength, that was stabilized by the heterobifunctional linker t-PEG-c described above, was taken. The t-GNR-PEG-c were resuspended in 100 mM MES buffer (Sigma #M-0164) at pH of 6.1 and concentrated by sedimentation to a volume of 100 μL using an absorbance of greater than 10 at the LSPR peak wavelength. A solution containing 96 mg of 1-ethyl-[3-dimethylaminopropyl]carbodiimides (EDC, Sigma #1769), 29 mg of N-hydroxysuccinimde (NHS, Sigma, #1306762), and 10 mL of MES buffer pH 6.1 was prepared, and thoroughly mixed and 10 μL this solution was immediately added to the 100 μL t-GNR-PEG-c solution. This mixture was allowed to react for 15 minutes, at room temperature. Meanwhile 0.5 mL of 2-mercaptoethanol was diluted into 14.5 mL MES buffer pH 6.1, this being a 1:29 ratio, then 10 μL of the diluted mercaptoethanol solution was added into the nanorod solution following the 15 minute incubation. The mixture was allowed to react for 10 minutes, at room temperature, after which 400 μL of antibody solution at 2 mg/mL in 1X Phosphate buffered saline (PBS, Fisher #NC9826748) pH 7.1 was added.

The final 500 μL nanorod bioconjugate solution was incubated for 2 hours at room temperature. The nanorod bioconjugates were separated from excess reactants and byproducts by sedimentation at 10,000 RPM (6,800 rcf) for 10 minutes, and decantation of 95% of the supernatant without disturbing the pellet. The nanorod bioconjugates were then resuspended in 500 μL of 1X PBS pH 7.1, and used immediately, or stored for a short period at 4°C. As a means to confirm the changes to the surface chemistry of the

antibody conjugated GNR termed t-GNR-PEG-c-Ab, LSPR absorbance and zeta potentional measurements were obtained.

3.1.3 Zeta Potential

To confirm the altered GNR surface chemistry at various stages, zeta potential measurements were performed using a Malvern Zetasizer Nano. Zeta potential data of diluted samples in water and 1X PBS pH 7.1, 100 mM MES pH 6.1, and 50 mM Borate buffer pH 8.6, were tested using the Zetasizer Nano cuvettes (Malvern, #DTS1060) using a refractive index of 0.2 and absorption coefficient of 3.32. A control zeta of colloidal gold particles was obtained using similar conditions. The resulting data ranging from the original CTAB-GNR solution, t-GNR-PEG-c, and with the final bound conjugated antibody (t-GNR-PEG-c-Ab) were obtained.

3.1.4 Fluorimetry

Fluorimetry was used to determine the bound antibody to the GNR conjugates, therefore the conjugation procedure was followed with Fluorimetry using an Alexa Fluor 488 labeled rabbit Immunoglobulin G (AF-Ab, Invitrogen, #A11059). A buffer blank, control antibody-buffer solution of known concentration, and sample were analyzed in a Horiba Jobin-Yvon FluoroLog-3 fluorimeter with CW Xenon excitation. The AF-Ab-GNR (AF-Ab-GNR) bioconjugates were put through subsequent rounds of sedimentation using a 90% decant and resuspended in PBS. The free AF-Ab served as a standard curve to determine the concentration of the AF-Ab bound to the GNR. The calibration curve

was tabulated using the average number of bound peptides obtained by dividing the measured molar antibody concentration by the molar GNR concentration.

3.1.5 Nanoparticle ELISA

The GNR conjugated to mouse anti-human HER2 antibodies (NeoMarkers, #MS-301-PABX) were incubated with horseradish peroxidase (HRP)-labeled anti-mouse Immunoglobulin (IgG, Sigma, #A4416) for 1 hour. Nonspecific reaction sites were blocked with a 3% solution of Bovine Serum Albumin (BSA). t-GNR-PEG-c-Ab were rinsed twice by sedimentation and resuspended in 3% BSA to remove any unbound IgG. The HRP bound to the conjugates were then developed with 3,3',5,5'-tetramethylbenzidine dihydrochloride (Sigma, #T3405), and compared with HRP anti-mouse IgG standard curve by determining the absorbance at 450 nm with a spectrophotometer. The resulting number of active antibodies per GNR conjugates could be determined and these results could be further confirmed using fluorimetry.

3.1.6 Cell Culture & Imaging

The t-GNR-PEG-c-Ab conjugates with anti-HER2 antibodies were then incubated with two cell types, these being the HER2-overexpressing epithelial breast cancer cell line SK-BR-3 and the normal mammary epithelial cell line MCF10A (American Type Culture Collection). The SK-BR-3 cells were grown in McCoy's 5A medium supplemented with 10% fetal bovine serum (FBS) and 1% penicillin-streptomycin and maintained at 37°C in a 5% CO_2 atmosphere. The MCF10A cells were cultured in Mammary Epithelial Basal Medium (MEBM) supplemented with a BulletKit (Clonetics)

and maintained at 37°C in 5% CO_2. Both cell lines were prepared for the experiment by putting 6 x 10^5 cells in chambered cover slips and allowing them 30 minutes to attach to the surface. The cells were rinsed once with PBS, then incubated with nanorod conjugates for 1 hour in 5% CO_2 at 37°C. The LSPR peak absorbance of the nanorod conjugate solution was 1.5. Post the incubation, cells were rinsed 3x with 1xPBS and then the appropriate cell media was added prior to imaging. The cells were imaged by TPL microscopy at 50X with 780 nm illumination and 400-700 nm detection.[66]

KU7 cells were then grown in MEM medium supplemented with 10% FBS and 1% penicillin-streptomycin and maintained at 37°C in a 5% CO_2 atmosphere. The cell line was prepared by placing 4x10^5 cells on cover slips and allowing them to attach to the surface for 24 hours. Prior to treatment, the cell media was changed to OptiMEM and the GNR conjugates were added for 4 hours. Post the 4 hours, the OptiMEM media was changed to MEM medium supplemented with 10% serum and incubated in 5% CO_2 at 37°C atmosphere for another 20 hours. Twenty minutes prior to fixation, the cells were rinsed once with warm PBS, then incubated with 100 nM Alexa-488-wheat germ agglutinin (WGA) and left for 10 minutes in the cell incubator for WGA cellular internalization. After 10 minutes the cells were rinsed three times with warm PBS then fixed in 3.7 paraformaldehyde for 15 minutes then washed three times with cold PBS and mounted on slides using Slow-Fade Antifade (all reagents were purchased from Molecular Probes). Imaging was carried out using a Leica SP5RS AOBS confocal microscope using a 63x/1.4 objective. GNR were detected using 633 nm illumination in reflection mode, and WGA was excited at 488 nm.

3.2 Results and Discussion

3.2.1 GNR Bioconjugates

To form stable bioconjugates, a heterobifunctional PEG with thiol and carboxyl end groups was used, which is similar to the $mPEG_{(5000)}$-SH stabilization discussed in Chapter 3. The carboxy-terminated GNR were conjugated to antibodies using the zero-length crosslinker EDC that was stabilized by NHS.[55] Standard procedures for EDC protein crosslinking were followed with modifications to the unique carboxyl end group chemistry.[56] Here the NHS and EDC groups are reacted in order to mediate the formation of an amide bond between amino and carboxylic groups. The highly reactive O-acylisourea intermediate allows nucleophilic substitution with an antibodies' primary amino group, thereby increasing the low efficiency of the carbodiimide-catalyzed reaction, this conjugation strategy is shown in Figure 3.1.[56]

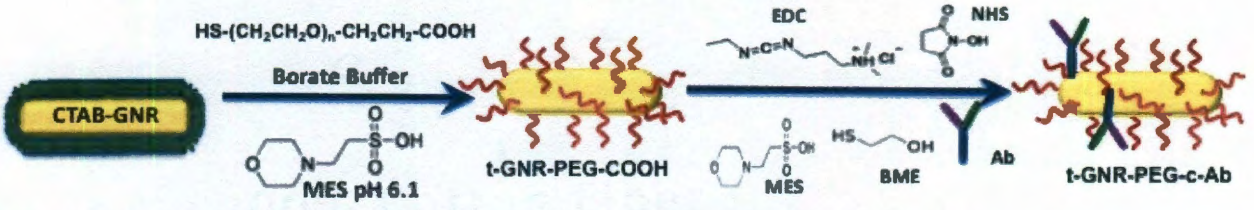

Figure 3-1. Schematic representation of the NHS-EDC-antibody chemistry, with the GNR being 15 x 50 nm, and PEG chain makes a 5 nm above the GNR.

Since the GNR do not contain amine groups, there is no aggregation issues stemming from amide bond formation between the rods, this helps to minimize the criticality for the initial EDC exposure. To avoid buffer exchange or sedimentation methods, the change in pH from 6.1 to activation at 7.1 for conjugation was achieved by diluting the GNR into a larger volume of antibody solution. Excess reactants and products were then removed from the bioconjugate solution by sedimentation and LSPR

spectra was used to monitor changes to aggregation, this is shown in **Figure 3-2.** Antibody binding to the t-GNR-PEG-c conjugates leads to an altered refractive index, and dielectric constant around the surface of the nanoparticles due to the antibody layers. This would then cause the slightly red-shifted spectra, which serves to identify that the antibody has been bound to the gold nanoparticle, this is evidenced in the LSPR spectra.[70] The t-GNR-PEG-c-Ab conjugates were then checked for antibody aggregation through the peak wavelength and full width height max (FWHM) of the LSPR spectra. Any t-GNR-PEG-c-Ab aggregates were removed by pelleting-decantation-resuspension, and changes to the LSPR optical spectra showed their aggregation tendencies throughout the procedure, note that such aggregates decreased the overall product yield.

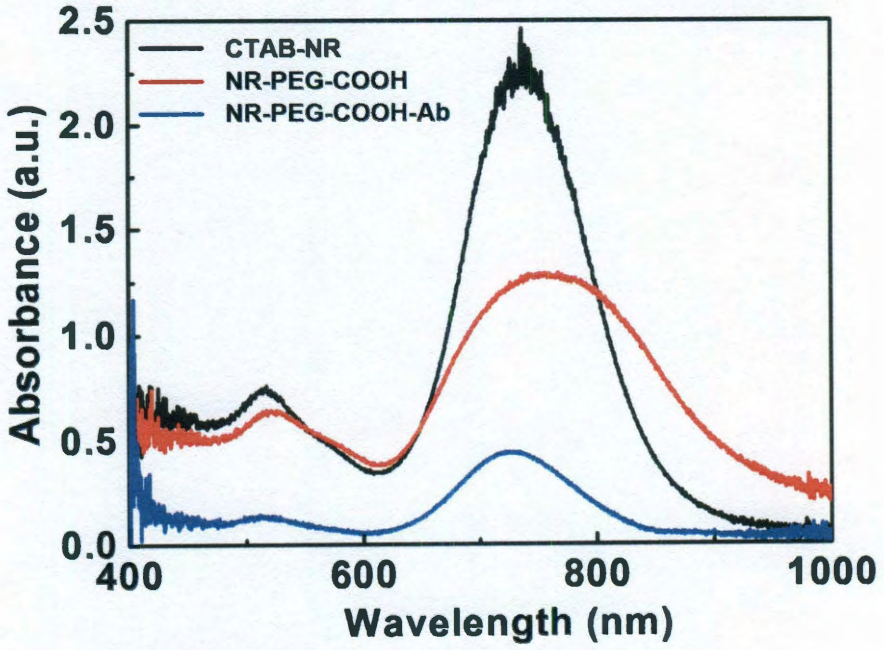

Figure 3-2. Spectra of the resulting GNR bioconjugates.

3.2.2 GNR Charge

As particle charges are relevant for binding and aggregation purposes, the particle charge was measured with zeta potential, this is shown in **Table 3-1**. Zeta potential measures the effective surface potential at the hydrodynamic shear plane that is close to the solid-liquid interface, as this is the parameter that governs the electrokinetic behavior of particles in solution, which determines their electrophoretic mobility with an applied electric field. The ensuing electrostatic repulsion between particles is what dictates, their charge, and ensuing particle attraction and binding to substrates.[67] Zeta potential measurements confirmed that the GNR-CTAB initial charge of +83 mV was altered to -19 mV for the carboxyl conjugated rods, to -6 mV for the antibody bound bioconjugates. This change is consistent with the cationic, anionic, and zwitterionic surface charges, associated with the three states of the bioconjugated GNR. This particle charge would be significant for the targeted binding of the cell since all cells contain an outermost negative zone composed of negatively charged glycolipid and glycoproteins which makes each cell act as a negatively charged body, this charge influences other nearby charged bodies/cells.[68] In effect, a negative or slightly negative charge in the antibody conjugated nanoparticles would be needed for successful in vitro receptor binding, and this negative charge was evidenced in the zeta potential data taken from the nanorod bioconjugates.

Nanoparticle	Zeta Potential (mV)
NR-CTAB	+83
NR-S-PEG-COOH	-19
NR-S-PEG-Ab	-6

Table 3-1. Zeta potential measurements confirm surface chemistry modification.

3.2.3 GNR Bioconjugate Fluorimetry

To characterize the final bioconjugates, the t-GNR-PEG-c were conjugated to AF-Ab for fluorimetric analysis. The GNR bioconjugates were put through successive rounds of sedimentation, 90% decantation and resuspension in buffer to dilute the unbound AF-Ab by factors of 10. Fluorimetry of unbound AF-Ab in the decants is shown in **Figure 3-3**, and served to make the standard titration curve. Background fluorescence noise was evident by the 4th round, which is when the AF-Ab concentration is at 0.1 nM. Fluorimetry of the t-GNR-PEG-c-Ab bioconjugates indicated that the nanorod bound AF-Ab concentration was 1 nM, this yields approximately two antibodies per GNR, given a concentration of 0.5 nM from the LSPR extinction peak.[73]

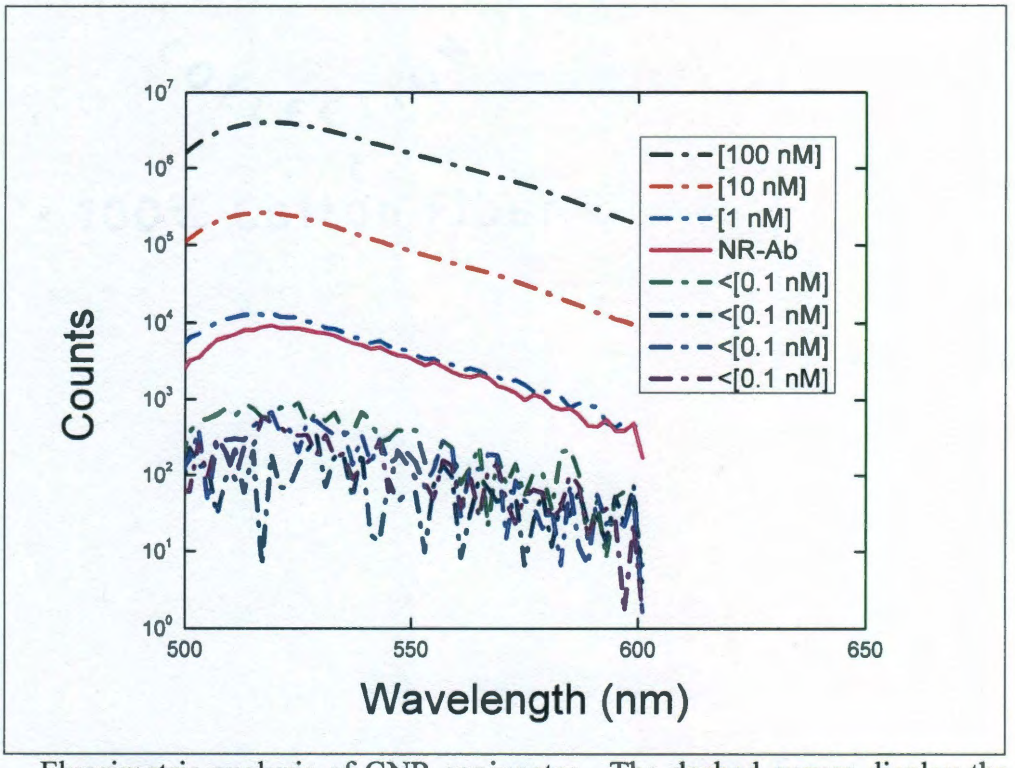

Figure 3-3. Fluorimetric analysis of GNR conjugates. The dashed curves display the signal from free labeled antibodies in solution at the stated concentrations. The solid curve displays the signal from nanorod conjugates.

3.2.4 Antibody Conjugation Yield

An ELISA antibody test was performed in order to tabulate the number of active antibodies per t-PEG-c-GNR-Ab bioconjugates.[84] The Nanoparticle ELISA method used, is similar to the traditional ELISA except that the immunosorbent surface is that of the nanoparticles in solution. The nanoparticle ELISA indicated that there were 2.28 +/- 0.05 antibodies per nanorod, which agrees with the fluorimetry results. A control ELISA of GNR prepared with mPEG-SH and no capture antibodies yielded 0.68 +/- 0.2 antibodies per nanorod. This latter result possibly stemmed from an artifact due to the label antibody chemisorbing to the GNR surface or antibody adsorption, however the control targeting showed to be insignificant.

3.2.5 Nanorod Targeting

The resulting GNR bioconjugation scheme was tested in vitro using two cancer cell lines and respective cancer antibodies. t-GNR-PEG-c were conjugated to Anti-HER2 and also to rabbit IgG as a control. Each GNR bioconjugate was incubated with the HER2-overexpressing epithelial breast cancer cell line SK-BR-3 and the normal mammary epithelial cell line MCF10A (American Type Culture Collection) for 30 minutes under identical conditions. The respective cells were washed and immediately imaged using TPL, which highlighted the presence of the GNR, as well as phase contrast which evidenced the respective cell locations, this is shown in **Figure 3-4.** The TPL was conducted at 0.1 mW, 780 nm illumination with detection at 400-700 nm, using a 50X objective, with a scanning area of 60 μm x 60 μm, and a total irradiation time of 1.05 seconds per scan. The TPL image showed the resulting GNR-anti-HER2 targeting

results, with red being indicative of a significant level of GNR binding to cells that only occurred for the specific antibody-cancer cell combination. **Figure 3-5** shows dark-field images of targeted GNR and control cells from the same sample, and evidenced that the GNR were not visible. To test the antibody targeted t-GNR-PEG-c-Ab conjugate visibility under dark field microscopy, isolated GNR were deposited on glass substrates near alignment marks and compared to easily visible spherical gold nanoparticles, this is shown in **Figure 3-6**. Here images of a single GNR and single gold nanosphere were taken under dark field microscopy using a high sensitivity black and color charge-coupled device (CCD) cameras, and AFM imaging which was performed on the same area. The GNR was not detectable using either the high-sensitivity monochromatic or color CCD cameras. In vitro GNR imaging of GNR bioconjugates of C225 and human IgG control were tested in the KU7 bladder cancer cell line by confocal reflectance, this is shown in **Figure 3-7**. The t-GNR-PEG-c-Ab bioconjugates were imaged by confocal reflectance at 633 nm. The cells were visualized with a WGA fluorescence label, yielding the cell location in green, and bound GNR by confocal reflectance in red. t-GNR-PEG-c-Ab bioconjugate binding is only observed for the specific C225 conjugates and the KU7 cells and not the control IgG, as noted in **Figure 3-7**.

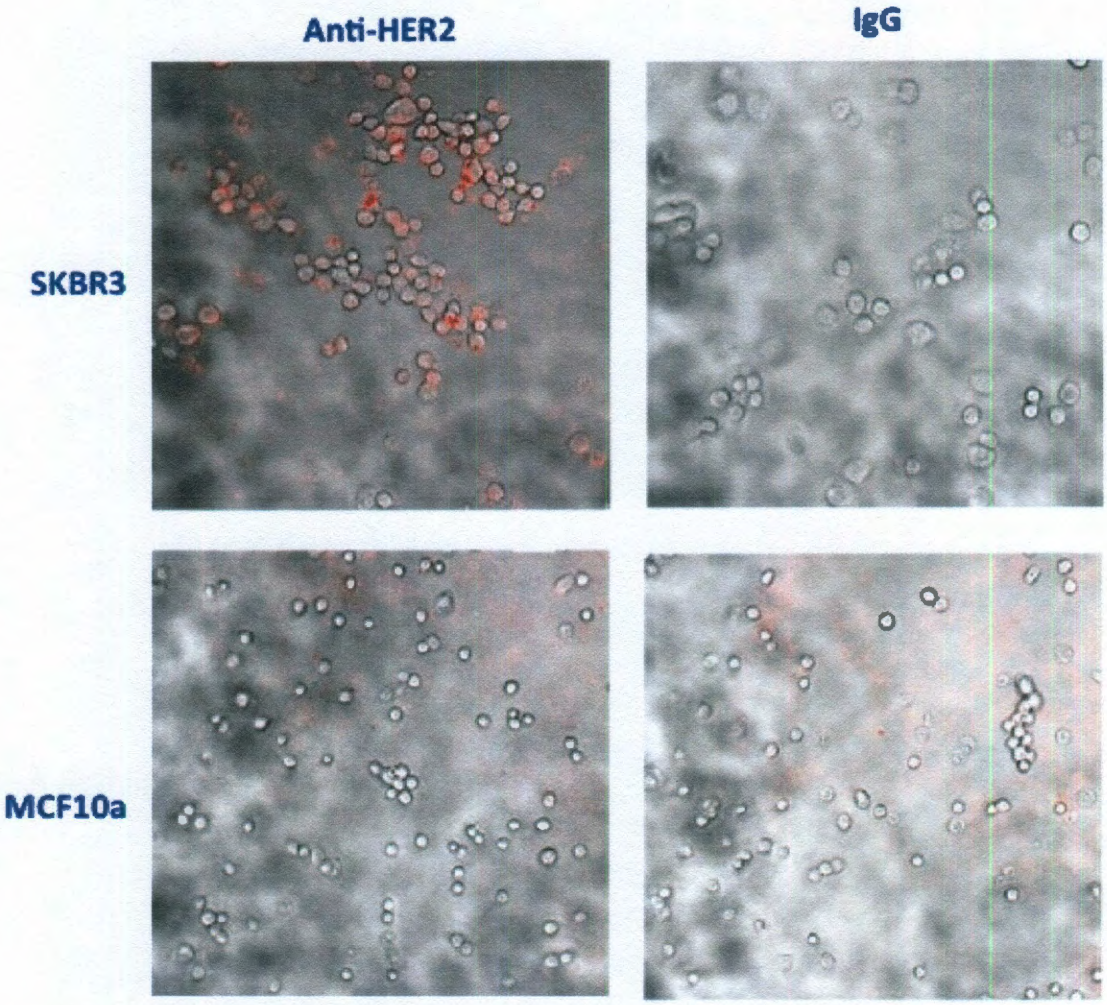

Figure 3-4. GNR conjugate targeting. Phase contrast shows the cell locations in grayscale, and TPL is displayed in red. Binding was only observed for the Anti-HER2 conjugates and SKBR3 cells.

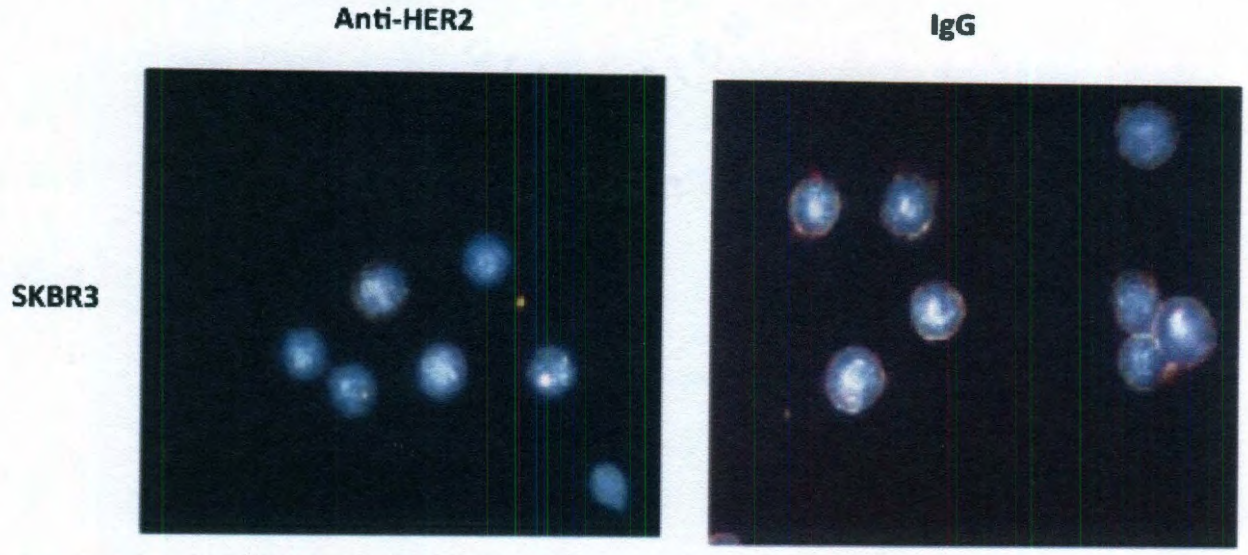

Figure 3-5. Dark field microscopy images of the samples as in **Figure 3-4**.

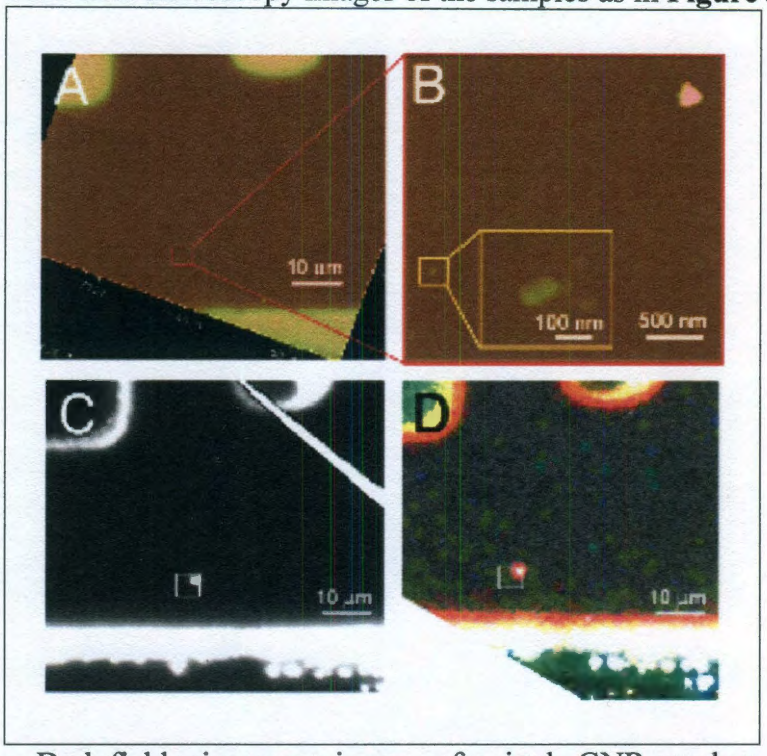

Figure 3-6. Dark field microscopy images of a single GNR on glass. The first AFM image (A) shows a region near alignment marks that are also visible in the optical images (C and D). A zoomed AFM image (B) reveals a large nanosphere in the upper right (triangular shape is a tip artifact) and a nanorod in the lower left. The GNR is clearly revealed in the inset. Its size is exaggerated by the tip. The true size is approximately 50 nm length and 15 nm width. Dark field images captured with a high sensitivity CCD (C) and color CCD (D) clearly show the nanosphere, but show no sign of the nanorod in the expected region, even with significant contrast enhancement. The inset boxes in A, C, and D are all shown at the same size and position.

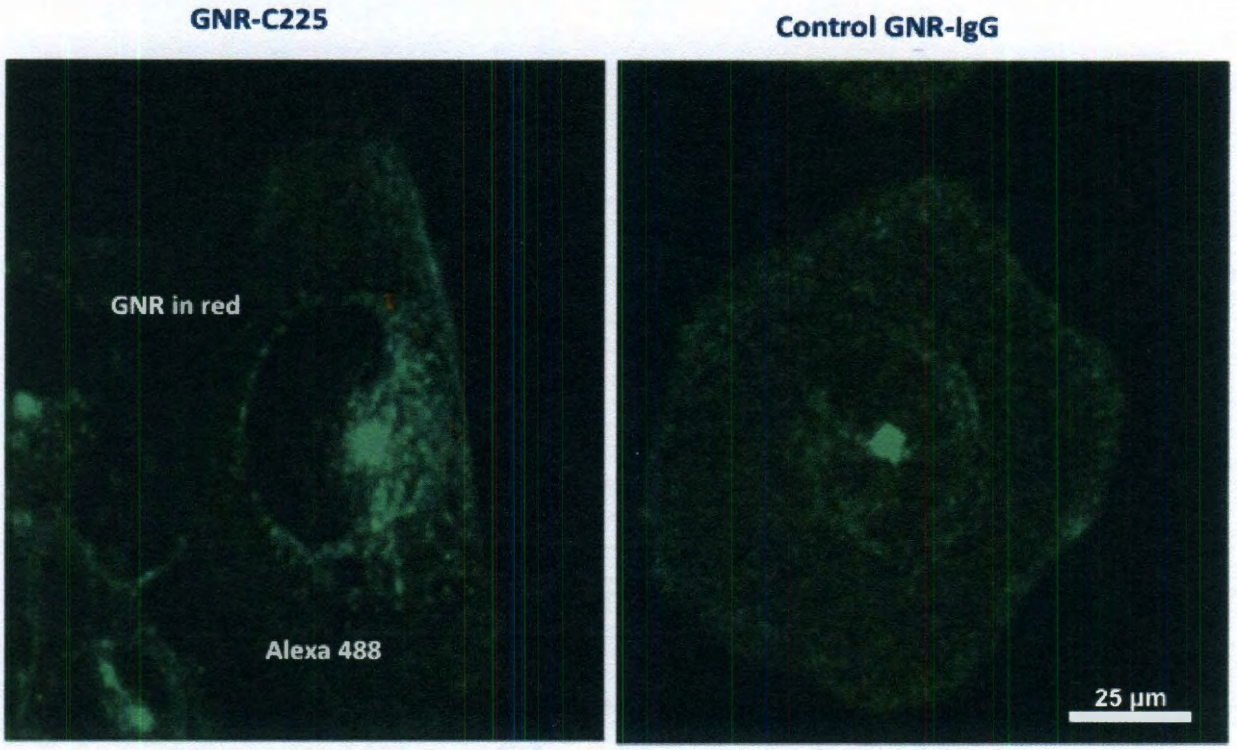

Figure 3-7. In vitro nanorod imaging by confocal reflectance. WGA fluorescence shows the cell location in green, and confocal reflectance at 633 nm illustrates nanorod binding in red. Nanorod binding is only observed for the specific C225 conjugates and KU7 cells.

3.2.6 Conjugation Discussion

To date in vitro and in vivo GNR targeting experiments have been mostly carried out with CTAB-capped gold GNR stabilized with polyelectrolytes, followed by the mixing and non-covalent binding of antibodies or other targeting agents.[35-36,38-40,42-43] These strategies compare to the antibody bound citrate-capped gold nanoparticles that are often used for immunoelectron microscopy where the binding often results from weak electrostatic and hydrophobic interactions.[85-86] The t-GNR-PEG-c functionalization described in this work makes use of an amide bond between the linker and antibody, and a strong gold-thiol bond between the thiol linker and the GNR. Amide bond formation

with antibodies has likewise been explored with various methods which included, polyelectrolytes that housed exposed carboxyl groups, or with alkanethiols that contained bifunctional PEG linkers.[37,44,87] This latter method often remains problematic due to the low aqueous solubility of alkanethiols, which makes it necessary to employ elevated temperature and sonication to achieve the concentrations needed to displace CTAB.[87] In vivo applications can benefit from more optimized gold-thiol and covalent bond conjugations that are application tailored, however the bioconjugation described here is reproducible for cancer cell targeting in spite of the strong CTAB-gold interaction.[35] Zeta potential testing showed that changes to the intended surface chemistry were altered for the negatively charged t-GNR-PEG-c, near neutral for the zwitterionic antibody t-GNR-PEG-c-Ab bioconjugates, and positive for the original CTAB-GNR. Fluorimetric assays confirmed that there were two antibodies per GNR, and Nanoparticle-ELISA suggested that a large fraction of these antibodies were active. Successful in vitro cell targeting was then shown with two cell types and different antibodies.

3.2.7 Microscopy & Scattering Characterization

Sensitive characterization techniques, allow for the detection and spectroscopies of individual nanoparticles, however the optical detection of single nanoparticles remains a challenge.[12] In order to overcome this, total internal reflection, and Rayleigh intensity scattering have been used, as these are able to detect particles above 40 nm.[12] Such methods have been unsuccessful in smaller sized particles as it is difficult to differentiate the scattered intensity of nanoparticles from the background of fellow scatterers.[12,71] Under confocal microscopy the nanoparticles can function as optical contrast agents that increase the visibility of the cells under reflectance mode imaging.[12,71] Since the targeted

t-GNR-PEG-c-Ab bioconjugates are able to bind to cancer cells, they can produce reflective signals that function as biomarkers that can discriminate between cancer and normal cells. The strong resonant light scattering response of gold nanoparticles is enhanced when the gold nanoparticles cluster around the cell membrane, as their surface plasmons are able to interact with each other upon excitation by light.[12,71] Once this dipole oscillation is induced it produces the scattering of particles, and oscillations that are of the same polarization as the incident light beam.[12] The oscillating dipoles will then reradiate the light with the same polarization, and the intensity of the scattered light from the particles will be asymmetric about the GNR. The laser-nanoparticle interaction, then produces strain waves and surface polarization currents that cause the scattered electromagnetic energy to re-radiate from the particles, leading to the ultimate signal that the observer sees.[12] Photothermal methods which also rely on the absorption properties of the GNR, which vary with the third power of the particle size, also present an advantage to highly scattering environments, and finds applicability in absorption spectroscopy and live cell imaging studies.[71] The photothermal effect arises from the excitation of the surface plasmon resonance of the metal nanoparticles, which have a large absorption cross-section, and exhibits a fast electron-phonon relaxation time, which makes them very efficient light absorbers. Since the luminescent yield is quite weak, almost all the absorbed energy is converted into heat, leading to increased temperatures that cause variations in the refractive index of the absorbing particle.[12]

3.2.8 Conjugate Imaging Discussion

Different imaging methods were used to visualize the bioconjugates in and around cells. TPL images shown in **Figure 3-4** clearly reveal the GNR in the samples. What was

also evidenced in the figure is the nonspecific binding of the antibody to a bare plastic surface which had not been substrate modified. This often occurs due to a hydrophobic substrate-protein interaction due to the water molecules on the plastic substrate having a much higher affinities for each other. This exclusion of hydrophobic sites in the aqueous solution can lead to parts of proteins being adsorbed onto the hydrophobic parts of the plastic substrate. The nonspecific binding of the antibody to the hydrophobic portions of the plastic substrate, which is noted in red, is the background signal noted in **Figure 3-4**. Note that this behavior was also seen in the PET vials used for the initial t-GNR-PEG-c conjugation.

Dark field microscopy results, which are shown in **Figure 3-5**, was also used to detect the GNR in cells, as this technique is likewise able to pick up the striking modalities of the plasmon resonant nanoparticles.[88] The complication of dark field microscopy is that the optical scattering needed to provide the dark field constant is a strong function of the nanoparticle size. An additional issue stems from the size range at which the nanoparticles become visible by dark-field methods, which is tens of nanometers, and which is similar to the range of nanoparticles that have been used in biomedical applications. Visibility issues are also sensitive to the illumination, imaging numerical apertures, spectral range, nanoparticle aggregation, and background scattering from the cells. This poses a complication for dark field, as the strong background scattering of the cells complicates the scattering stemming from the cross-section of the GNR. This makes it necessary to cautiously analyze the targeting of the t-GNR-PEG-c-Ab bioconjugates by dark-field methods. Dark-field images in **Figure 3-5** reveal no evidence of scattering the t-GNR-PEG-c-Ab bioconjugates, while TPL imaging in **Figure**

3-4 clearly shows the presence of the GNR. This suggests that the 15 x 50 nm GNR do not scatter sufficiently to be visible against the background scattering of the cells. This means that the dark field samples are unable to distinguish the t-GNR-PEG-c-Ab bioconjugates when compared to the cell scattering, this is further confirmed by the dark field images taken from the single GNR glass substrate sample as shown in **Figure 3-6**. While AFM and alignment marks were used to confirm the location of the single GNR relative to the larger spherical particle, the dark field images failed to confirm the rod with either a color CCD camera or back-illuminated electron multiplying CCD camera. This is indicative that visibility is lacking in both the cell and glass substrate samples.

Other methods could be used to increase the GNR imaging signals, and contrast such as spectrally filtering the scattered light, exciting with monochromatic illumination at the plasmon resonant wavelength, and using higher numerical aperture condensers and objectives can be implemented. However, confocal reflectance microscopy coupled with monochromatic illumination at the LSPR wavelength and reduced background signal, was sufficient to detect the targeted GNR in the KU7 cells, this is shown in **Figure 3-7**. It would seem that the contrast levels between the TPL and confocal reflectance in the cell samples may be relevant. TPL however was enough to detect individual or a small cluster of GNR that were undetected in dark field microscopy, this is shown in **Figure 3-4**, this is expected as other groups have shown the use of TPL for GNR imaging.[66] This suggests that dark field methods would require spectral filtering of the scattered light, excitation with monochromatic light at the plasmon resonant wavelength, and/or use of higher numerical apertures, and condensers and objectives in order to increase the GNR imaging signals. However, GNR that are significantly aggregated due to high-density

binding, may become visible in dark field measurements. These results indicate that the targeted GNR can be visualized below the aggregated level using monochromatic illumination at the LSPR wavelength, with reduction in background noise.

3.3 Conclusion

GNR targeting experiments were successfully carried out with stable bioconjugates that resulted from the use of NHS-EDC chemistry and a bifunctional PEG with thiol and carboxyl end groups. This resulted in the formation of an amide bond between the linker and antibody, and the strong-gold thiol bond between the linker and GNR. The carbodiimide linking strategy was successful in producing carboxy-terminal PEGylated GNR that could undergo successful bioconjugation with antibodies. Furthermore this conjugation strategy was reproducible despite the strength of the original gold-CTAB interaction. Zeta potential measurements were able to confirm changes to the intended surface chemistry, leading to negative potentials for the carboxy-terminated GNR conjugates and near-neutral charge for the zwitterionic antibody protein GNR bioconjugates. Fluorimetric assays suggested that two antibodies per nanorod were present and Nanoparticle ELISA assay demonstrated that a large fraction of these bound antibodies were active. Successful in vitro targeting of the GNR bioconjugates were shown in two cell types using the HER-2 and C225 antibodies. TPL and confocal reflectance were then used to successfully image the t-GNR-PEG-c-Ab particles that were successfully internalized by the cells.

CHAPTER 4

NIR Plasmonic Gene Therapy Vector

Genetic diseases are unfortunate worldwide threats in human society that occur as a result of mutations in the DNA sequence of healthy cells. Gene therapy has the promising potential to create safe and effective treatments for genetic diseases ranging from inherited disorders and incurable cancers to viral infections. In gene therapy, the successful delivery and integration of genetic material such as DNA or RNA, can modify the encoding of the target proteins, and may restore their function as well as expression level to a disease-free state.[90] Yet, in order to successfully achieve a therapeutic effect, several methods and conditions have to be met, these include: (i) to synthesize a DNA or RNA sequence that contains the protein coding information; (ii) to deliver this safely inside the cell using a designed optimal vector; (iii) to design a system that caters to receptor mediated endocytosis in order to avoid the reticuloendothelial system (RES) clearance and macrophages, and (vi) to escape the endosomes and gain access to the cytoplasm and associated nuclear membrane without degradation.[90-91] Then in order to affect gene expression, the relatively short sequences of genetic material must be complementary to mRNA. Once this complementary match is achieved, then blocking of the translational initiation, or mRNA processing, and the subsequent destruction of the mRNA can occur.

4.1 Gene Therapy Introduction

4.1.1 Gene Therapeutics

Gene-, stem cell/protein-, and nano-based therapies are now becoming new approaches in molecular medicine, and this stems from their increased ability to deliver therapeutic drugs and genetic material to the target cells. Gene delivery therapies still present a variety of potential problems, and this may be due to the fact that oligonucleotides such as DNA, and RNA, are often unstable in an environment with high ionic strength such as blood, where charges from electrolytes and salts may lead to aggregation.[90-91] The short half-life of naked genetic material (less than five minutes in plasma) and its degradation and clearance following systemic injection, makes it is necessary to use a suitable delivery system, such as vectors.[90-91] Several delivery vectors, which are viral or nonviral in nature, have been developed to facilitate the transfer of genetic information into a cell. Determining the size of the genetic material being transferred, identifying the target cells and their optimal ability to be transfected, and subsequent longevity of expression, may also help address some of these issues.[90-93]

4.1.2 Delivery

A major hurdle in gene therapy, is the difficulty in being able to efficiently transfer a highly negatively charged DNA, RNA molecule or other genetic material into a cell using either ex vivo or in vivo delivery methods.[90-93] For ex vivo delivery, DNA/RNA can be transferred into cells using calcium-phosphate precipitation, electroporation, cationic or anionic lipids, liposomes, dendrimers, polymers, or nanoparticles.[90-92] The transfected cells can then be selected by virtue of a selectable marker that is recognized by the DNA, RNA, or oligonucleotide. Some genetic material

requires the use of a combination of delivery vehicles such as liposomes, cationic or anionic lipids, polymers, and nanoparticles in order to increase the low transfer efficiency.[90-94] Plasma membrane fusion proteins, polymer, or nanoparticle-assisted delivery systems that wrap or shield the genetic material have also been employed.[94] Yet changes to the chemical composition of the delivery vectors must be optimal in order to ensure that they are physiologically compatible and successfully internalized often by exploiting receptor-mediated endocytosis targeting strategies into endosomal compartments. The nuclear delivery and binding of the DNA/RNA material will then turn genes on or off, by adding, replacing, or correcting the diseased genes. This allows the endogenous target mRNA to be modified in order to alter its transcription, which leads to a therapeutic effect. While viral and nonviral vectors differ in terms of their overall efficiency the latter specifically lag behind viruses in terms of transfection ability.[90-94] Existing technologies currently exploit the binding and condensing of nucleic acids, subsequent vector unpackaging, endocytic escape, and cytoplasmic mobility. Novel emerging technologies are being developed to fine tune the protection of the nucleic acid cargo material, its endosomal delivery and escape, and nuclear localization.[94] Appropriate formulation conditions are still being investigated in order to avoid toxicity issues.

4.1.3 Gene Delivery vectors

To increase the efficiency of gene therapy by non-viral means, plasmid DNA vectors can be complexed by physico-chemical methods to either polymeric, lipid, and/or plasmonic vectors.[90-100] Plasmid vectors are small circular molecules of double stranded DNA that are naturally derived from plasmids found in bacteria. Plasmids are

transferrable genetic elements of DNA that are capable of autonomous replication within a suitable host. Being able to function similar to viruses, plasmids can transfer genetic information non-genomically, however their lack of a protein coat hinders their ability to move from cell to cell, thereby restricting movement within a single cell. Plasmid vectors have three main components, these being an origin of replication which facilitates extraction and allows for replication inside the host cell, an encoded antibiotic resistance gene that is selective to growth, and polylinker DNA sequence that contains enzyme restriction sites that allows for the insertion of mammalian DNA/RNA sequence of interest.[93-100] Plasmid vectors help to facilitate the nuclear delivery and subsequent protein expression of the gene of interest. Except during mitosis, which is when the nuclear envelope breaks down, the only way molecules can enter the nucleus is by taking advantage of the nuclear pore complex which allows for the passive diffusion or active transport of molecules. Plasmid vectors are able to enhance the transfectability of mitotic cells whose nuclear envelope breaks down during reproduction.[93-100] Yet the diffusional barrier of the nuclear envelope continues to pose a problem to the cytoplasmic stability of plasmid DNA, resulting in their low nuclear delivery and gene transfer abilities.

Among all the various gene carriers, viral vectors are the most widely investigated to date because of their efficient transformation efficiency.[90-94] Lentiviral, adeno-associated virus, and other retroviral vectors have been extensively researched for stable expression of short hairpin RNA due to viral vectors ability to successfully insert into the host genome.[95,90-94] However, due to viral re-activation, gene control, and immunogenicity, safety issues are still problematic for benchside medical and human trials. Molecular encapsulation by liposomes, polymers, and dendrimers has also been

used, but these are less efficient than viral vectors and can suffer from increased toxicity.[90-100] Plasmonic nanostructure based vectors are now being actively researched due to their low immunogenicity, non-toxicity, and compatibility.[92,99-100] In addition these vectors are more effective at achieving gene delivery and can be engineered for controlled release upon laser irradiation.[100]

4.1.4 Viral vectors

The viral gene therapy approach uses replication defective viruses where part or all of the viral coding sequence is replaced by therapeutic genetic material. Viral vectors confer highly efficient delivery as they avoid plasma components by using their capsid proteins to attach to cells, which often significantly reduce and/or lead to the elimination of transfection agents. Types of viral vectors include retroviruses, which are a type of lentivirus that uses a reverse transcriptase to transcribe RNA to DNA.[90-95] Retrovirus vectors can achieve a long-term expression in cycling cells, resulting in high viral titers that can enable the transduction of non-dividing cells.[90-95] A drawback of the use of retroviruses rests in the integration of the viral genome into the host genome, which is a random process that carries a high risk of insertional mutagenesis. Other vectors such as the Adenovirus-based vectors, use an icosahedral virus with a large DNA genome that can infect dividing and non-dividing cells, leading to high viral titers. Adenovirus based vectors will transduce a wide range of target cells leading to high-level gene expression. However, since they are non-integrating vectors their expression in dividing cells is progressively lost. Adenoviral vectors are suitable for applications that require a transient, high level activity, and where immune responses to the vector and transgene expression are acceptable. Toxicity associated with the repeated administration of

adenovirus vectors is often problematic.[90-95] The adeno-associated virus is another viral vector type that often uses a small nonpathogenic DNA virus that can only produce progenies in the presence of helper viruses. In the absence of helper virus, it incorporates a genome into the chromosome of host cells.[90-95] Adeno-associated virus vectors can yield high viral titers and transfect both dividing and non-dividing cells. However, their application is limited by toxicity and packaging size constraints.

While viral vectors are great for in vitro gene therapy, problems arise with non-replicating cells, and in vivo studies. The infectivity and compatibility match up of viral-cell types often restricts their use, while packaging and size limitations hinders associated insertional sequences. Viral self-replicating capabilities with unique recombination and complement activation are also problematic, as is the inability to bypass the host's defense mechanisms.[90-95] Insufficient pharmaceutical quantities, termed viral titers, and the limitation of the amount of genomic information that can be introduced into these vectors are also complications.[90-95]

4.1.5 Nonviral vectors

The aforementioned problems associated with the use of viral vectors have led to the development of a nonviral approach to gene therapy, which abstains from the use of any viral particle but uses instead a combination of plasmid vectors, polymers, cations, anions, nanoparticles, lipids, and oligonucleotides, which work together to emulate viral gene delivery vectors.[90-100] RNA, DNA, or other genetic material that can undergo amplification in bacteria and cells, and/or which can be chemically synthesized can be used. Nonviral vectors differ from each other only in their self-assembly which is

controlled by the order of addition of components, subsequent charge, and resulting polydispersity.

Types of nonviral vectors include naked or free DNA, which is often given as an intratumoral injection.[94] While naked DNA can induce a transgene expression that is high enough to confer a therapeutic response, its systemic administration needs to be protected from endonuclease degradation. More efficient DNA transfer can result from the use of ballistic DNA injection which use micron sized gold particles that are coated with a plasmid DNA that encodes the gene of interest.[94] The plasmid coated gold particles are then placed onto a carrier sheet that is housed in a discharge chamber, which can be accelerated by a motive force to penetrate cell membranes. Lipoplexes are another type of nonviral vector that are often used for cancer-based studies. The lipoplex uses lipid-encapsulated plasmid DNA creating an organized and complexed structure resembling that of a micelle or liposome.[96] Lipids, which can be anionic, cationic, or neutral, can then complex to DNA through a charge interaction. Often helper lipids are included in the formulation because they can increase the intracellular trafficking of the genetic material.[96] Helper lipids have been shown to fuse with the endosomal membrane to deliver the internalized cargo molecules, and facilitate their diffusion into the cytoplasm. For example, a helper lipid such as polylysine, uses weak intermolecular forces that arise from interactions between charges and dipoles, and hydrogen-bonding (H-bonding) between amino and phosphate groups, to create particles that are small enough to enter cells.[96] By virtue of their ability to exploit weak intermolecular forces such as ionic, H-bonding, hydrophobic, and solvent exclusion, lipoplexes can also produce a tight condensation of the DNA into a heterochromatin structure, which further

favors delivery. Another nonviral gene delivery vehicle is a polyplex, which is a polymer-DNA complex that often consists of positive cationic polymers, complexed with anionic DNA. DNA interactions with cationic polymers and liposomes occur through charges that help to compact the DNA/RNA molecules and promote binding. To date, lipoplexes and polyplexes are the most successful non-viral gene delivery vehicles.[96]

Given the immune system's lack of exposure to non-viral vectors, there is little chance of patients having high titers of neutralizing antibodies against them.[93-94] Furthermore, their size can compare to viral vectors, which makes them small enough for endocytosis. The non-immunogenicity, low acute toxicity, and simplicity of non-viral vectors makes them attractive candidates for gene delivery. Yet the inefficient delivery of non-viral vectors can result from size and charge constraints, which can lead to overwhelming van der Waals forces in the particles resulting in aggregation.[93] Major delivery barriers/obstacles include transfection, which can be influenced by the interactions between the colloidal and surface properties of the delivery vector, and the compacted or condensed nucleic acid cargo material.[93-94] A variety of strategies have been developed to improve the efficiency of non-viral vectors, for instance through enhanced cellular internalization by receptor mediated endocytosis, the endosomal escape and nuclear localization of the genetic material is encouraged. [93-94,96-102] Drawbacks of non-viral vectors include their large-scale production, lower efficiency in gene transfer, and transient gene expression. Formulation barriers, batch-to-batch variability, and issues with synthetic material synthesis, and purification are also still plaguing.[93]

4.1.6 Colloidal Gene Vectors

Less expensive synthetic delivery vectors such as charged colloidal gene therapy vehicles with excess positive or negative charge have also been researched.[94] A drawback with colloidal systems is that they often fail to reach the target cells due to interactions with the extracellular matrix (ECM) proteins and cell surface lipids. Current research has shown that nanotechnology based, plasmonic-vectors that are non-viral in nature can be used for gene delivery.[99-100] Plasmonic nanoparticle-based vectors have already been used to successfully deliver genetic materials into cells, and in some cases are helpful in overcoming the packaging size constraints that plague the established viral and non-viral vectors.[103-109] Nanotechnology-based approaches have also shown to have minimal toxicity or side effects both in cell culture and animal models.[99-100,103-109]

4.1.7 Gold Nanoparticle based therapies

GNR are 20 nm in diameter and 80-nm long, solid-gold cylinders and exhibit tunable NIR extinction that allows for their extensive use in cancer therapeutics/diagnostics, photo-thermal cancer therapies, and in diagnostic molecular imaging.[110-111] While bulk gold has been deemed safe, the biocompatibility and environmental risks of nanoscale gold particles need to be clarified prior to their large scale manufacturing for in vivo use.[112-113] The non-toxic nature of the GNR comes to light after the cytotoxic dispersants (CTAB) have been replaced by biopolymers. It has been shown that a three-day in-vitro exposure of K562 leukemia cells to 100 nM concentrations of nanoparticles was in fact nontoxic.[114] However, free CTAB has the potential to lyse cell membranes and cause nonspecific binding interactions that are detrimental to gene therapies.[114] Therefore a key step for in vivo work is the removal of

CTAB combined with an appropriate nanorod purification step. The cytotoxicity of GNR can also be reduced by overcoating them with PEG polymers, which helps reduce nonspecific binding of biological molecules to cell surfaces in general.[115-116] GNR coated with CTAB and subsequently overcoated with polyelectrolytes show 90% viability for HeLa cells and cause little change in the levels of gene expression: only 35 out of 10,000 genes were mildly down-regulated.[116] However, polyelectrolyte stabilization of GNR can suffer from instabilities at certain pH values and ionic strengths. Although standard assays of polymer functionalized nanoparticles do not evidence cytotoxicity, they may still cause serious cellular damage, such as an increase in actin filaments and decrease in cell proliferation and adhesion.[117] Cytotoxicity may also depend on the cell type used and the type of material used to construct the nanoparticles.[118]

4.2 RNA therapeutics

4.2.1 RNA Silencing

RNA based therapies such as silencing RNA (siRNA), are now highly sought after for non-actively dividing cells.[96,102] The post-transcriptional gene silencing by RNA interference is known as RNAi, was first observed in plants, and is a mechanism that can be exploited by cells to conduct gene regulation and as a strategy of defense against foreign (viral) RNA.[96,102] siRNA gene therapies work by silencing target mRNA by binding complementarily to small RNA molecules, which takes advantage of the extreme specificity of Watson-Crick base pairing. siRNA molecules contain a catalytic component that enables a single siRNA molecule to silence or destroy thousands of copies of mRNA molecules. When compared to regular anti-sense technology where nucleic acid molecules can bind to and silence only a single mRNA molecule, siRNA

silencing is extremely efficient. In mammalian cell lines, siRNA is generated by a cleavage of larger double stranded RNA (dsRNA) precursors through the RNAse II endonuclease dicer. [96,102,119] Dicer forms a complex with the TAR-RNA binding protein (TRBP) which hands siRNA to the RNA-induced silencing complex (RISC), which contains the protein that conducts the silencing activity by cleaving the target mRNA molecule between bases at the 5' end of the antisense siRNA. The core of RISC contains Ago-2 (a member of the Argonaute protein family), which carries out the catalytic cleavage activity and releases the passenger strand, leading to an activated form of RISC with single stranded RNA (ssRNA). [96,102,119] mRNA with perfect or near perfect complementarity to the guide RNA is then used by Ago-2 to recognize and cleave the target. Partial complementarity to siRNA and target mRNA, represses translation and destabilizes transcripts if the binding mimics micro RNA (miRNA) interactions with target sites. The miRNA is the endogenous substrate for the RNAi machinery and is expressed as a long primary transcript (pre-miRNA). This pre-miRNA is then processed within the nucleus into a 60-70 base pair (bp) hairpin by a microprocessor complex. Further processing in the cytoplasm by the RNAse III dicer complex removes the hairpin loop of the pre-miRNA. Only one of the two strands of the pre-miRNA is then loaded into the cytoplasmic RISC complex. Partial complementarity of the miRNA with the sequences 3' untranslated region (UTR) of the target mRNA allows for the translation repression and associated message degradation. [96,102,119] It becomes possible to exploit this native gene-silencing pathway for the regulation of genes, if a siRNA effector molecule with one strand of complementarity matches that of the target nucleotide sequence. [96,102,119] This complex can then be delivered into a cell to activate RISC

directly, resulting in specific silencing of the target mRNA. This is often the method of choice for silencing and controlling disease-associated cancer genes in mammalian cell lines. [96,102,119] However, the cytoplasmic delivery of such molecules is still very problematic, making it necessary to use gene delivery systems in order to prolong the genetic materials cytoplasmic stability.

4.2.2 Bladder Cancer Therapeutics

Urothelial carcinoma of the bladder (UC) is a significant health threat to the U.S. population, and the integrated clinical and laboratory investigations of this disease have lagged behind those of other forms of cancer.[120-122] Rapid advances in our understanding of cancer biology have not been translated into improved patient care, and there have been no major advances in therapy for this disease since Methotrexate-Vinblastine-Adriamycin-Cisplatin (M-VAC) chemotherapy was introduced over 20 years ago.[120-122] Despite the obvious need to make the most of the available cytotoxic drugs, there is an undeniable reality that such efforts are unlikely to provide a quantum leap in survival. There is a pressing need to expand the paradigm as many of the newer biologic cancer therapeutic agents such as growth factor antagonists, tyrosine kinase inhibitors, and anti-angiogenic agents have yet to be fully utilized in urothelial cancers. There are also many potential therapeutic targets for gene transfer strategies that are relevant to the pathogenesis of bladder cancer. For example, some studies have shown that some growth factors, such as Heparin Binding-EGF (HB-EGF), Basic Fibroblast Growth Factor (bFGF), and Cripto which are often found in highly malignant cancers are of interest in bladder cancer based gene therapies.[123] Although the biologic activity of the nuclear-localized growth factors is not fully understood, it appears that by targeting the

expression of these ligands through siRNA, one could efficiently block their nuclear function.[123]

4.2.3 siRNA-GNR Plasmonic Vector

In this investigation we studied untreatable forms of bladder cancer with antibody targeted thiol-PEG-carboxyl functionalized GNR that trapped a glyceraldehyde-3-phosphate (GAPDH), Fluorescein isothiocyanate (FITC) labeled siRNA, termed GAPDH-siRNA-FITC that was housed within a Luciferase based plasmid vector. The targeted thiol-PEG-carboxyl-GNR (t-PEG-c-GNR) conjugates were covalently bonded to the EGFR/C225 antibody, in order to enhance C225-induced EGFR receptor-based endocytosis. Receptor-mediated targeting was used to deliver the kinetically trapped GAPDH-siRNA-FITC that was housed within the PEG layer. Heating methods were used to trap and release the GAPDH-siRNA-FITC from the PEG, based on activation of the polymer pour point and salt based electrostatic screening of the PEG-COOH groups. The advantage of this strategy is that it allows for the preferential delivery of the GAPDH-siRNA-FITC into tissues and cell types that differentially express the EGFR receptor, and facilitates delivery into the appropriate endosomal compartment.[120] The down regulation of the GAPDH gene was targeted by the siRNA as GAPDH has been shown to be up-regulated in many cancers and down-regulated by chemotherapeutic drugs.[124] Changes to the GAPDH mRNA expression are therefore highly relevant to cancer-based gene therapies. Cell culture, and subsequent imaging by TEM, TPL and confocal microscopy were used to view the internalized conjugates, while RT-PCR determined if the release of the GAPDH-siRNA-FITC caused a reduction in the

expression of GAPDH mRNA. Plasmonic gene silencing of the gene by the GAPDH-siRNA-FITC will be compared to the lipid based Dharmafect control in terms of transfection ability. GAPDH was chosen as the protein target of the siRNA since its expression is highly correlated with cell proliferation, increased metastasis, and tumor aggressiveness, where any decrease in overexpression correlates with inhibition of cancer cell proliferation, invasive tumor growth, and decreased metastatic potential.

4.3 Methods

4.3.1 GNR Bioconjugates

A 5 mL aliquot of GNR with an OD~10 at the LSPR peak wavelength which was stabilized by the t-PEG-c-GNR conjugation protocol described in Chapter 3. The GNR were resuspended in 100 mM MES buffer at pH of 6.1 and concentrated by sedimentation to a volume of 100 μL using an absorbance of greater than 10 at the LSPR peak wavelength, and filtered using a low-protein binding filter (0.22 μ pore size). A solution containing 96 mg of EDC, 29 mg of NHS, and 10 mL of MES buffer pH 6.1 was filtered using a low protein binding filter (0.22 μ pore size) and 10 μL of this solution was immediately added to the 100 μL nanorod solution. This mixture was allowed to react for 15 minutes at room temperature. Meanwhile 0.5 mL of 2-mercaptoethanol was diluted into 14.5 mL MES buffer pH 6.1 (1:29 ratio), and filtered using the low protein binding filter (0.22 μ pore size), and 10 μL of the diluted mercaptoethanol solution was added into the nanorod solution following the 15-minute incubation. The mixture was allowed to react for 10 minutes at room temperature, after which 400 μL of filtered antibody solution at 2 mg/mL in Phosphate buffered saline (PBS), pH 7.1, was added. The final 500 mL nanorod bioconjugate solution was incubated for 2 hours at room

temperature. The nanorod bioconjugates were separated from excess reactants and byproducts by sedimentation at 10,000 RPM (6,800 rcf) for 10 minutes, which lead to a pellet that underwent a 95% decantation. The pelleted GNR bioconjugates were then resuspended in appropriate buffers.

4.3.2 Zeta Potential

As a means to confirm the changes to the surface chemistry of the conjugated GNR, LSPR absorbance spectra and zeta potential measurements were performed using a Malvern Zetasizer Nano at various stages of GNR conjugation ranging from the original CTAB solution, t-GNR-PEG-c, and the final t-GNR-PEG-c-Ab. Zeta potential data of diluted samples in water and 1X PBS pH 7.1, 100 mM MES pH 6.1, and 50 mM Borate buffer pH 8.6, were tested in Zetasizer Nano cuvettes using a refractive index of 0.2 and absorption coefficient of 3.32. A control zeta of colloidal gold particles was obtained using similar conditions. The resulting data ranging from the original CTAB solution, and the final t-GNR-PEG-c-Ab were obtained.

4.3.3 Cell Lines and culture conditions

The SK-BR-3 breast cancer cells were obtained from Dr. Liana Adam's laboratory at MD Anderson Cancer Center, and grown in McCoy's 5A medium supplemented with 10% fetal bovine serum (FBS) and 1% penicillin-streptomycin and maintained at 37°C in a 5% CO_2 atmosphere. The MCF10A breast epithelial cells were also obtained from Dr. Adams and were cultured in Mammary Epithelial Basal Medium (MEBM) supplemented with a BulletKit (Clonetics) and maintained at 37°C in 5% CO_2. Both cell lines were prepared for the experiment by seeding 6 x 10^5 cells in chambered cover slips and allowing them 30 minutes to attach to the surface. The cells were rinsed

once with PBS before they were incubated with nanorod conjugates for 1 hour in 5% CO_2 at 37°C. The LSPR peak absorbance of the nanorod conjugate solution was 1.5. Post the incubation, cells were rinsed 3 times with 1xPBS and then the appropriate cell media was added prior to imaging. The cells were imaged by TPL microscopy at 50X magnification with 780 nm illumination and 400-700 nm detection.[84]

KU7 bladder cancer cells were then grown in MEM medium supplemented with 10% FBS and 1% penicillin-streptomycin and maintained at 37°C in a 5% CO_2 atmosphere. The samples were prepared by seeding $4x10^5$ cells on cover slips and allowing them to attach to the surface for 24 hours. Prior to treatment, the cell media was changed to OptiMEM and the GNR conjugates were for 4 hours. After the 4 hour incubation, the OptiMEM media was changed to MEM medium supplemented with 10% serum and incubated in 5% CO_2 at 37°C atmosphere for another 20 hours. Twenty minutes prior to fixation, the cells were rinsed once with warm PBS, then incubated with 100 nM Alexa-488-wheat germ agglutinin (WGA) and left for 10 minutes in the cell incubator for WGA cellular internalization. After 10 minutes the cells were rinsed three times with warm PBS then fixed in 3.7% paraformaldehyde for 15 minutes and then washed three times with cold PBS and mounted on slides using Slow-Fade Antifade (all reagents were purchased from Molecular Probes).

4.3.4 siRNA Plasmids construction

The si-Genome On-Target, SMARTpool selection designed GAPDH-siRNA-FITC were obtained from MD Anderson, in annealed, desalted, and 2'-hydroxyl form. The 3'-Untranslated region (3'-UTR) reporter plasmids for the siRNA were constructed via insertion of the hairpin GAPDH-siRNA-FITC sequence into the Bacteriophage

(pRNA)-U6.1/Neo/siRLuc, which is a GenScript siRNA expression vector. This expression vector is used for mammalian cell transfection and uses Renilla luciferase expression. The GAPDH-siRNA-FITC was inserted downstream of its U6 promoter, between the BamHI and HindIII restriction sites as shown in Figure 4.1. The Liana Adams lab provided the Si-Genome On-Target plus Smart pool duplex sense and antisense sequences, these are listed in Table 4.1. The GAPDH-siRNA-FITC plasmid construct was inserted into the Luciferase vector into the BamH*I* and Hind*III* restriction sites, using the associated restriction endonucleases, in the 10x SURE Cut Buffer B (100 mM Tris-HCl pH 8.0, 50 mM $MgCl_2$, 100 mM NaCl, and 10 mM 2-Beta mercaptoethanol), and subjected to T4 DNA ligase using the 10X T4 DNA Ligase Buffer (300 mM Trish-HCl at pH 7.8, 100 mM $MgCl_2$, 100 mM DTT, and 10 mM ATP). The QIAquick DNA clean up systems from Qiagen was used for the plasmid construct. The pRNA-U6.1/Neo/siRLuc plasmid and GADPH-siRNA-FITC were obtained from MD Anderson, here 200 μL of 2 μM GADPH-siRNA-FITC was added to 300 μL of the 2 nM t-GNR-PEG-c-Ab with bound EGFR/C225, and mixed with a 1 mL aliquot of RNAse-free buffer, the usual plasmid construction reaction was used above.

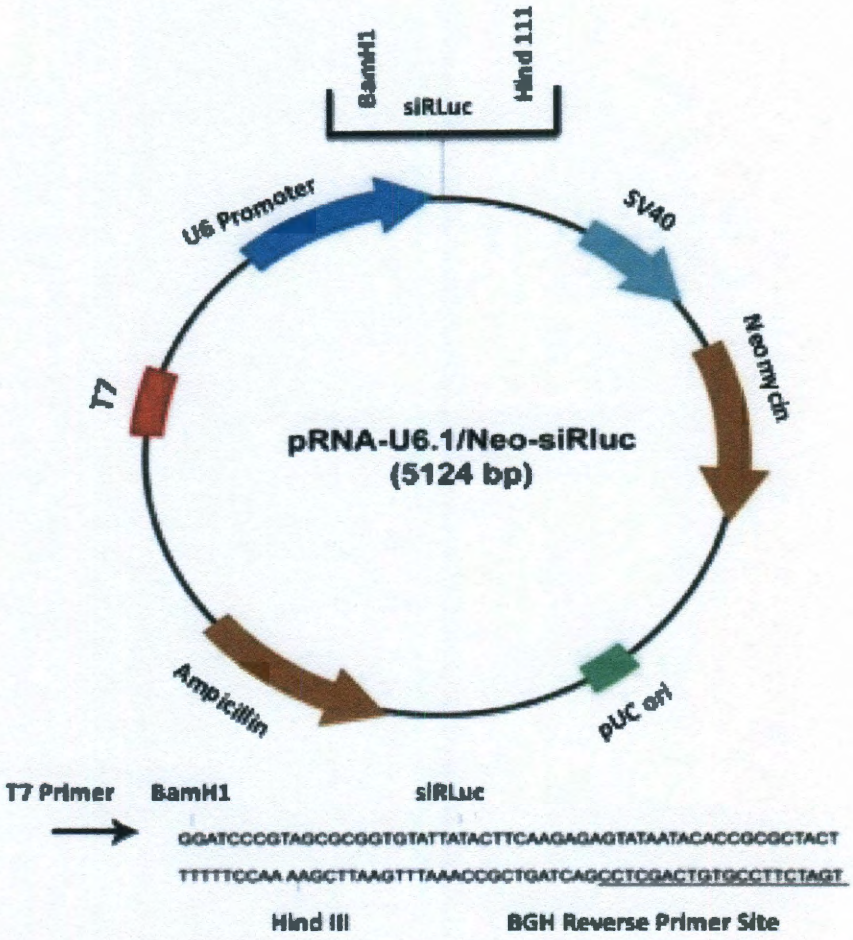

Figure 4-1. Bacteriophage (pRNA)-U6.1/Neo/siRLuc is a GenScript siRNA Renilla Luciferase expression vector. It was designed for mammalian transfection and uses a U6 promoter for siRNA expression and BamHI and HindIII sites.

C,A,A,C,G,G,A,U,U,U,G,G,U,C,G,U,A,U,U,U	5'-A,P,A,A,U,A,C,G,A,C,C,A,A,A,U,C,C,G,U,U,G,U,U
G,A,C,C,U,G,A,C,C,U,G,C,C,G,U,C,U,A,G,U,U	5'-P,C,U,A,G,A,C,G,G,C,A,G,G,U,C,A,G,G,U,C,U,U
C,A,A,U,A,U,G,A,U,U,V,V,S,V,V,V,S,U,G,U,U	5'-P,C,A,U,G,G,G,U,G,G,A,A,U,C,A,U,A,U,U,G,U,U
G,C,G,A,U,G,C,U,G,G,C,G,C,U,G,A,G,U,A,U,U	5'-P,U,A,C,UC,A,G,C,G,C,C,A,G,C,A,U,C,G,C,U,U

Table 4.1. The si-Genome On-Target, GAPDH SMARTpool siRNA sense (left) and antisense (right) sequences were obtained from MD Anderson.

siRNA encapsulation into the t-GNR-PEG-c-Ab plasmonic vector was achieved using PBS salt, which functions as an electrostatic shielding agent that neutralized the

PEG-COOH and siRNA charged entities. The shielding is based on a salting-in effect, which is a concentration and temperature dependant effect that imparts changes to the hydrophobic nature of the PEG. The combination of heat and salt affect the hydrogen bonding and water binding ability of the PEG allowing its water restructuring and amphiphilic properties to make it more hydrophobic. The salt bridges and temperature then alter the RNA charge, which promotes the RNA-PEG adsorption, and shielding, this is shown in **Figure 4.2.**

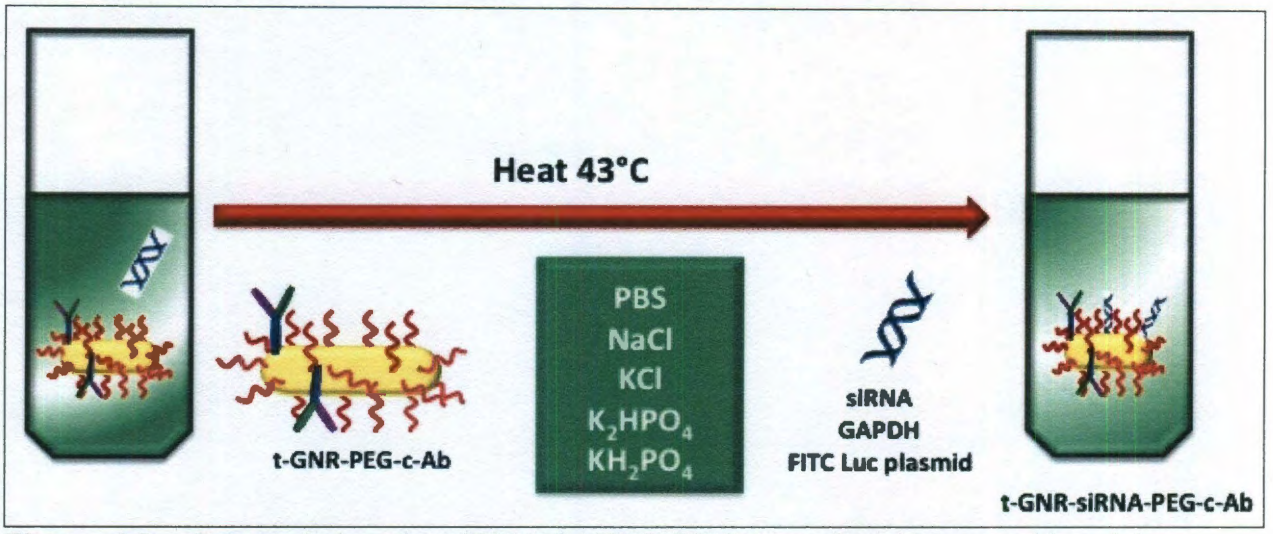

Figure 4.2. Encapsulating the siRNA-GAPDH-FITC-Luc plasmid was achieved by using the PBS salting-in effect, in combination with temperature, leading to the GNR plasmonic vector. The PBS and temperature were used to encapsulate the siRNA due to the hydration and charge changes that were imparted to the PEG and siRNA.

The trypsinized and counted cells were diluted into an antibiotic-free complete medium to achieve the necessary seeding density in 100 μL solution and plated into 6 well plates. The cells were incubated at 37°C with 5% CO_2 overnight.

4.3.5 siRNA Trapping and Transfection

The KU7 cells were incubated with t-GNR-siRNA-PEG-c-Ab complex in a 6-well plate for 1 hour using Serum-free OptiMem. The conjugates were gently mixed and

heated for 4 minutes at 43°C, to this was added 3 mL of Opti-MEM (no serum) and conjugates were ready for cell transfection, this is shown in **Figure 4.3.**

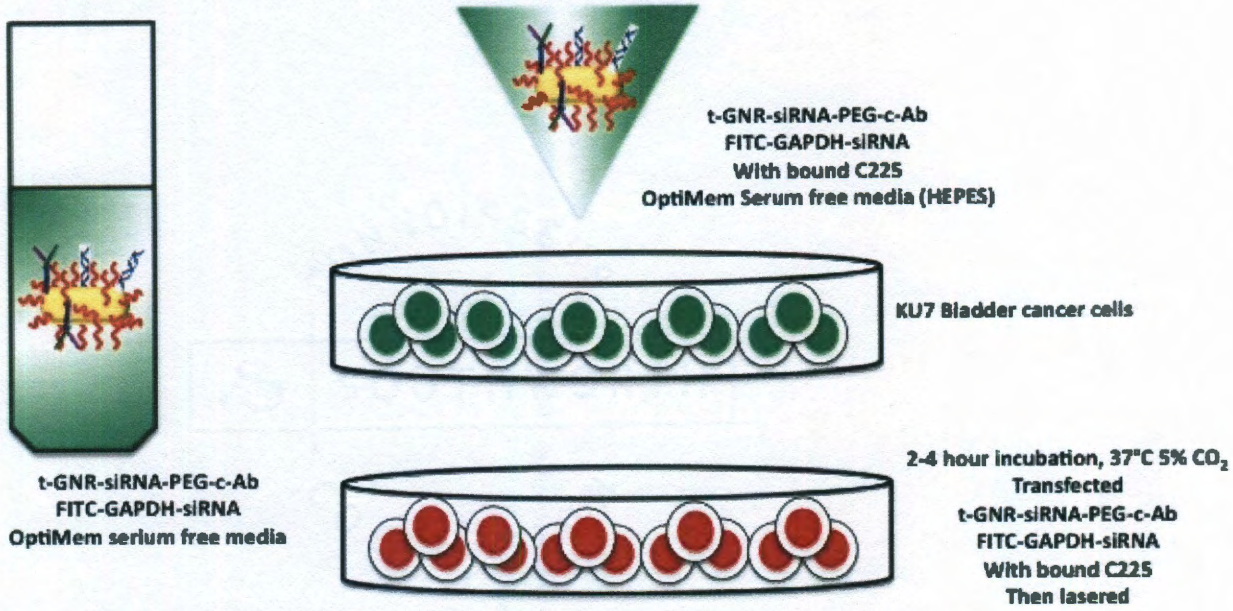

Figure 4.3. Cell transfection of KU7 bladder cancer cells with the GNR-plasmonic vector.

4.3.6 Cell Transfection

A 500 μL aliquot of the 2 nM FITC labeled t-GNR-siRNA-PEG-c-Ab conjugates with bound C-225 were then added to Opti-MEM serum free media, and pipetted into each well for transfection of cancer cells. The resulting plasmonic vector was subjected to a two hour incubation at 37°C with 5% CO_2. Lipid transfection of KU7 cells was achieved using the DharmaFect (DF-1) General Transfection protocol system, where 2 μM of GAPDH-siRNA-FITC was mixed into 1X siRNA buffer and diluted into the DF-1 transfection agent using serum-free media, and gently mixed. This was then incubated for 5 minutes at room temperature, followed by a 20-minute incubation in antibiotic free complete media. The culture media was then removed from the wells and 100 μL of the

appropriate DF-lipid-GAPDH-siRNA-FITC transfection vector was added to each well. The cells were incubated at 37°C in 5% CO_2 for 2 hours.

4.3.7 siRNA Laser Release

The plasmonic GAPDH-siRNA-FITC transfected cells were then subjected to laser treatment using a 1-Watt, 800 nm laser, which provided an energy density of 11.66 Joules/cm^2 (J/cm^2). The conjugate-cell samples were irradiated for 60 seconds, and 5 minutes using the fiber optic laser, at a height that was 3 cm above the well. A schematic of the plasmonic prepared vector is shown below in **Figure 4.4.** After irradiation, the samples were incubated for 48 hours with 2 mL of full-serum media Opti-Mem, and analyzed by

Reverse Transcriptase Polymerase Reaction (RT-PCR).

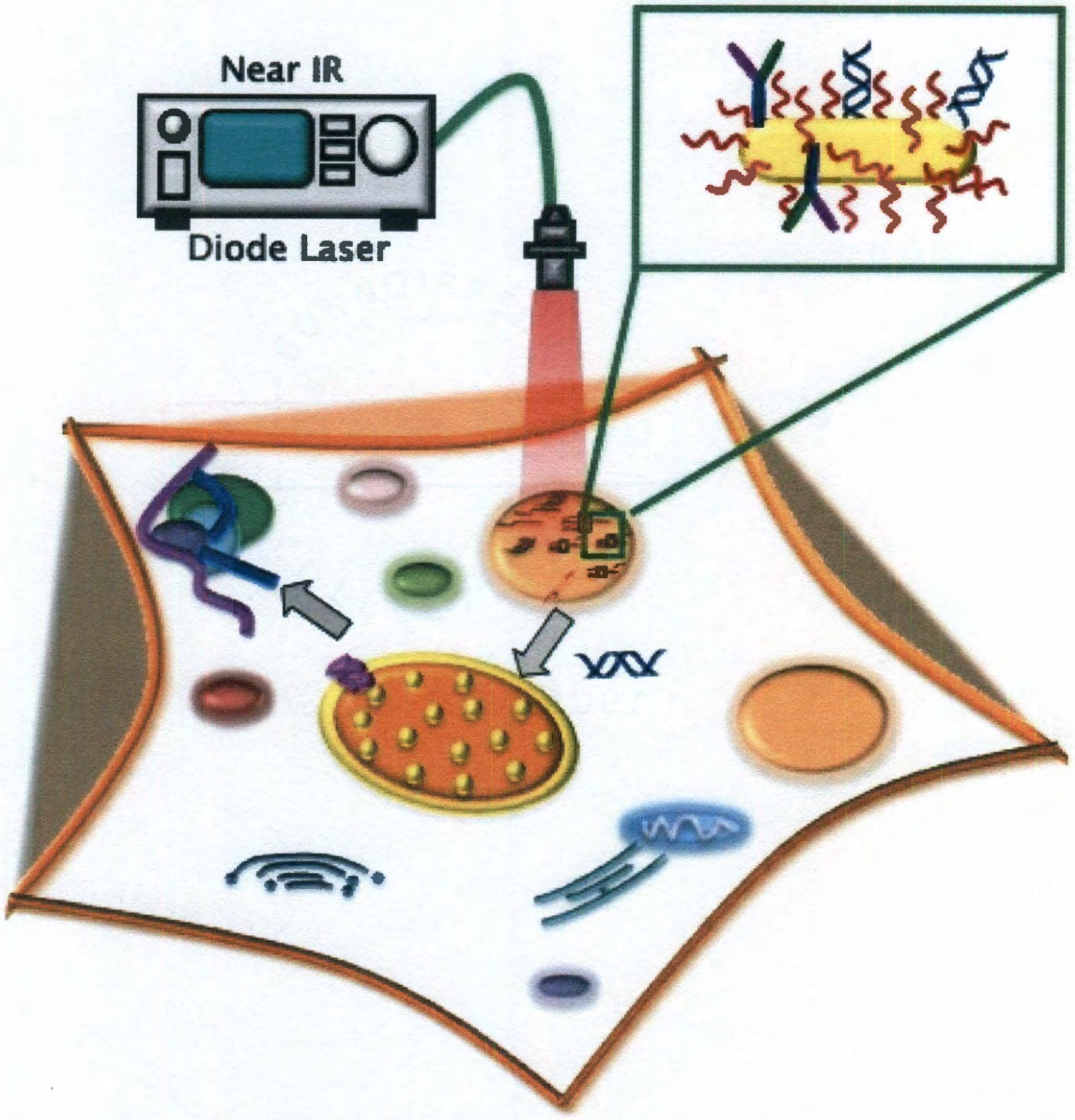

Figure 4.4. Schematic illustration of the GNR-PEG-COO-Ab-siRNA targeted carriers with energy controlled release of genes into cancer cell line. The GNR are coated with a biocompatible PEG polymer, and EGFR conjugated peptides.

4.3.8 RT-PCR

Measurement of GAPDH-mRNA was achieved using RT-PCR. Total RNA was extracted using a Minerva extraction reverse transcription kit (Applied Biosystems) and 10 ng of RNA along with GAPDH specific primer siRNA were used for expression

analysis, using a 18S ribosomal RNA as an internal control. cDNA was synthesized using First Choice RACE-Ready cDNA kit. RT-PCR was performed using the PCR program on ABI prisms SDS 7000 (Applied Biosystems). KU7 cells were incubated with non-targeting Glyceraldehyde (NTG) and GAPDH-targeted GNR for 48 hrs. The RNA was extracted and GAPDH-mRNA was measured.

4.3.9 Imaging methods

Various microscopic methods were used to image the internalized GNR in the cancer cells. Confocal imaging was carried out using the Leica SPR5RS AOBS microscope with a 63x/1.4 objective. GNR were detected at 633 nm illumination in reflection mode. Unmodified TPL microscopy was conducted at 50X with 780 nm illumination, and 400-700 nm detection. Bioconjugates were also analyzed in a Horiba Jobin-Yvon FluoroLog-3 fluorimeter with CW Xenon excitation. TEM was conducted at MD Anderson's High Resolution Electron Microscopy Facility (HREMF) using standard fixation and embedding of cells on a JEM1010 transmission electron microscope (TEM).

4.4 Results and Discussion

4.4.1 Nanorod conjugation

Protein and peptide conjugation to the GNR was carried out using commercially available functionalities, which strongly bind gold surfaces. To deliver the nucleic acid material to the specific tissue, the GNR were bound to monoclonal antibodies. In our strategy, we started out by PEGylating the GNR with a t-PEG-c linker to attach antibodies to the nanorod surface. These t-GNR-PEG-c conjugates were then coupled to antibodies by standard NHS-EDC carbodiimide chemistry. EGFR-C225, a disulfide-bond containing peptide, was the first choice for GNR-peptide conjugation because

EGFR is over-expressed in superficial bladder cancers.[120] We used a conjugation scheme where the antibody was placed on the outside of the PEG layer by using a PEG carboxyl group at the free end, this is shown in **Figure 4-5.**

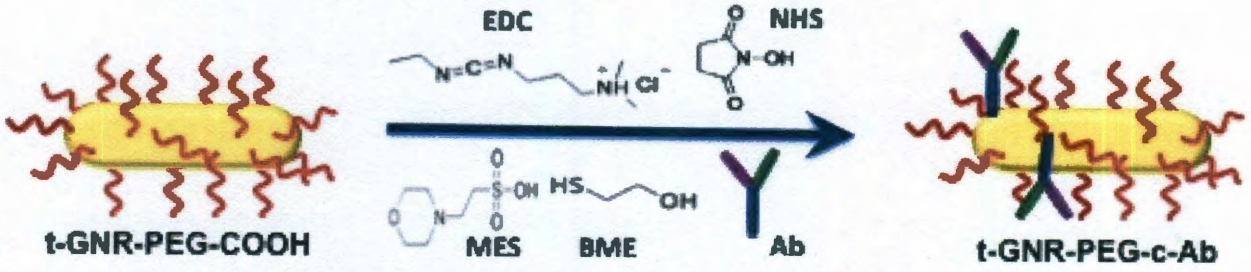

Figure 4-5. GNR bioconjugation strategy, with NHS-EDC, and subsequent antibody binding.

The EDC carbodiimide chemistry activated the carboxylate end groups of the PEG-COOH which allowed for the PEG-antibody functionalization through NHS. The NHS stabilized amine reactive acylisourea intermediate created an NHS ester that could form an amide bond with the hydrophobic amine of the antibody.[125,56] This resulted in a complex containing a GNR that was 50 nm long and 15 nm in diameter, a PEG-COO- coating (5,000 Dalton) with antibody bound at the end groups that was 30 nm in length, and unreacted hydrophilic COOH groups with a Debye length that was 1 nm. Salt screening of any non-antibody containing COOH-PEG molecules allowed for the fine tailoring of the electrostatics of the GNR-PEG-COO-Ab complex.[125] The conjugation of the C225 antibody was pursued, as this targets EGFR expressing cells and tissues which are frequently found in human bladder cancers that exhibit chemotherapy resistance.[120] The down regulation of EGFR has shown to reverse malignancy in bladder cancer associated tumors and is being actively researched.[120]

4.4.2 Fluorimetry

To visualize the cellular internalization of the GNR coupled with the anti-EGFR blocking antibody EGFR-C225, we labeled the conjugates with anti-rabbit IgG carrying an Alexa Fluor-488 dye (AF-488-IgG) and developed simple analytical assays to test for successful conjugation, this is shown in **Figure 4-6**. During conjugation, the GNR had a concentration of 1 nM while the AF-488-IgG had a concentration of 200 nM and therefore the fluorescence of the resulting solution was dominated by free AF-488-IgG. Subsequent rounds of centrifugation produced decants with increasingly lower concentrations of free AF-488-IgG yielding a lower sample fluorescence, until the signal reached the noise level. Following the centrifugation and decantation steps, the fluorimetry of the resuspended pellet was found to be equivalent to the 3rd decant. The fluorescence from the AF-488-IgG bound to the GNR indicated a concentration on the order of 1 nM, suggesting that approximately 2 IgG molecules were bound to each GNR, which is reasonable considering their small size. The results of this measurement represent actually a lower limit since the fluorescence signal of the GNR solution is reduced due to the absorption of the GNR.[132]

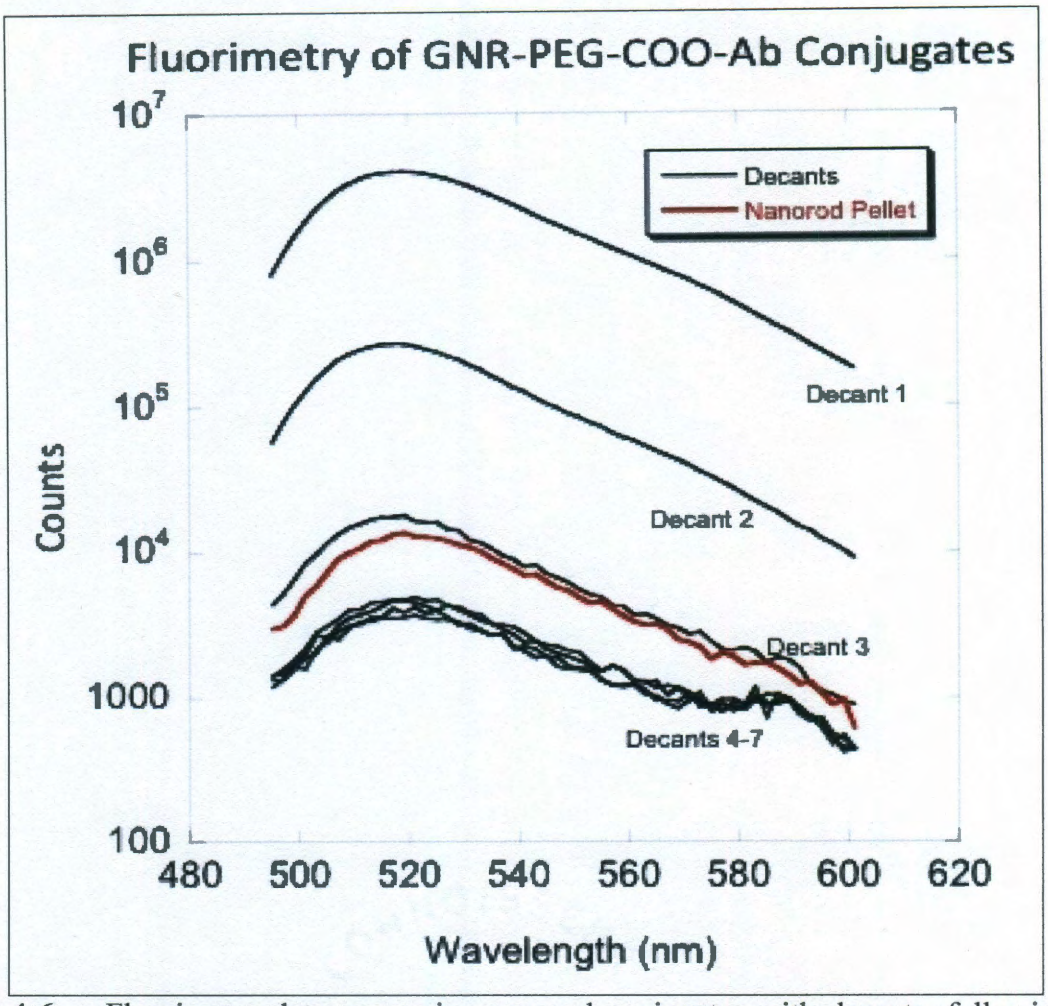

Figure 4-6. Fluorimetry data comparing nanorod conjugates with decants, following several rounds of centrifugation to reduce unbound antibody and CTAB concentrations.

4.4.3 Zeta Potential

Electrokinetic analysis was used to monitor the reduction and purification of the CTAB conjugates. **Table 4-2** lists the zeta potential of CTAB stabilized GNR, t-GNR-PEG-c conjugates, and finally the AF-488-IgG conjugated to the t-GNR-PEG-c-Ab bioconjugates. The positive and negative values for cationic CTAB and anionic COOH-PEG were expected due to changes to the GNR surface chemistry. Upon antibody conjugation, the zeta potential change to -5 ± 2 mV suggesting the binding of the antibody molecule at the surface of the GNR, this is shown in **Table 4-2**. The expected

value is difficult to pin down, since IgG isoelectric points (PIs) vary significantly and this experiment was carried out with polyclonal antibodies. However, the zeta potential data confirms that a molecular change at the surface of the GNR conjugates occurred due to the antibody binding.

Nanoparticle	Zeta Potential (mV)
GNR-CTAB	+85±2
GNR-S-PEG-COOH	-19±2
GNR-S-PEG-IgG	-5±2

Table 4-2. Zeta potential of antibody GNR conjugates.

4.4.4 Cell-specific Internalization

The confocal analysis of the KU7 bladder cancer cells that were treated with the 10 nM t-GNR-PEG-c-Ab conjugates with bound C225, and stained with a DNA-specific dye, Alexa-633-Topro3 (blue pixels), is shown in **Figure 4-7**, left panel. GNR were detected with 633 nm illumination in reflection mode, and Wheat Germ Agglutinized-AF-488 (WGA-AF-488) was excited at 488 nm and detected at 495-530 nm. It is notable that a non-specific Alexa-488 labeled WGA-IgM antibody coupled to the GNR did not show cellular internalization using this imaging method, **Figure 4-7**, right panel. Importantly, KU7 cells that are resistant to the EGFR blockade, either by antibodies or small inhibitory molecules such as Iressa, are still displaying the internalized GNR complexes that are expressing the EGFR protein.[121]

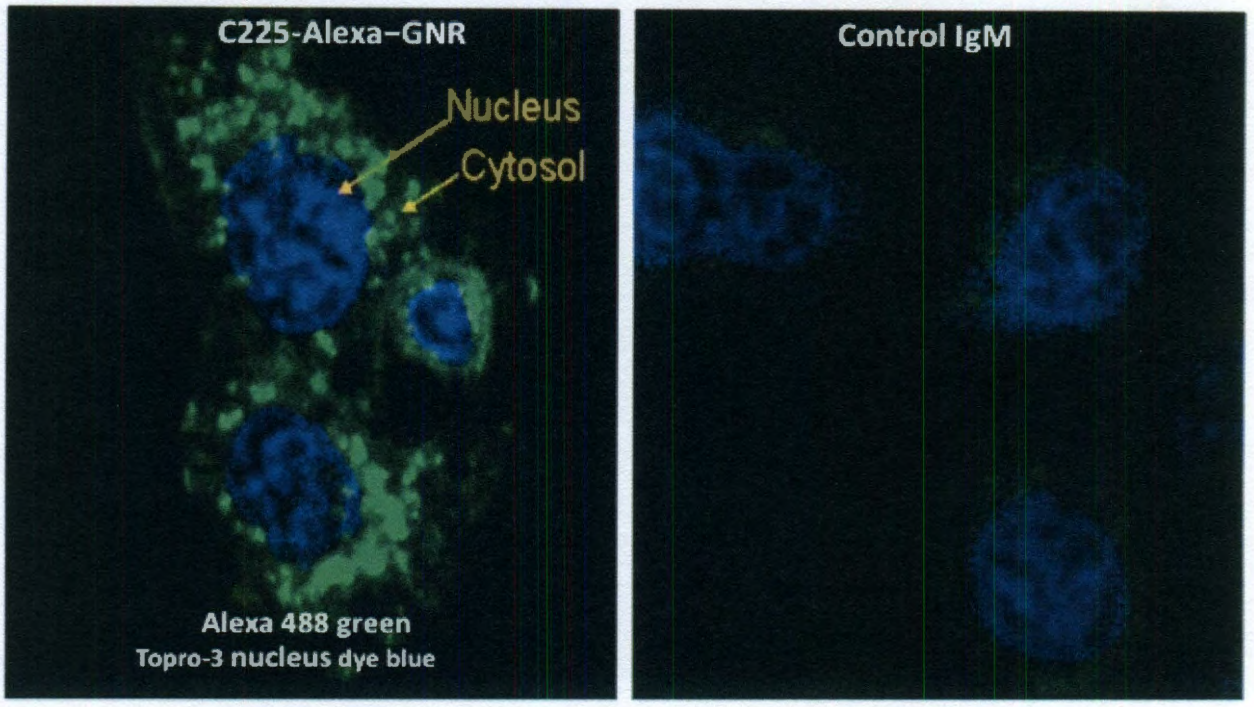

Figure 4-7. Confocal analysis of KU7 cells treated with 10 nM C225-conjugated GNR. The C225 (left panel) and non-specific IgM (right panel) antibodies were labeled with Alexa-488 fluorochrome, The KU7 cells were fixed in paraffin (3.7%), and nuclei were stained using a DNA die, Topro-3 labeled with the Alexa-633 fluorochrome (Molecular Probes). Both panels show the merged images from both channels.

4.4.5 TEM

A complimentary technique such as Transmission Electron Microscopy (TEM) was used to image the particles inside the cells. UMUC5 cells treated with GNR coupled to C225, are shown in **Figure 4-8,** left-lower panel, red circle. The UMUC5 cell line is one of the most sensitive cells lines to the EGFR blockade tested by the Adams lab thus far.[122] The naked GNR were internalized by the mouse 3T3 fibroblasts in lysosomes and thus prone to immediate degradation through a non-specific pathway, this is shown in **Figure 4-8,** lower right panel. By contrast, the C225-targeted GNR do not appear to reside inside well-defined structures, such as lysosomes, but they were found free in the cytoplasm of cells, close to the ribosomal cell-transcription machinery. These ribosomes

can be easily identified along the endoplasmic reticulum (ER), giving the rough ER. The differences in the targeted GNR subcellular locations are due to internalization mechanisms that initially follow an active pathway through EGFR internalization, and later undergo a passive mechanism that is of lesser amplitude. The location of the GNR in each case was different, especially since the GNR were engineered to be cargos for non-coding RNAs (ncRNAs). This strongly suggested that the use non-specific antibodies or naked GNR would result in ncRNA degradation through lysosomes.

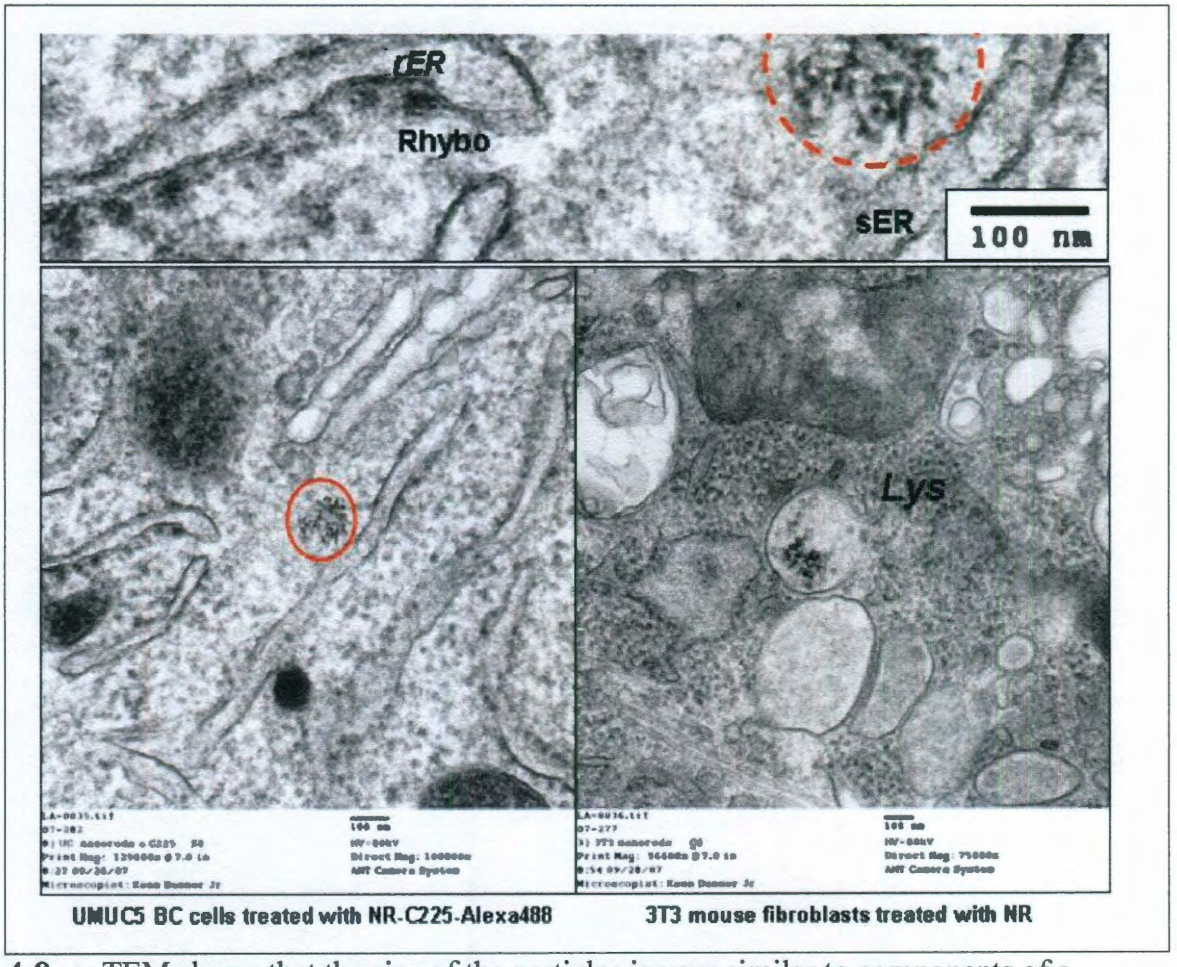

Figure 4-8. TEM shows that the size of the particles is very similar to components of a cellular ribosome, *Rhybo*.

4.4.6 Internalization of siRNA Plasmonic Vector

The overall goal of this study was to introduce siRNAs into somatic cells and provide additional biologic functions as well as to stop the production of detrimental genes implicated in the resistance to EGFR-targeted therapy in bladder cancer cell lines. Compared with viral vectors, synthetic gene-delivery systems such as liposomes and polymers, offer several advantages, including ease of production and reduced risk of cytotoxicity and immunogenicity, but their use has been limited by the relatively low transfection efficiency and their lack of specificity. These problems are mainly due to the difficulty in controlling properties at the nanoscale. Our application focuses on using a non-viral gene delivery system based on biocompatible plasmonic GNR. This plasmonic vector can simultaneously bind nucleic acid sequences encoding for specific siRNAs and targeting antibodies in order to release the functional material in the targeted cells. This approach will allow for the precise control of composition, size and multi-functionality of the delivery system. To determine whether siRNA could also be delivered into cancer cells, we used an original protocol in which the FITC labeled t-GNR-siRNA-PEG-c-Ab conjugates with bound C225 are formed at 43°C and then delivered into cells by direct incubation and receptor mediated endocytosis. Since the internalized GNR can be tracked by using fluorophore-labeled antibodies or nucleic acids, we decided to exploit the light scattering of the GNR. Their exposure to 700-800 nm light could be used as a method of tracking GNR in cells and tissues, **Figure 4-9,** right panel, arrows. In this experiment, the cells were incubated and targeted with t-GNR-PEG-c-Ab with bound C225, and immediately imaged using 800 nm TPL at different time points to estimate the

degree of GNR integration. We also used fluorochrome labeled antibodies (anti-EGFR, -AXL or -non-specific IgG) coupled to the GNR to determine whether the GNR were internalized through an active or a passive mechanism into the cells. The GNR internalization was tracked in KU7 cells using organelle-specific fluorochrome dyes and chemical inhibitors to determine which pathway is responsible for the active GNR internalization. Intracellular trafficking was studied using the Lysotracker (lysosomes) and membrane dyes, such as Die-I and Sito-9 live cell imaging.

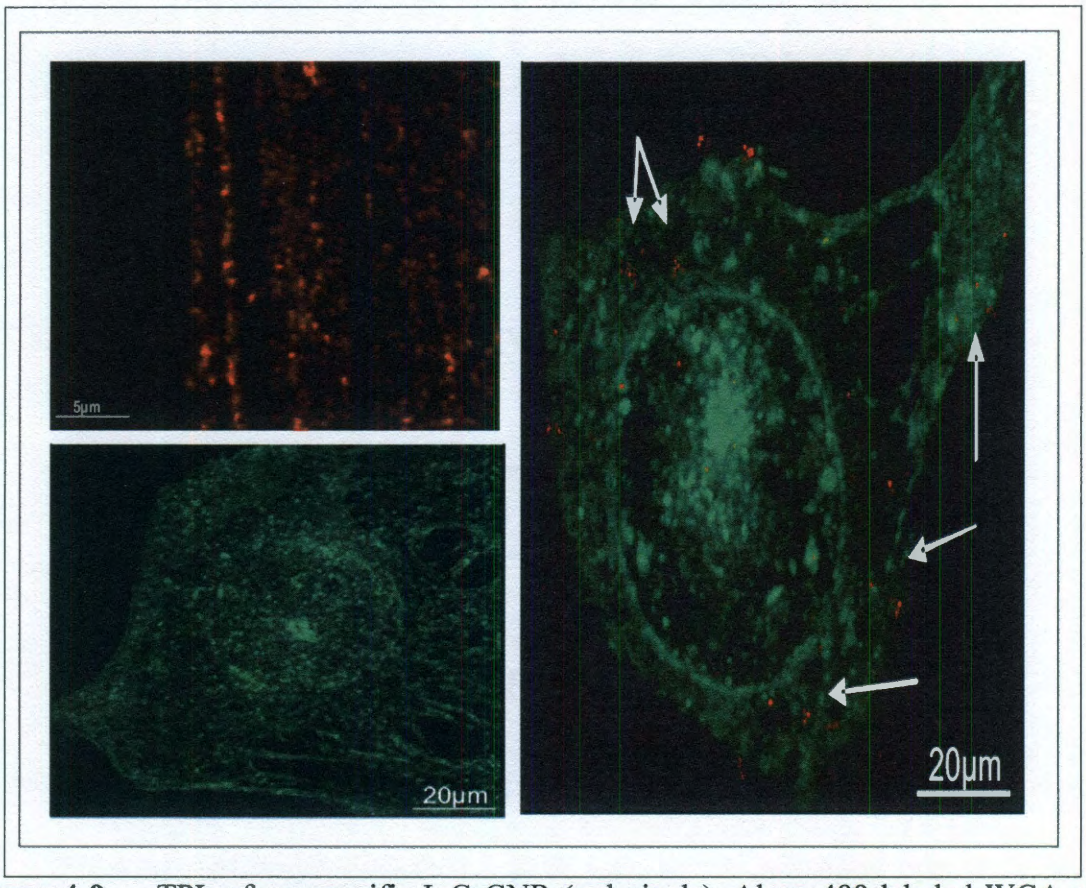

Figure 4-9. TPL of nonspecific IgG-GNR (red pixels). Alexa-488 labeled WGA was added to live bladder mesenchymal UC3 cells cell 10 min before fixation Alexa-488 WGA with C225-GNR seen in red (far right), and Alexa488-WGA in green no GNR (lower left).

Confocal microscopy images of KU7 cells exposed to the t-GNR-PEG-c-Ab conjugated to the EGFR/C225-Fluorescein isothiocyanate (FITC) and controls are shown in **Figure 4-10**. EGFR/C225 was chosen as port of entry into the cells because its expression level is high in bladder cancer cells compared with normal urothelium. EGFR-mediated cell internalization occurs through a well-known mechanism involving the endosomal pathway which is a form of active transport. [120-123,126]

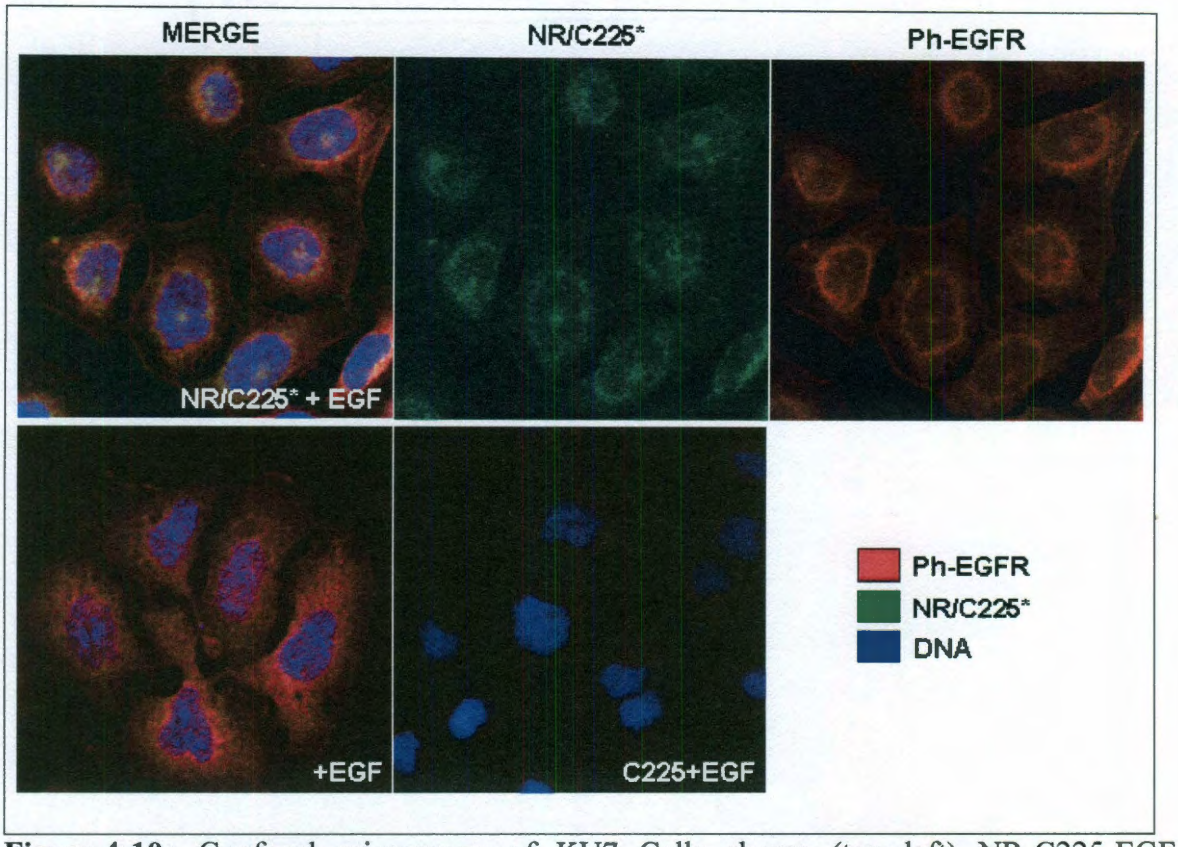

Figure 4-10. Confocal microscopy of KU7 Cells shown (top left) NR-C225-EGF, (middle top) NR-C225, (top right) Phenyl red-EGFR, (bottom left) EGF control, (bottom right) C225-EGF control. Green images shown GNR binding in KU7 cells with and without EGF, DNA is shown in blue.

To compare the FITC-siRNA transfection and its ability to achieve endosomal release and gene silencing, we used a charge neutral plasmonic transfection system composed of the FITC labeled t-GNR-siRNA-PEG-c-Ab bound to C225 and compared it

to a cationic liposome-based Dharmafect (DF-1) transfection reagent from Dharmacon shown in **Figure 4-11.** Lipid-mediated transfection which is common to siRNA delivery is most often used, however, it can be problematic as many cell types may suffer from chemical, cytotoxic and immunological shock in reaction to exposure to cationic lipid reagents. [96,102,119] This often makes it necessary to use DF-1 reagents, which overcome these limitations in hard-to-transfect cell types. [127] DF-1 allows for the successful delivery of GAPDH-siRNA-FITC with low toxicity, and can achieve robust siRNA uptake for gene silencing. Our results showed that lipid transfection was minimally successful in delivering GAPDH-siRNA-FITC into the cells, however, this did not compare to the plasmonic FITC labeled t-GNR-siRNA-PEG-c-Ab complex which evidenced higher internalized bioconjugates, **Figure 4-11** lower left. The controls of the GNR-siRNA-FITC and siRNA-FITC show no internalization, when compared to the t-GNR-siRNA-PEG-c-C225 bioconjugates. These results indicated that the physical and chemical interactions between the t-GNR-PEG-c-C225 complex and the GAPDH-siRNA-FITC could be easily manipulated within physiological temperature ranges.

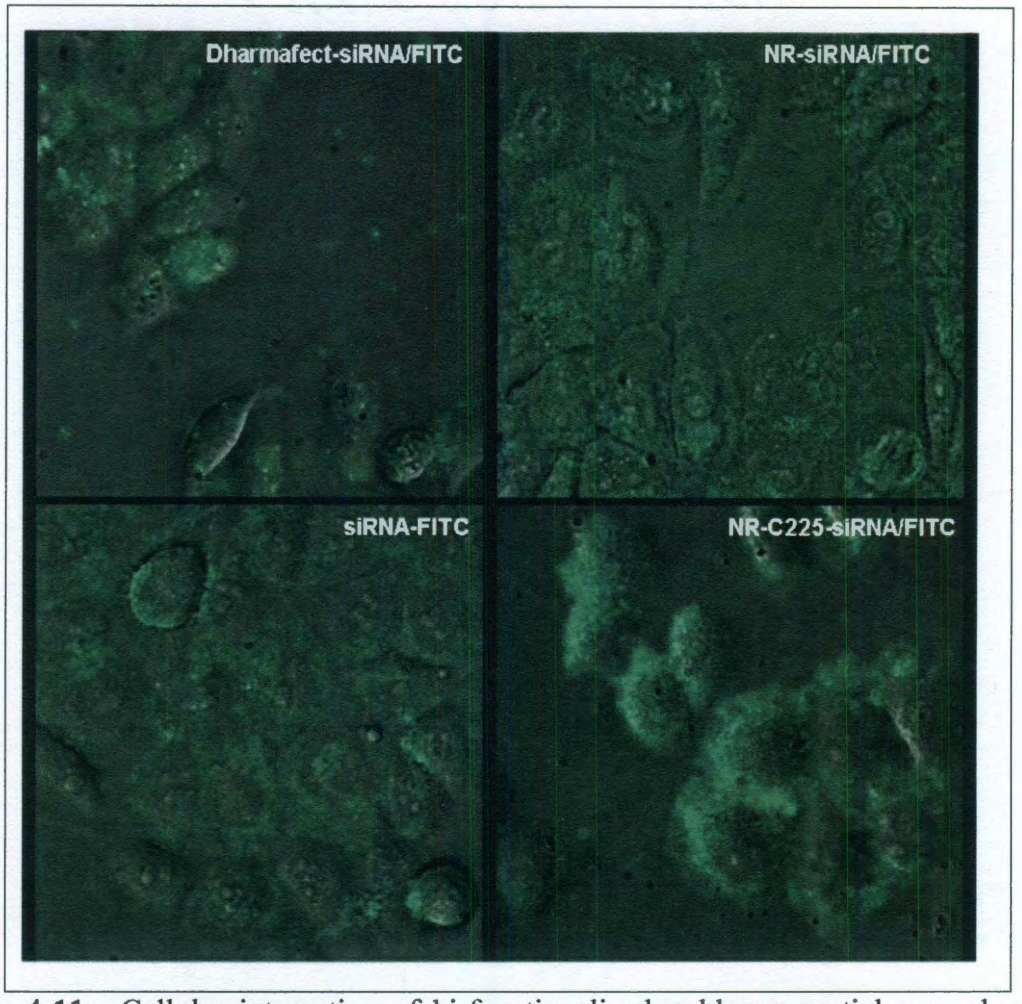

Figure 4-11. Cellular integration of bi-functionalized gold nanoparticles as observed by confocal. The images of live cells were taken 12 hrs post-transfection using a 40x objective-Zeiss Observer-Z1.

4.4.7 Plasmonic Vector Trapping/Release

The t-GNR-PEG-c-Ab plasmonic vector kinetically trapped the GAPDH-siRNA-FITC in the PEG polymer layer, to protect the GAPDH-siRNA-FITC for its internalization and release inside the cell. To overcome additional physical barriers such as receptor-mediated endocytosis, a PEG shield was included to reduce nonspecific binding and C225 was used as the targeting antibody. The PEG-COOH end groups were then salt screened using the cations from the PBS buffer leading to salt bridge formation.

[125,128-129] A thermally induced gradient from the heating block then allowed for the kinetic trapping of the GAPDH-siRNA-FITC material. This combined temperature increase and salt screening was able to alter the structure of the PEG-COO- layers by changing the H-bonding network, and with it the degree of hydration.[128-129] Increased temperature activated the flow, or pour point of the PEG which occurs around the glass transition temperature of 35-40-45°C, leading to a liquid-like structure, with melting of the PEG polymer which occurs at 50-60°C, being avoided.[128-129] An attractive force between PEG chains occurs at 43°C leading to a reduction in the repulsive forces, which decreases the number of bound water molecules onto the inert hydrophilic polymer chains. Structural changes brought about by heat also affect the GAPDH-siRNA-FITC, which likewise undergoes dehydration, and structure rearrangement. The combined temperature and salt screening allows for the encapsulation of the siRNA. With an equilibration to 25°C the hydrophilic PEG chains are again able to bind water molecules, thereby shielding the encapsulated siRNA. Numerous methods such as temperature, laser heating, ionization, salt, and pH can be used to bring about structural changes to the PEG layers which alter the number of water cages and degree of hydration.[128-129] This can be of interest for the drug delivery of encapsulated pharmaceutical agents.

4.4.8 NIR Laser Heating

Following incubation, the GNR underwent receptor-based endocytosis into its targeted intracellular compartments, and were irradiated by a non-collimated NIR laser light to locally heat and release the genetic material within the cells. Activation of the PEG pour point would cause the trapped GAPDH-siRNA-FITC to be released into a medium were electrostatic screening from a high salt media was lacking. This allowed

the GAPDH-siRNA-FITC to be released into the cytoplasm and ensuing cytosol for subsequent protein inactivation through mRNA silencing. The laser output power was optimized to accomplish the desired degree of NIR irradiation and subsequent plasmon heating by the GNR, namely 45°C, which in turn controls the extent of the GAPDH-siRNA-FITC release. Laser settings can be optimized such that the target tissues and therapeutic oligonucleotide molecules are not negatively affected.[104] On the basis of the preliminary results, we show that the photothermal strategy is able to successfully release GAPDH-siRNA-FITC from the PEG-NR-C225 complexes, at specific power density parameters and irradiance settings, this is shown in **Figure 4-11**.

4.4.9 RT-PCR

To determine whether the RNA released from the GNR after NIR exposure is functional, we exposed cells to GAPDH-siRNA-FITC which was targeted to the GAPDH gene, and exposed the cells to a low-power non-collimated NIR laser. After 48 hours we measured the GAPDH-mRNA expression by real-time RT-PCR. The GAPDH gene is ideal for optimizing siRNA transfection conditions by helping to confirm that transfection procedures and cell cultures support gene silencing. Furthermore, GAPDH expression is actively correlated with tissues and cell types that differentially express the EGFR receptor. The down-regulation of the GAPDH gene is highly relevant for bladder cancer as it is up-regulated in malignant cancer cells and can be down-regulated by cancer based therapies. Changes to the expression of the GAPDH-mRNA are therefore highly relevant to bladder cancer-based gene therapies. The results shown in **Figure 4-12** demonstrate that NIR exposure resulted in a minimal reduction of GAPDH expression with no cell death evidenced, whereas cells that were not exposed to NIR showed no

change in GAPDH levels (**Figure 4-12, white boxes**). This signifies that some gene silencing of GAPDH-mRNA is occurring with the laser-treated, FITC labeled t-GNR-siRNA-PEG-c-Ab particles. The FITC labeled t-GNR-siRNA-PEG-c-Ab conjugates were able to confirm that the transfection procedure achieved moderate gene silencing following laser GAPDH-siRNA-FITC delivery inside the bladder cancer cell lines, without achieving any cell damage. Therefore, future studies that are more optimized would be needed to silence the gene further.

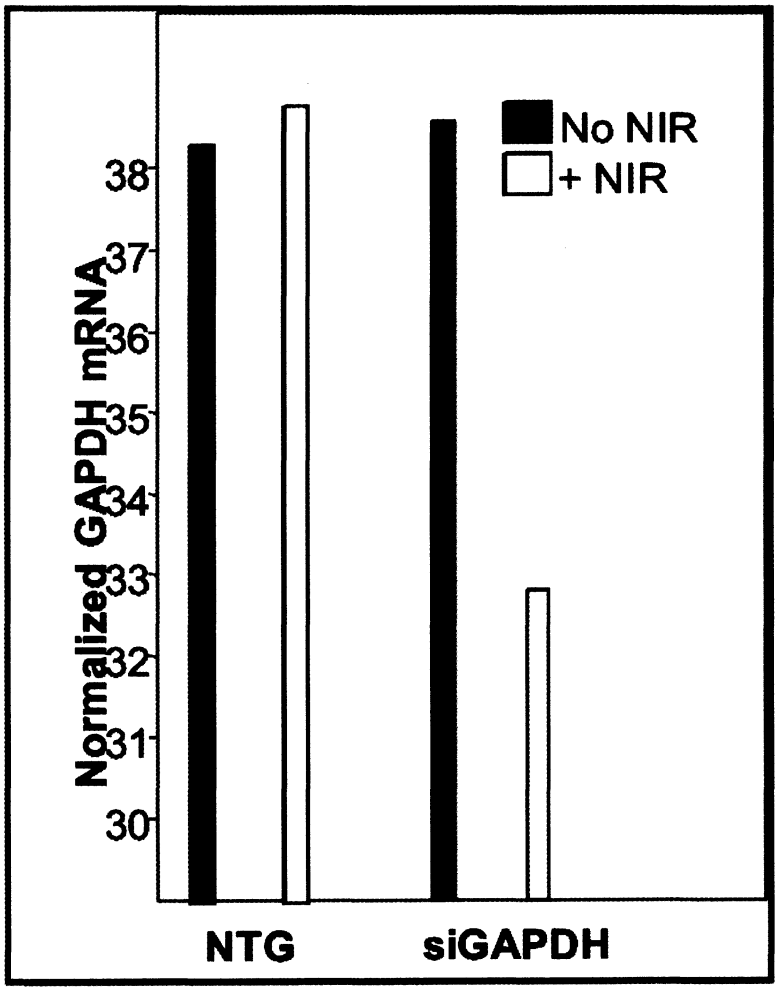

Figure 4-12. Measurement of GAPDH-mRNA using real-time RT-PCR. KU7 cells were incubated for 48 hours with non-targeting Glyceraldehyde (NTG) and GAPDH targeted siRNA-FITC that was housed with the t-GNR-PEG-Ab with C225. The RNA was extracted and GAPDH-mRNA was measured. The mRNA normalization was done by measurement of 18S ribosomal RNA (internal control).

4.4.10 Plasmonic Vector Discussion

The goal of gene therapy is to introduce foreign genes into somatic cells and provide additional biological functions to stop the production or function of detrimental genes. This can be achieved using various vector based delivery methods. Compared to viral vectors, synthetic gene-delivery systems (such as liposomes and polymers) offer several advantages, including ease of production and a reduced risk of cytotoxicity and

immunogenicity, but their use is often limited by the relatively low transfection efficiency and nonspecificity. These problems are mainly due to the difficulty in controlling their properties at the nanoscale. Our application used a targeted non-viral gene delivery system based on biocompatible GNR plasmonic vector that could simultaneously trap the GAPDH-siRNA-FITC, and used the targeting of C225 antibodies to ensure the delivery and cytoplasmic release of the functional siRNA material inside the endosomal compartments. This approach allowed for the precise control of composition, size and multifunctionality of the gene delivery system, which could be assayed with microscopic, fluorescence, zeta potential, TPL, and RT-PCR methods. The FITC labeled t-GNR-siRNA-PEG-c-Ab vector, whose size is below 100 nm, used a PEG shield to enhance the GAPDH-siRNA-FITC delivery. Furthermore the PEG-C225 antibody targeted delivery vehicle allowed for receptor-mediated endocytosis into its appropriate endosomal compartment. The GAPDH-siRNA-FITC was trapped by temperature increases in the hydrophilic, salt screened PEG layer resulting from the use of a heating block, while the release of the siRNA resulted from laser treatment and subsequent NIR plasmons in the GNR. The resulting plasmonic vector was able to achieve successful delivery when compared with the DF-1 liposome vector and modest gene silencing of the GADPH housekeeping genes was confirmed by RT-PCR. Thus, we have produced a proof of concept experiment where a suitable transfection with a targeted plasmonic FITC labeled t-GNR-siRNA-PEG-c-Ab vector can be further optimized to ensure silencing of the GADPH housekeeping gene, as well as other bladder cancer associated genes.

4.5 Conclusion

An untreatable form of bladder cancer was studied using the t-GNR-PEG-c-Ab bioconjugates with C225 antibody. The t-GNR-PEG-c-Ab were used to create as plasmonic vector that housed a GAPDH-FITC labeled siRNA, termed GAPDH-siRNA-FITC, which was included within a Luciferase based plasmid. A salt based electrostatic heating method was used to trap the GAPDH-siRNA-FITC from the PEG layer by activating the PEG polymer pour point, while a laser based heating system was used for in vitro release inside cancer cells. The down regulation of the GAPDH gene was targeted by the siRNA, as GAPDH has been shown to be up-regulated in many cancers and down-regulated by chemotherapeutic drugs. Cell culture, and subsequent imaging by TEM, TPL and confocal microscopy were used to view the internalized conjugates, and RT-PCR were used to determine if the release of the GAPDH-siRNA caused a reduction in the expression of GAPDH-mRNA. Plasmonic gene silencing of the gene by the GAPDH-siRNA was then compared to a lipid based Dharmafect control in terms of transfection ability, and suggested that the plasmonic vector was a more optimal choice.

CHAPTER 5

Conclusions

The material surface properties of gold nanoparticles govern interactions at visible and NIR wavelengths, which lead to the ability to manipulate light at the nanometer scale. The gold nanoparticles can then manipulate light through resonant collective oscillations of the conduction electrons, which are LSPR that result in strong optical absorption and scattering, at visible and NIR wavelengths. This can be of considerable interest in biomedical applications, since the plasmon resonances can affect localized heating and light scattering, which can benefit biological systems that require relatively inert gold nanoparticle based therapies. The CTAB-gold absorption is quite strong and it is often difficult to remove the bound CTAB, which is problematic for in vivo, cell-based applications. Chloroform extractions of CTAB showed that a critical CTAB/GNR ratio is needed in order to maintain colloidal stability of the GNR, this was found to be 740,000:1. $mPEG_{(5000)}$-SH functionalization was shown to displace the CTAB while polyelectrolytes can wrap the CTAB present on the surface of the GNR. Both the $mPEG_{(5000)}$-SH and PSS stabilization methods were effective methods by which to stabilize the GNR. However, the $mPEG_{(5000)}$-SH covalent functionalization method leads to higher yields and more monodisperse GNR samples. Yet in spite of $mPEG_{(5000)}$-SH covalent functionalization methods, some residual CTAB remains bound to the particles, as shown by the MS data. Nevertheless at these CTAB concentrations, which are below 10 μM, cell cytotoxic effects are typically absent.

GNR targeting experiments were successfully carried out with stable bioconjugates that resulted from the use of NHS-EDC chemistry and a bifunctional PEG with thiol and carboxyl end groups. This resulted in the formation of an amide bond between the linker and antibody, and the strong-gold thiol bond between the linker and GNR. The carbodiimide linking strategy was successful in producing carboxy-terminal PEGylated GNR that could undergo successful bioconjugation with antibodies. Furthermore this conjugation strategy was reproducible despite the strength of the original gold-CTAB interaction. Zeta potential measurements were able to confirm changes to the intended surface chemistry, leading to negative potentials for the carboxy-terminated GNR conjugates and near-neutral charge for the zwitterionic antibody protein GNR bioconjugates. Fluorimetric assays suggested that two antibodies per nanorod were present and Nanoparticle ELISA assay demonstrated that a large fraction of these bound antibodies were active. Successful in vitro targeting of the GNR bioconjugates was shown in two cell types using the HER-2 and C225 antibodies. TPL and confocal reflectance were then used to successfully image the t-GNR-PEG-c-Ab particles that were successfully internalized by the cells.

Our gene therapy application used a targeted nonviral gene-delivery system based on biocompatible GNR that could simultaneously trap GAPDH-siRNA-FITC and used the targeting of C225 antibodies to ensure the delivery and cytoplasmic release of the functional siRNA material. The FITC labeled t-GNR-siRNA-PEG-c-Ab vector, used a PEG shield to enhance the GAPDH-siRNA-FITC delivery. Furthermore the PEG-C225 antibody targeted delivery vehicle allowed for receptor-mediated endocytosis into its appropriate endosomal compartment. The GAPDH-siRNA-FITC was trapped by

temperature increases in the hydrophilic salt screened PEG layer resulting from the use of a heating block, while the release of the siRNA resulted from laser treatment and subsequent NIR plasmons in the GNR. The resulting plasmonic vector was able to achieve successful delivery when compared with the DF-1 liposome vector and modest gene silencing of the GADPH housekeeping genes was confirmed by RT-PCR. Thus, we have produced a proof of concept experiment where a suitable transfection with a targeted plasmonic FITC labeled t-GNR-siRNA-PEG-c-Ab vector can be further optimized to ensure silencing of the GADPH housekeeping gene, as well as other bladder cancer associated genes. This approach allowed for the precise control of composition, size and multifunctionality of the gene-delivery system, which could be assayed with microscopic, fluorescence, zeta potential, TPL, and RT-PCR methods.

REFERENCES

[1] Daniel, M. and Astruc, D., 2004: Gold nanoparticles: assembly, supramolecular chemistry, quantum-size-related properties, and applications toward biology, catalysis, and nanotechnology. *Chemical Reviews*, **104(1)**, 293-346.

[2] Link, S. and El-Sayed, M.A., 1999: Size and temperature dependence of the plasmon absorption of colloidal gold nanoparticles. *Journal of Physical Chemistry B*, **103**, 4212-4217.

[3] Burda, C., Chen, X., Narayan, R., El-Sayed, M.A., 2005: Chemistry and properties of nanocrystals of different shapes. *Chemical Reviews*, **105(4)**, 1025-1102.

[4] Mulvaney, P., 1996: Surface plasmon spectroscopy of nanosized metal particles. *Langmuir*, **12(3)**, 788-800.

[5] Perez-Juste, J., Pastoriza-Santos, I., Liz-Marzan, L., Mulvaney, P., 2005: Gold nanorods: synthesis, characterization and applications. *Coordination Chemistry Reviews*, **249(17-18)**, 1870-1901.

[6] Nehl, C. and Hafner, J., 2008: Shape-dependent plasmon resonances of gold nanoparticles. *Journal of Materials Chemistry*, **18(21),** 2415-2419.

[7] Kelly, K., Coronado, E., Zhao, L.L., Schatz, G.C., 2003: The optical properties of metal nanoparticles: the influence of size, shape, and dielectric environment. *Journal of Physical Chemistry B-Condensed Phase,* **107(3)**, 668-677.

[8] Liz-Marzan, L.M., 2006: Tailoring surface plasmons through the morphology and assembly of metal nanoparticles. *Langmuir,* **22(1)**, 32-41.

[9] Pileni, M., 2007: Control of the Size and Shape of Inorganic Nanocrystals at Various Scales from Nano to Macrodomains. *Journal of Physical Chemistry C*, **111(26)**, 9019-9038.

[10] Mulvaney, P., 2001: Not all that's gold does glitter. *Materials Research Society Bulletin (USA)*, **26(12)**, 1009-1014.

[11] Haes, A.J., Stuart, D.A., Nie, S., Van Duyne, R.P.V., 2004: Using solution-phase nanoparticles, surface-confined nanoparticle arrays and single nanoparticles as biological sensing platforms. *Journal of Fluorescence*, **14(4)**, 355-367.

[12] Cognet, L. and Lounis, B., 2008: Ultra-sensitive detection of individual gold nanoparticles: spectroscopy and applications to biology. *Gold Bulletin*, **41(2)**, 139-146(8).

[13] Sau, T., Murphy, C., 2004: Seeded high yield synthesis of short Au nanorods in aqueous solution. *Langmuir*, **20(15)**, 6414-6420.

[14] Murphy, C.J., Sau, T.K., Gole, A.M., Orendorff, C.J., Gao, J., Gou, L., Hunyadi, S.E., Li, T., 2005: Anisotropic metal nanoparticles: Synthesis, assembly, and optical applications. *Journal of Physical Chemistry B*, **109(29)**, 13857-13870.

[15] Jana, N.R., Gearheart, L., Murphy, C.J., 2001: Seeding growth for size control of 5-40 nm diameter gold nanoparticles. *Langmuir*, **17(22)**, 6782-6786.

[16] Takahashi, H., Niidome, Y., Yamada, S., 2005: Controlled release of plasmid DNA from gold nanorods induced by pulsed near-infrared light. *Chemical Communications,* **17**, 2247-2249.

[17] Roca, M. Haes, A., 2008: Probing cells with noble metal nanoparticle aggregates. *Nanomedicine*, **3(4)**, 555-565.

[18] Connor, E.E., Mwamuka, J., Gole, A., Murphy, C.J., Wyatt, M.D., 2005: Gold nanoparticles are taken up by human cells but do not cause acute cytotoxicity. *Small*, **1(3)**, 325-327.

[19] Park, H.-S., Agarwal, A., Kotov, N.A., Lavrentovich, O., 2008: Controllable side-by-side and end-to-end assembly of Au nanorods by lyotropic chromonic materials. *Langmuir*, **24(24),** 13833-13837.

[20] Szymula, M., Narkiewicz-Michalek, J., 2003: Atmospheric and electrochemical oxidation of ascorbic acid in anionic, nonionic and cationic surfactant systems. *Colloidal Polymer Science*, **281**, 1142-1148.

[21] Wang, C., Wang, T., Ma, Zhanfang, Su, Z., 2005: pH-tuned synthesis of gold nanostructures from gold nanorods with different aspect ratios. *Nanotechnology*, **16**, 2555-2560.

[22] Weichold, O., Dederichs, T., Möller, M., 2007: The dispersion-stability diagram of boehmite nanoparticles in aqueous AOT solutions. *Journal of Colloid and Interface Science,* **306(2)**, 300-306.

[23] Funston, A.M., Novo, C., Davis, T.J., Mulvaney, P., 2009: Plasmon coupling of gold nanorods at short distances and in different geometries. *Nano Letters*, **9(4)**, 651-1658.

[24] Dai, Q., Coutts, J., Zou, J., Huo, Q., 2008: Surface modification of gold nanorods through a place exchange reaction inside an ionic exchange resin. *Chemical Communications*, **25**, 2858-2860.

[25] Alper, J.D., Schmidt, A.J., Chiesa, M., Chen, G., Schifferli, K.H., Das, S.K., 2008: Probing the Gold Nanorod− Ligand− Solvent Interface by Plasmonic Absorption and Thermal Decay. *The Journal of Physical Chemistry C*, **112**, 13320-13323.

[26] Sun, X., L. Yang, Chaikof, E., 2008: Chemoselective immobilization of biomolecules through aqueous Diels–Alder and PEG chemistry. *Tetrahedron Letters*, **49(16)**, 2510-2513.

[27] Kumar, S., Aaron, J., Sokolov, K., 2008: Directional conjugation of antibodies to nanoparticles for synthesis of multiplexed optical contrast agents with both delivery and targeting moieties. *Nature Protocols*, **3(2)**, 314-320.

[28] Takahashi, H., Niidome, T., Kawano, T., Yamada, S., Niidome, Y., 2008: Surface modification of gold nanorods using layer-by-layer technique for cellular uptake. *Journal of Nanoparticle Research*, **10(1)**, 221-228.

[29] Qian, X., Peng, X.H., Ansari, D.O., Yin-Goen, Q., Chen, G.Z., Shin, D.M., Yang, L., Young, A.N., Wang, M.D., Nie, S., 2008: In vivo tumor targeting and spectroscopic detection with surface-enhanced Raman nanoparticle tags. Nature Biotechnology, **26(1)**, 83-90.

[30] Liao, H., Hafner, J. H., 2005: Gold nanorod bioconjugates. *Chemistry of Materials*, **17**, 4636-4641.

[31] Gole, A.; Murphy, C. J., 2005: Polyelectrolyte-coated gold nanorods: Synthesis, characterization and immobilization. *Chemistry of Materials*, **17(6)**, 1325-1330.

[32] Sun, Z. H.; Ni, W. H.; Yang, Z.; Kou, X. S.; Li, L.; Wang, J. F., 2008: pH-controlled reversible assembly and disassembly of gold nanorods. *Small*, **4(9)**, 1287-1292.

[33] Niidome, Y.; Honda, K.; Higashimoto, K.; Kawazumi, H.; Yamada, S.; Nakashima, N.; Sasaki, Y.; Ishida, Y.; Kikuchi, J., 2007: Surface modification of gold nanorods with synthetic cationic lipids. *Chemical Communications*, **36,** 3777-3779.

[34] Pirollo, K. F.; Chang, E. H., 2008: Does a targeting ligand influence nanoparticle tumor localization or uptake? *Trends in Biotechnology*, **26(10)**, 552-558.

[35] Javier, D. J.; Nitin, N.; Roblyer, D. M.; Richards-Kortum, R., 2008: Metal-based nanorods as molecule-specific contrast agents for reflectance imaging in 3D tissues. *Journal of Nanophotonics*, **2**, 023506.

[36] Tong, L.; Zhao, Y.; Huff, T. B.; Hansen, M. N.; Wei, A.; Cheng, J. X., 2007: Gold nanorods mediate tumor cell death by compromising membrane integrity. *Advanced Materials,* **19(20)**, 3136-3141.

[37] Popovtzer, R.; Agrawal, A.; Kotov, N. A.; Popovtzer, A.; Balter, J.; Carey, T. E.; Kopelman, R., 2008: Targeted Gold Nanoparticles Enable Molecular CT Imaging of Cancer. *Nano Letters*, **8(12)**, 4593-4596.

[38] Huang, X. H.; El-Sayed, I. H.; Qian, W.; El-Sayed, M. A., 2007: Cancer cells assemble and align gold nanorods conjugated to antibodies to produce highly enhanced, sharp, and polarized surface Raman spectra: A potential cancer diagnostic marker. *Nano Letters*, **7(6)**, 1591-1597.

[39] Huang, X. H.; El-Sayed, I. H.; Qian, W.; El-Sayed, M. A., 2006: Cancer cell imaging and photothermal therapy in the near-infrared region by using gold nanorods. *Journal of the American Chemical Society,* **128(6),** 2115-2120.

[40] Hu, R.; Yong, K. T.; Roy, I.; Ding, H.; He, S.; Prasad, P. N., 2009: Metallic Nanostructures as Localized Plasmon Resonance Enhanced Scattering Probes for Multiplex Dark-Field Targeted Imaging of Cancer Cells. *Journal of Physical Chemistry C*, **113(7)**, 2676-2684.

[41] Hauck, T. S.; Ghazani, A. A.; Chan, W. C. W., 2008: Assessing the effect of surface chemistry on gold nanorod uptake, toxicity, and gene expression in mammalian cells. *Small*, **4(1)**, 153-159.

[42] Durr, N. J.; Larson, T.; Smith, D. K.; Korgel, B. A.; Sokolov, K.; Ben-Yakar, A., 2007: Two-photon luminescence imaging of cancer cells using molecularly targeted gold nanorods. *Nano Letters*, **7(4)**, 941-945.

[43] Ding, H.; Yong, K. T.; Roy, I.; Pudavar, H. E.; Law, W. C.; Bergey, E. J.; Prasad, P. N., 2007: Gold nanorods coated with multilayer polyelectrolyte as contrast agents for multimodal imaging. *Journal of Physical Chemistry C*, **111(34)**, 12552-12557.

[44] Agarwal, A.; Huang, S. W.; O'Donnell, M.; Day, K. C.; Day, M.; Kotov, N.; Ashkenazi, S., 2007: Targeted gold nanorod contrast agent for prostate cancer detection by photoacoustic imaging. *Journal of Applied Physics*, **102(6)**, 064701-064701-4.

[45] Sirk, K.M., Saleh, N.B., Phenrat, T., Kim, H.-J., Dufour, B., Ok, J., Golas, P.L., Matyjaszewski, K., Lowry, G.V., Tilton, R.D., 2009: Effect of adsorbed

polyelectrolytes on nanoscale zero valent iron particle attachment to soil surface models. *Environmental Science & Technology*, **43**, 3803-3808.

[46] Kong, H.J., Bike, S.G., Li, V.C., 2006: Electrosteric stabilization of concentrated cement suspensions imparted by a strong anionic polyelectrolyte and non-ionic polymer. *Cement and Concrete Research*, **36**, 842-850.

[47] Saleh, N., Phenrat, T., Sirk, K., Dufour, B., Ok, J., Sarbu, T., Matyjaszewski, K., Tilton, R.D., Lowry, G.V., 2005: Adsorbed triblock copolymers deliver reactive iron nanoparticles to the oil/water interface. *Nano Letters*, **5**, 2489-2494.

[48] Pierrat, S., Zins, I., Breivogel, A., Sonnichsen, C., 2007: Self-assembly of small gold colloids with functionalized gold nanorods. *Nano Letters*, **7(2)**, 259-263.

[49] Ferhan, A.R., Guo, L., Kim, D.-H., 2010: Influence of ionic strength and surfactant concentration on electrostatic surfacial assembly on cetyltrimethylammonium bromide-capped gold nanorods on fully immersed glass. *Langmuir*, **26(14)**, 12433-12442.

[50] Gutig, C., Grady, B., Striolo, A., 2008: Experimental studies on the adsorption of two surfactants on solid-aqueous interfaces: adsorption isotherms and kinetics. *Langmuir*, **24(9)**, 4806-4816.

[51] Smith, D., Korgel, B., 2008: The importance of the CTAB surfactant on the colloidal seed-mediated synthesis of gold nanorods. *Langmuir*, **24(3)**, 644-649.

[52] Takahashi, H., Niidome, T., Nariai, A., Niidome, Y., Yamada, S., 2006: Gold Nanorod-sensitized Cell Death: Microscopic Observation of Single Living Cells Irradiated by Pulsed Near-infrared Laser Light in the Presence of Gold Nanorods. *Chemistry Letters*, **35(5)**, 500-501.

[53] Huff, T., Hansen, M.N., Tong, L., Zhao, Y., Wang, H., Zweifel, D.A., Cheng, J.-X., Wei, A., 2007: Plasmon-resonant nanorods as multimodal agents for two- photon luminescent imaging and photothermal therapy. *Progress in Biomedical Optics and Imaging*, **8(25)**, 64280D.1-64280D.9.

[54] Mukherjee, P., Bhattacharya, R., Bone, N., Lee, Y.K., Patra, C.R., Wang, S., Lu, L., Secreto, C., Banerjee, P.C., Yaszemski, M.J., Kay, N.E., Mukhopadhyay, D., 2007: Potential therapeutic application of gold nanoparticles in B-chronic lymphocytic leukemia (BCLL): enhancing apoptosis. *Journal of Nanobiotechnology,* **5(1)**, 1-13.

[55] Grabarek, Z.; Gergely, J., 1990: Zero-Length Crosslinking Procedure with the Use of Active Esters. *Analytical Biochemistry*, **185(1)**, 131-135.

[56] Hermanson, G. T., 1996: *Bioconjugate Techniques*. **1st ed.**; Academic Press, 785.

[57] Jain, P. K.; Huang, X. H.; El-Sayed, I. H.; El-Sayed, M. A., 2008: Noble Metals on the Nanoscale: Optical and Photothermal Properties and Some Applications in Imaging, Sensing, Biology, and Medicine. *Accounts of Chemical Research*, **41(12)**, 1578-1586.

[58] Murphy, C. J.; Gole, A. M.; Stone, J. W.; Sisco, P. N.; Alkilany, A. M.; Goldsmith, E. C.; Baxter, S. C., 2008: Gold Nanoparticles in Biology: Beyond Toxicity to Cellular Imaging. *Accounts of Chemical Research*, **41(12)**, 1721-1730.

[59] Lal, S.; Clare, S. E.; Halas, N. J., 2008: Nanoshell-Enabled Photothermal Cancer Therapy: Impending Clinical Impact. *Accounts of Chemical Research*, **41(12)**, 1842-1851.

[60] Bikram, M.; West, J. L., 2008: Thermo-responsive systems for controlled drug delivery. *Expert Opinion on Drug Delivery*, **5(10)**, 1077-1091.

[61] Tong, L.; Wei, Q. S.; Wei, A.; Cheng, J. X., 2009: Gold Nanorods as Contrast Agents for Biological Imaging: Optical Properties, Surface Conjugation and Photothermal Effects. *Photochemistry and Photobiology*, **85(1)**, 21-32.

[62] Hleb, E. Y.; Hu, Y.; Drezek, R. A.; Hafner, J. H.; Lapotko, D. O., 2008: Photothermal bubbles as optical scattering probes for imaging living cells. *Nanomedicine*, **3(6)**, 797-812.

[63] Pirollo, K. F.; Chang, E. H., 2008: Does a targeting ligand influence nanoparticle tumor localization or uptake? *Trends in Biotechnology*, **26(10)**, 552-558.

[64] Farokhzad, O.C., Jon, S., Khademhosseini, A., Tran, T.N., Lavan, D.A., Langer, R., 2004: Nanoparticle-Aptamer Bioconjugates A New Approach for Targeting Prostate Cancer Cells. *Cancer Research*, **64(21),** 7668-7672.

[65] Kynclova, E., Elsner, E., Kopf, A., Hawa, G., Schalkhammer, T., Pittner, F., 1996: Novel method for coupling of poly (ethyleneglycol) to carboxylic acid moieties of proteins. *Journal of Molecular Recognition*, **9(5-6)**, 644-651.

[66] Wang, H.; Huff, T. B.; Zweifel, D. A.; He, W.; Low, P. S.; Wei, A.; Cheng, J.-X., 2005: In vitro and in vivo two-photon luminescence imaging of single gold nanorods. *Proceedings of the National Academy of Sciences of the United States of America*, **102(44)**, 15752-15756.

[67] Dougherty, G.M., Rose, K.A., Tok, J.B., Pannu, S.S., Chuang, F.Y., Sha, M.Y., Chakarova, G., Penn, S.G., 2008: The zeta potential of surface-functionalized metallic nanorod particles in aqueous solution. *Electrophoresis*, **29(5)**,1131-1139.

[68] Seidl, J., Knuechel, R., Kunz-Schughart, L.A., 1999: Evaluation of Membrane Physiology Following Fluorescence Activated or Magnetic Cell Separation. *Cytometry*, **36(2)**, 102-111.

[69] Geoghegan, W. D.; Ackerman, G. A., 1977: Adsorption of Horseradish-Peroxidase, Ovomucoid and Antiimmunoglobulin to Colloidal Gold for Indirect Detection of Concanavalin-a, Wheat-Germ Agglutinin and Goat Antihuman Immunoglobulin-G on Cell-Surfaces at Electron-Microscopic Level - New Method, Theory and Application. *Journal of Histochemistry & Cytochemistry*, **25(11)**, 1187-1200.

[70] Kah, J., Olivo, M.C., Lee, C.G.L., Sheppard, C.J.R., 2008: Molecular contrast of EGFR expression using gold nanoparticles as a reflectance-based imaging probe. *Molecular and Cellular Probes*, **22(1)**, 14-23.

[71] Lowery, A. R.; Gobin, A. M.; Day, E. S.; Halas, N. J.; West, J. L., 2006: Immunonanoshells for targeted photothermal ablation of tumor cells. *International Journal of Nanomedicine*, **1(2)**, 149-154.

[72] Nikoobakht, B., El-Sayed, M.A., 2001: Evidence for bilayer assembly of Cationic surfactants on the surface of gold Nanorods. *Langmuir* **17(20)**, 6368-6374.

[73] Liao, H., Nehl, C.L., Hafner, J.H., 2006: Biomedical applications of plasmon resonant metal nanoparticles. *Nanomedicine*, **1,** 201–208.

[74] Jain, P.K., Huang, X.H., El-Sayed, I.H., El-Sayed, M.A., 2008: Noble metals on the nanoscale: optical and photothermal properties and some applications in imaging, sensing, biology, and medicine. *Accounts of Chemical Reseach,* **41,** 1578–15786.

[75] Murphy, C.J., Gole, A.M., Stone, J.W., Sisco, P.N., Alkilany, A., Goldsmith, E.C., Baxter, S.C., 2008: Gold nanoparticles in biology: beyond toxicity to cellular imaging. *Accounts of Chemical Reseach,* **41,** 1721–1730.

[76] Lal, S., Clare, S.E., and Halas, N.J., 2008: Nanoshell-enabled photothermal cancer therapy: impending clinical impact. *Accounts of Chemical Reseach,* **41,** 1842–1851.

[77] Bikram, M., West, J.L., 2008: Thermo-responsive systems for controlled drug delivery. *Expert Opinion in Drug Delivery,* **5,** 1077–1091.

[78] Tong, L., Wei, Q.S., Wei, A., Cheng, J.X., 2009: Gold nanorods as contrast agents for biological imaging: optical properties, surface conjugation and photothermal effects. *Photochemistry and Photobioliogy,* **85,** 21–32.

[79] Hleb, E.Y., Hu, Y., Drezek, R.A., Hafner, J.H., Lapotko, D.O., 2008: Photothermal bubbles as optical scattering probes for imaging living cells. *Nanomedicine,* **3,** 797–812.

[80] Jana, N.R., Gearheart, L., Murphy, C.J., 2001: Wet chemical synthesis of high aspect ratio cylindrical gold nanorods. *Journal of Physical Chemistry* B, **105** 4065–4067.

[81] Sau, T.K., Murphy, C.J., 2004: Seeded high yield synthesis of short Au nanorods in aqueous solution. *Langmuir*, **20** 6414–6420

[82] Nikoobakht, B., El-Sayed, M.A., 2003: Preparation and growth mechanism of gold nanorods (NRs) using seed-mediated growth method. *Chemistry of Materials,* **15** 1957–1962.

[83] Rostro-Kohanloo, B.C., Bickford, L.R., Payne, C.M., Day, E.S., Anderson, L.J.E., Zhong, M., Lee, S., Mayer, K.M., Zal, T., Adam, L., Dinney, C.P.. Drezek, R.A.. West, J.L., Hafner, J.H., 2009: The stabilization and targeting of surfactant-synthesized gold nanorods. *Nanotechnology*, **20**, 434005-434014.

[84] Lowery, A.R., Gobin, A.M., Day, E.S., Halas, N.J., West, J.L., 2006: Immunonanoshells for targeted photothermal ablation of tumor cells. *International Journal of Nanomedicine,* **1,** 149–154.

[85] Geoghegan, W.D., Ackerman, G.A., 1977: Adsorption of horseradish-peroxidase, ovomucoid and antiimmunoglobulin to colloidal gold for indirect detection of concanavalin-a,wheat-germ agglutinin and goat antihuman immunoglobulin-g on cell-surfaces at electron-microscopic level new method, theory and application. *Journal of Histochemistry and Cytochemistry,* **25,** 1187–1200.

[86] Nuzzo, R.G., Zegarski, B.R., Dubois, L.H., 1987: Fundamental-studies of the chemisorption of organosulfur compounds on Au(111)—implications for molecular self-assembly on gold surfaces. *Journal of the American Chemical Society*, **109**, 733–740.

[87] Eghtedari, M., Liopo, A.V., Copland, J.A., Oraevslty, A.A., Motamedi, M, 2009: Engineering of hetero-functional gold nanorods for the *in vivo* molecular targeting of breast cancer cells. *Nano Letters,* **9,** 287–291.

[88] Mock, J.J., Barbic, M., Smith, D.R., Schultz, D.A., Schultz, S, 2002: Shape effects in plasmon resonance of individual colloidal silver nanoparticles. *Journal of Chemical Physics*, **116,** 6755–6759.

[89] Mock, J.J., Barbic, M., Smith, D.R., Schultz, D.A., Schultz, S, 2002: Shape effects in plasmon resonance of individual colloidal silver nanoparticles. *Journal of Chemical Physics*, **116,** 6755–6759.

[90] Pfeifer, A., Verma, I.M., 2001: Gene therapy: promises and problems. *Annual Review of Genomics and Human Genetics*, **2,** 177-211.

[91] Verma, I.M., Weitzman, M.D., 2005: Gene therapy: twenty-first century medicine. *Annual Review of Biochemistry*, **74,** 711-738.

[92] Schaffer, D.V., Zhou, W., 2005: Gene therapy and Gene Delivery Systems. *Advances in Biochemical Engineering/Biotechnology*, **99,** 1-39.

[93] Huang, L., Hung, M.-C., Wagner, E., 1999: Nonviral vectors for gene therapy. *Advances in Biochemical Engineering/Biotechnology*, London, England: Academic Press.

[94] Huang, L., Hung, M.-C., Wagner, E., 1999: Nonviral vectors for gene therapy. *Advances in Biochemical Engineering/Biotechnology*, London, England: Academic Press.

[95] Kay, M.A., Glorioso, J.C., Naldini, L., 2001: Viral vectors for gene therapy: the art of turning infectious agents into vehicles of therapeutics. *Nature Medicine*, **7(1),** 33-40.

[96] Tseng, Y.-C., Mozumdar, S., Huang, L., 2009: Lipid-based systemic delivery of siRNA. *Advanced Drug Delivery Reviews*, **61,** 721-731.

[98] Putnam, D., 2006: Polymers for gene delivery across length scales. *Nature Materials*, **5,** 439-451.

[99] Zhang, L., Radovic-Moreno, A.F., Alexis, F., Gu, F., Basto, P.A., Bagalkot, V., Jon, S., Langer, R.S., Farokhzad, O.C., 2007: Co-Delivery of Hydrophobic and Hydrophilic Drugs from Nanoparticle–Aptamer Bioconjugates. *ChemMedChem*, **2,** 1268-1271.

[100] Barhoumi, A., Huschka, R., Bardhan, R., Knight, M.W., Halas, N., 2009: Light-

induced release of DNA from plasmon-resonant nanoparticles: towards light-controlled gene therapy. *Chemical Physics Letters,* **482**, 171–179.

[101] Yang, N.-S., Wang, J.-H., Turner, J., 2004: Molecular strategies for improving cytokine transgene expression in normal and malignant tissues. *Gene Therapy*, **11**, 100-108.

[102] Ryther, R.C.C., Flynt, A.S., Phillips III, J.A., Patton, J.G., 2005: siRNA therapeutics: big potential from small RNAs. *Gene Therapy*, **12**, 5-11.

[103] Kawano, T., Yamagata, M., Takahashi, H., Niidome, Y., Yamada, S., Katayama, Y., Niidome, T., 2006: Stabilizing of plasmid DNA in vivo by PEG-modified cationic gold nanoparticles and the gene expression assisted with electrical pulses. *Journal of Controlled Release*, **111**, 382-389.

[104] Yao, C.-P., Zhang, Z.-X., Rahmanzadeh, R., Huettmann, G., 2008: Laser-based gene transfection and gene therapy. *IEEE Transactions of Nanobioscience*, **7**, 111-119.

[105] Sullivan, M.M.O., Green, J.J., Przybycien, T.M., 2003: Development of a novel gene delivery scaffold utilizing colloidal gold-polyethylenimine conjugates for DNA condensation. *Gene Therapy*, **10**, 1882-1890.

[106] Sandhu, K.K., McIntosh, C.M., Simard, J.M., Smith, S.W., Rotello, V.M., 2002: Gold-nanoparticle mediated transfection of cells. *Bioconjugate Chemistry*, **13(1)**, 3-6

[107] Huff, T.B., Tong, L., Zhao, Y., Hansen, M.N., Cheng, J.-X., Wei, A., 2007: Hyperthermic effects of gold nanorods on tumor cells. *Nanomedicine*, **2**, 125-132.

[108] Mukherjee, P., Bhattacharya, R., Bone, N., Lee, Y.K., Patra, C.R., Wang, S., Lu, L., Secreto, C., Banerjee, P.C., Yaszemski, M.J., Kay, N.E., and Mukhopadhyay, D., 2007: Potential therapeutic application of gold nanoparticles in B-chronic lymphocytic leukemia (BCLL): enhancing apoptosis. *Journal of Nanobiotechnology*, **5(4),** 1-13.

[109] Wijaya, A., Schaffer, S.B., Pallares, I.G., Hamad-Schifferli, K., 2008: Selective release of multiple DNA oligonucleotides from gold nanorods. *ACS Nano*, **3**, 80-86.

[110] Loo, C., Lowery, A., Halas, N., West, J., Drezek, R., 2005: Immunotargeted nanoshells for integrated cancer imaging and therapy. *Nano Letters,* **5(4)**, 709-711.

[111] Gobin, A.M., Lee, M.H., Halas, N.J., James, W.D., Drezek, R.A., West, J.L., 2007: Near-infrared resonant nanoshells for combined optical imaging and photothermal cancer therapy. *Nano Letters*, **7(7)**, 1929-1934.

[112] Colvin, V.L., 2003: The potential environmental impact of engineered nanomaterials. *Nature Biotechnology*, **21(10)**, 1166-1170.

[113] Shukla, R., Bansal, V., Chaudhary, M., Basu, A., Bhonde, R.R., Sastry, M., 2005: Biocompatibility of gold nanoparticles and their endocytic fate inside the cellular compartment: a microscopic overview. *Langmuir*, **21(23)**, 10644-10654.

[114] Connor, E.E., Mwamuka, J., Gole, A., Murphy, C.J., Wyatt, M.D., 2005: Gold nanoparticles are taken up by human cells but do not cause acute cytotoxicity. *Small*, **1(3),** 325-327.

[115] Niidome, T., Yamagata, M., Okamoto, Y., Akiyama, Y., Takahashi, H., Kawano, T., Katayama, Y., and Niidome, Y., 2006: PEG-Modified Gold Nanorods with a Stealth Character for in vivo application. □*Journal of Controlled Release*, *114(3),* 243-347.

[116] Hauck, T.S., Ghazani, A.A., Chan, W.C.W., 2008: Assessing the effect of surface chemistry on gold nanorods uptake, toxicity, and gene expression in mammalian cells. *Small*, **4(1)**, 153-159.

[117] Pernodet, N., Fang, X., Sun, Y., Bakhtina, A., Ramakrishnan, A., Sokolov, J., Ulman, A., Rafailovich, M., 2006: Adverse effects of citrate/gold nanoparticles on human dermal fibroblasts. *Small*, **2(6),** 766-773.

[118] Lewinsky N., Colvin, V., Drezek, R., 2008: Cytoxicity of nanoparticles. *Small*, **4(1)**, 26-49.

[119] Devi, G.R., 2006: siRNA-based approaches in cancer therapy. *Cancer Gene Therapy,* **13**, 819-829.

[120] Villares, G.J., Zigler, M., Blehm, K., Bogdan, C., McCokey, D., Colin, D., Bar-Eli, M., 2007: Targeting EGFR in bladder cancer. *World Journal of Urology*, **25(6)**, 573-579.

[121] Kassouf, W., Luongo, T., Brown, G., Adam, L., Dinney, C.P.N., 2006: Schedule dependent efficacy of Gefitinib and Docetaxel for bladder cancer. *Journal of Urology*, **176(2)**, 787-792.

[122] Kassouf, W., Dinney, C.P.N., Brown, G., McConkey, D.J., Diehl, A.J., Bar-Eli, M., Adam, L., 2005: Uncoupling between epidermal growth factor receptor and downstream signals defines resistance to the antiproliferative effect of Gefitinib in bladder cancer cells. *Cancer Research*, **65(22)**, 10524-10535.

[123] Huang, Z., Brdlik, C., Jin, P., Shepard, H.M., 2009: A pan-HER approach for cancer therapy: background, current status and future development. *Expert Opinion in Biological Therapy*, **9(1)**, 97-110.

[124] Revillion, F., Pawlowski, V., Hornez, L., Peyrat, J.-P., 2000: Glyceraldehyde-3-phosphate dehydrogenase gene expression in human breast cancer. *European Journal of Cancer*, **36(8),** 1038-1042.

[125] Sperling, R.A., V., Parak, W.J., 2010: Surface modification, functionalization and bioconjugation of colloidalinorganic nanoparticles. *Philosophical Transactions of the Royal Society A*, **368,** 1333-1383.

[126] Weiler, J., Hunziker, J., Hall, J., 2006: Anti-miRNA oligonucleotides (AMOs): ammunition to target miRNAs implicated in human disease? *Gene Therapy*, **13**, 496-502.

[127] Bonetta, L., 2005: The inside-scoop—evaluating gene delivery methods. *Nature Methods*, **2**, 875-883.

[128] Zhu, P., Yang, H., Peng, C., Zhang, X., 2001: The Influence of solvent and temperature upon the aggregation of poly(ethylene glycol). *Macromolecular Chemistry and Physics*, **202**, 1380-1383.

[129] Lee, J., Govorov, A.O., Kotov, N.A., 2005: Nanoparticle assemblies with molecular springs: a nanoscale thermometer. *Angewandte Chemie International Edition*, **202(44)**, 7439 –7442.

[130] Scheper, T., Rao, G., 2009: Optical sensor systems in biotechnology. *Advances in Biochemical Engineering/Biotechnology*, **116,** 29-72.

[130] Scheper, T., Rao, G., 2009: Optical sensor systems in biotechnology. *Advances in Biochemical Engineering/Biotechnology*, **116,** 29-72.

[131] Adam L, Zhong M, Choi W, Qi W, Nicoloso M, Arora A, Calin G, Wang H, Siefker-Radtke A, McConkey D, Bar-Eli M, Dinney C., 2009: miR-200 Expression Regulates Epithelial-to-Mesenchymal Transition in Bladder Cancer Cells and Reverses Resistance to Epidermal Growth Factor Receptor Therapy. Clinical Cancer Research (Cover Illustration), **15**(16), 5060-72.